NASA Technical Memorandum 102267 USAAVSCOM Technical Memorandum 90-A-004

A Flight-Dynamic Helicopter Mathematical Model with a Single Flap-Lag-Torsion Main Rotor

M. D. Takahashi

February 1990

National Aeronautics and Space Administration

US ARMY AVIATION SYSTEMS COMMAND
AVIATION RESEARCH AND TECHNOLOGY ACTIVITY

NASA Technical Memorandum 102267 USAAVSCOM Technical Memorandum 90-A-004

A Flight-Dynamic Helicopter Mathematical Model with a Single Flap-Lag-Torsion Main Rotor

M. D. Takahashi, Aeroflightdynamics Directorate, U.S. Army Aviation Research and Technology Activity, Ames Research Center, Moffett Field, California

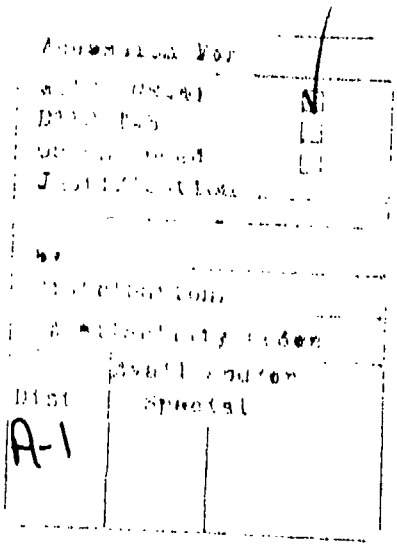

February 1990

National Aeronautics and Space Administration

Ames Research Center
Moffett Field, California 94035-1000

US ARMY
AVIATION
SYSTEMS COMMAND

AVIATION RESEARCH AND
TECHNOLOGY ACTIVITY
MOFFETT FIELD, CA 94035-1099

CONTENTS

	Page
NOMENCLATURE	v
SUMMARY	1
INTRODUCTION	1
HELICOPTER EQUATIONS OF MOTION	2
Fuselage	2
Main Rotor	6
Inflow	11
Tail Surfaces	13
Tail Rotor	14
Main-Rotor Downwash	15
Mass Matrix	17
Multiblade Coordinate Transformation	21
OPERATIONS	22
Basic Setup	22
Initialization	24
Trim	24
Integration	26
Linearization	28
RESULTS	29
CONCLUDING REMARKS	34
REFERENCES	35
TABLES	37
FIGURES	54

NOMENCLATURE

A vector is denoted with an over-arrow (e.g., the position vector $\vec{r}_{ab}$), and the column matrix representation of a vector, or any other type of column matrix, is represented with an underbar (e.g., $\underline{v}$). Points in the system are designated by lowercase letters, so the position vector $\vec{r}_{ab}$ in the above example is read "the position from point a to point b." Coordinate frames are designated by capital letters (e.g., $\hat{x}_A$ is the x unit vector in the A system). Coordinate-frame rotation rates are represented as $\vec{\omega}_{F/I}$, which is read as "the rotation rate of frame F relative to frame I." Rotation vectors are always resolved in the frame of the first subscript. Nondimensional quantities are represented with an overbar and are nondimensionalized by the blade mass, rotor radius, and nominal rotor rotational rate.The sine and cosine functions are abbreviated to S_θ and C_θ, where the subscript is the argument. In the following list, the abbreviation DOF is used for degrees of freedom.

a	blade-section lift-curve slope
a_{snd}	speed of sound
a_{TR}	tail-rotor lift-curve slope
$a_{0_{TS}}, b_{0_{TS}}, a_{TS}, b_{TS}$	tail-surface dynamic pressure loss angles
b	blade-section semichord
b_{TR}	tail-rotor semichord
$C_{D_0}, C_{D_1}, C_{D_2}, C_{D_3}, C_{D_4}, C_{D_5}$	tail-surface-drag coefficient values at break angles
$C_{F_x}, C_{F_y}, C_{F_z}$	fuselage-mount damping constants
$C_{L_S}, C_{L_1}, C_{L_2}$	tail-surface-lift coefficient values at break angles
C_T, C_M, C_L	main-rotor thrust, pitch, and roll coefficients
C_{TS}	tail-surface dynamic pressure loss factor
C_x, C_y, C_z	hinge damping constants
$C_{0_{TR}}, C_{1_{TR}}$	tail-rotor drag function constants
d_0, d_1, d_2	blade-section drag function constants
e, f	first and second offsets
e_{TR}	tail-rotor flapping-hinge offset
$\underline{f}, \underline{\dot{f}}, \underline{\ddot{f}}$	fixed-DOF array and derivatives
$\underline{f}_{eq}$	fixed equations
F_x, F_y, F_z	applied-forces components at mount in F system
g	gravity constant
h	shaft length
i_{Aero}	apparent-mass-term flag
$i_f(n_{i_f})$	fixed DOF indices (number selected)
$i_{f_{eq}}(n_{f_{eq}})$	fixed equation indices (number selected)
$i_{\dot{f}}(n_{i_{\dot{f}}})$	first-derivative fixed DOF indices (number selected)
$i_{\ddot{f}}(n_{i_{\ddot{f}}})$	second-derivative fixed DOF indices (number selected)
$i_u(n_{i_u})$	fixed control indices (number selected)
$i_y(n_{i_y})$	feedback fixed-output indices (number selected)
$i_{\tilde{y}}(n_{i_{\tilde{y}}})$	auxiliary fixed-output indices (number selected)
$i_X(n_{i_X})$	feedback X-output indices (number selected)

$i_{\tilde{\mathbf{X}}}(n_{i_{\tilde{\mathbf{X}}}})$	auxiliary X-output indices (number selected)
$i_1(n_{i_1})$	first-order variable/equation indices (number selected)
$I_{b_{TR}}$	tail-rotor flap inertia about flapping hinge
I_B	blade inertia matrix
I_F	fuselage inertia matrix
I_R	rotor-hub inertia matrix
$j_r(n_{j_r})$	rotor DOF/equation indices (number selected)
$j_{\dot{r}}(n_{j_{\dot{r}}})$	first-derivative rotor DOF indices (number selected)
$j_w(n_{j_w})$	feedback-rotor output indices (number selected)
$j_{\tilde{w}}(n_{j_{\tilde{w}}})$	auxiliary-rotor output indices (number selected)
$j_\theta(n_{j_\theta})$	rotor control indices (number selected)
$K(n_K)$	rotor control blade indices (number selected)
$K_{b_{TR}}$	tail-rotor flap-spring constant
$K_{F_x}, K_{F_y}, K_{F_z}$	mount spring constants
K_x, K_y, K_z	hinge spring constants
$K_{1_{TR}}$	tail-rotor tangent of δ_3
L_I, M_I	inflow matrices
M_B	blade mass
$M_{B_{TR}}$	tail-rotor blade mass
M_F	fuselage mass
M_R	rotor-hub mass
m_0, m_1	blade-section moment function constants
$n_{A_{bld}}$	number of blade accelerometer measurements
$n_{A_{fus}}$	number of fuselage accelerometer measurements
n_b	number of blades
$n_{b_{TR}}$	number of blades in tail rotor
n_f	number of fixed DOF
$n_{h_{LIN}}$	number of harmonics in periodic system linear coefficient matrices
$n_{h_{TRM}}$	number of harmonics in trim blade equilibrium solution
n_r	number of rotor blade DOF
n_s	number of empennage surfaces
n_u	number of fixed inputs
$n_{u_A}, n_{u_C}, n_{u_P}, n_{u_S}, n_{u_G}$	number of controls in blocks A, C, P, S, and G
n_w	number of rotor outputs
$n_{x_A}, n_{x_C}, n_{x_P}, n_{x_S}, n_{x_G}$	number of states in blocks A, C, P, S, and G
n_y	number of fixed outputs
$n_{y_A}, n_{y_C}, n_{y_P}, n_{y_S}, n_{y_G}$	number of outputs in blocks A, C, P, S, and G
$n_{\alpha_{mid}}, n_{\alpha_{end}}$	number of divisions in middle/end region of α for surface downwash table
$n_{\beta_{mid}}, n_{\beta_{end}}$	number of divisions in middle/end region of β for surface downwash table
n_θ	number of rotor blade inputs
n_1	number of augmented states

r_{co}	trim Fourier coefficients matrix $\left[(2n_{h_{TRM}}+1) \text{ by } n_r\right]$ of the blade DOF
r_1, r_2	integration limits in downwash table calculation
$\underline{r}, \underline{\dot{r}}, \underline{\ddot{r}}$	blade DOF arrays and derivatives
r_{eq}	rotor equations
R	rotor radius
R_{TR}	tail-rotor radius
$\underline{R}^T = \left[R_{m_x} R_{m_y} R_{m_z}\right]^T$	translation DOF of fuselage
S_f	reference area of fuselage aerodynamic forces
ST_a, BL_a, WL_a	aerodynamic force position a in station-buttline-waterline coordinate frame
ST_c, BL_c, WL_c	fuselage center-of-mass position c
ST_m, BL_m, WL_m	translational DOF position m
ST_r, BL_r, WL_r	tail-rotor position
ST_s, BL_s, WL_s	tail-surface position
ST_t, BL_t, WL_t	shaft tilt position
S_{TS}	tail-surface reference area
$t_{f_{INT}}$	final time of response
TR_{BRK}, TR_{LOSS}	tail-rotor loss function constants
T_{wc}, T_{wx}	blade linear twist constants
$\underline{U}$	fixed input array
x_A	blade-section torsion axis distance behind 1/4 chord
x_b, y_b, z_b	blade center-of-gravity position components in B system
$x_{b_{TR}}$	tail-rotor center of mass from hinge offset
x_1, x_2	aerodynamic forces integrated from x_1 to x_2 along $\hat{x}_B$
$\underline{x}_{eq}$	first-order equations
$\underline{x}_1$	first-order augmented state array
$\alpha_{D_1}, \alpha_{D_2}, \alpha_{D_3}, \alpha_{D_4}$	tail-surface-drag break angles
$\alpha_{L_S}, \alpha_{L_1}, \alpha_{L_2}$	tail-surface-lift break angles
$\alpha_{LO_{BND}}, \alpha_{LO}, \alpha_{UP}, \alpha_{UP_{BND}}$	downwash table α ranges
$\beta_{LO_{BND}}, \beta_{LO}, \beta_{UP}, \beta_{UP_{BND}}$	downwash table β ranges
β_k, ζ_k, ϕ_k	flap, lag, and torsion blade DOF
β_p, ζ_p	hinge offset angles
Δ_{DW}	nearest α to wake layer for surface downwash table calculations
$\Delta\underline{f}, \Delta\underline{\dot{f}}$	finite-difference perturbation for fixed DOF and derivative
$\Delta\underline{r}, \Delta\underline{\dot{r}}$	finite difference perturbation for rotor DOF and derivative
$\Delta\underline{U}$	finite-difference perturbation for fixed inputs
$\Delta\underline{x}_1$	finite-difference perturbation for augmented states
$\Delta\underline{\theta}$	finite-difference perturbation for rotor-blade inputs
$\underline{\theta}$	rotor inputs
θ_s, ϕ_s	shaft tilt in pitch (positive back) and roll (positive right)
$\theta_{t_{TR}}$	tail-rotor twist per unit length
$\theta_{x_o}, \theta_{y_o}, \theta_{z_o}$	zero moment angles at mount

$\underline{\Theta}^T = \left[\theta_x, \theta_y, \theta_z\right]^T$	fuselage Euler angles
λ	inflow at main rotor
μ	advance ratio
ρ_A	air density
ρ_x, ρ_y	tail-rotor orientation angles
σ_x, σ_y	tail-surface orientation angles
ψ	rotor DOF, $\psi_k = \psi + \frac{(k-1)}{n_b} 2\pi$
ω_f	rotor fundamental frequency
Ω	nominal rotor rotation rate
Ω_{TR}	tail-rotor rotation rate

For position vector $\vec{r}$:

$\dot{\vec{r}}$	time derivative
$\vec{r}'$	time derivative of a vector relative to vector frame
$\vec{r}^*$	nondimensional time derivative
$\vec{r}(F)$	a vector resolved in a particular frame
$\check{r}$	special matrix form of a vector, i.e., $\check{r} = \begin{bmatrix} 0 & r_z & -r_y \\ -r_z & 0 & r_x \\ r_y & -r_x & 0 \end{bmatrix}$

SUMMARY

A mathematical model of a helicopter system with a single main rotor that includes rigid, hinge-restrained rotor blades with flap, lag, and torsion degrees of freedom is described. The model allows several hinge sequences and two offsets in the hinges. Quasi-steady Greenberg theory is used to calculate the blade-section aerodynamic forces, and inflow effects are accounted for by using a three-state nonlinear dynamic inflow model. The motion of the rigid fuselage is defined by six degrees of freedom, and an optional rotor rpm degree of freedom is available. Empennage surfaces and the tail rotor are modeled, and the effect of main-rotor downwash on these elements is included. Model trim, linearization, and time-integration operations are described and can be applied to a subset of the model in the rotating or nonrotating coordinate frame. A preliminary validation of the model is made by comparing its results with those of other analytical and experimental studies. This publication presents the results of research completed in November 1989.

INTRODUCTION

Future requirements for helicopter flight performance place greater emphasis on high-bandwidth flight-control systems than current requirements. Low-order rigid-body models of helicopter systems can be used successfully to design feedback control systems, but these models impose bandwidth limitations on the controller, making them unsuitable for the design and evaluation of high-bandwidth systems (ref. 1). To meet the new requirements, higher order helicopter models must be used in the design of the flight-control systems. The higher order effects of primary interest are those of the rotor dynamics and the rotor inflow. In addition to capturing the blade-flap and lag dynamics, the effect of torsional dynamics on the control design problem needs to be understood. This last item is relevent to rotor designs using hingeless and bearingless rotors and to advanced concepts, such as servo–flap control, which require torsionally soft rotor blades (ref. 2).

This report documents a higher order helicopter mathematical model created to fill these needs. The helicopter model is described in detail in the next section. The rotor consists of rigid blades with flap, lag, torsion, and pitch motions; and with linear hinge springs and dampers. This gives the model the rotor dynamics of interest and allows for approximate modeling of hingeless rotor systems. The flap (f), lag (l), torsion (t), and pitch (p) hinge motions can have the order flpt, fplt, pflt, lfpt, lpft, or plft (only flpt and lfpt are currently available), and two hinge offsets are available to model various articulated configurations. The blade-section aerodynamics are linear, and the quasi-steady Greenberg model is used (ref. 3). Unsteady inflow effects are included using the three-state nonlinear Pitt/Peters dynamic inflow model (ref. 4). An rpm degree of freedom (DOF) of the main rotor is also available, making analysis of engine/rotor interaction possible. The rigid fuselage model has six degrees of freedom and includes an equivalent-drag-area aerodynamic model, a tail-rotor model, and an empennage-surface model. The empennage-surface models have main-rotor downwash effects that are calculated from the flat-wake model described in chapter 2 of reference 5. The tail rotor is the quasi-static flapping model described in reference 6. For greater flexibility, the spring/damper model, the blade-section aerodynamic model, and the fuselage aerodynamic model can be replaced with user-defined models.

Following the description of the model is the Operations section, which details the operations that are performed on the model. There are three operations: trim, linearization, and time-integration. Trim

places the helicopter system in some user-defined flight condition by satisfying the system equations of motion. After trimming, the model may be linearized about the trim condition, or the model may be initialized in the trim condition and then time-integrated. Linearization uses nonrotating rotor coordinates through a multiblade coordinate transformation (MBCT) (ref. 7). In forward flight, the periodic system matrices can be extracted from this linearization process. The time-integration uses rotating blade coordinates and allows for arbitrary inputs to the model controls. Additionally, the integration process has been cast in a general block form, allowing the introduction of user-specified actuator, sensor, feedback, and precompensator dynamics to the system.

In the Results section, a preliminary validation of the helicopter model is made by comparing results with those from other analytical and experimental studies. The rotor model results are compared with trimmed rotor-response results, from reference 8, of an isolated rotor. Rotor/fuselage results are compared with the experimental frequency and damping data presented in reference 9. The full helicopter model is validated by comparing trim and time-history data extracted from flight data on a UH-60A helicopter (ref. 10). Additionally, a comparison with the quasi-static eight-state linearized model from the GEN HEL program (refs. 11,12) is made.

HELICOPTER EQUATIONS OF MOTION

Fuselage

The fuselage is modeled as a rigid body whose motion is defined by the six degrees of freedom shown in figure 1. The fuselage coordinate frame F is body fixed, with its origin at point m. The location of point m is chosen by the user. The body translational motion is defined by the components of the inertial position vector $\vec{r}_{im}$, and body rotation is defined by the Euler angles. Other relevant points on the body are shown in figure 2. The positions of these points are chosen by the user in the body-fixed coordinate frame defined by the station, the buttline, and the waterline. The forces and moments at m result from mounting restraints, which can be set to simulate any mounting condition, such as in a wind-tunnel test. Point c is the center of mass of the fuselage, where inertial and gravitational forces are resolved, and point a is where fuselage aerodynamic forces are applied. The n_s empennage surfaces produce resultant forces at the s_j points, and the resultant tail-rotor force is at point r. There are $n_{A_{fus}}$ points designated as y_n, where accelerations are output measurements. Point h is the attachment point of the main-rotor hub, which can be set at tilt angles about point t. These tilt angles are defined by the transformation, shown in figure 3, which tips the hub coordinate frame H by constant pitch and roll angles, θ_s and ϕ_s.

The equations of motion for the fuselage are formed by summing the forces created by the main rotor, fuselage inertia and gravity, fuselage aerodynamics, the fuselage mount, the tail rotor, and the tail surfaces. This gives the vector equation

$$\vec{Q}_H + \vec{Q}_{IG} + \vec{Q}_A + \vec{Q}_M + \vec{Q}_R + \sum_j^{n_s} \vec{Q}_{S_j} = 0 \tag{1}$$

Summing the respective moments about point m gives

$$\vec{L}_H + \vec{L}_{IG} + \vec{L}_A + \vec{L}_M + \vec{L}_R + \vec{L}_S = 0 \tag{2}$$

where

$$\vec{L}_H = \vec{J}_H + (\vec{r}_{mt} + \vec{r}_{th}) \times \vec{Q}_H \tag{3}$$

$$\vec{L}_{IG} = \vec{J}_I + \left(\vec{r}_{mc} \times \vec{Q}_{IG}\right) \tag{4}$$

$$\vec{L}_A = \vec{J}_A + \left(\vec{r}_{ma} \times \vec{Q}_A\right) \tag{5}$$

$$\vec{L}_R = \vec{J}_R + \left(\vec{r}_{mr} \times \vec{Q}_R\right) \tag{6}$$

$$\vec{L}_S = \sum_j^{n_s} \vec{J}_{S_j} + \left(\vec{r}_{ms_j} \times \vec{Q}_{S_j}\right) \tag{7}$$

The final fuselage equations are resolved such that they correspond to the fuselage generalized coordinates. That is, if a Lagrangian approach had been used, the same fuselage equations would have resulted. This resolution of the equations facilitates the extraction of the system mass matrix, which is discussed in a subsequent section. The definition of the equations and their location in the fuselage-equation vector $\underline{f}_{eq}$ are

$$f_{eq}(1) = \sum \text{moments about } \hat{x}_F \tag{8}$$

$$f_{eq}(2) = \sum \text{moments about } \hat{y}_{\theta_y} \tag{9}$$

$$f_{eq}(3) = \sum \text{moments about } \hat{z}_{\theta_z} \tag{10}$$

$$f_{eq}(4) = \sum \text{forces in } \hat{x}_I \text{ direction} \tag{11}$$

$$f_{eq}(5) = \sum \text{forces in } \hat{y}_I \text{ direction} \tag{12}$$

$$f_{eq}(6) = \sum \text{forces in } \hat{z}_I \text{ direction} \tag{13}$$

Using the position vectors and coordinate frames as defined, the velocities and accelerations can be determined. At the main rotor hub, the angular velocity and acceleration are given by

$$\vec{\omega}_{H/I} = \vec{\omega}_{H/F} + \vec{\omega}_{F/I} \tag{14}$$

$$\dot{\vec{\omega}}_{F/I} = \vec{\omega}'_{F/I} \tag{15}$$

$$\dot{\vec{\omega}}_{H/I} = \vec{\omega}'_{H/I} = \vec{\omega}'_{H/F} + \vec{\omega}_{H/I} \times \vec{\omega}_{H/F} + \dot{\vec{\omega}}_{F/I} \tag{16}$$

Taking advantage of the constant components in the position vectors, the velocities at selected points are

$$\dot{\vec{r}}_{it} = \dot{\vec{r}}_{im} + \vec{\omega}_{F/I} \times \vec{r}_{mt} \tag{17}$$

$$\dot{\vec{r}}_{ih} = \dot{\vec{r}}_{it} + \vec{\omega}_{H/I} \times \vec{r}_{th} \tag{18}$$

$$\dot{\vec{r}}_{is_j} = \dot{\vec{r}}_{im} + \vec{\omega}_{F/I} \times \vec{r}_{ms_j} \tag{19}$$

$$\dot{\vec{r}}_{ir} = \dot{\vec{r}}_{im} + \vec{\omega}_{F/I} \times \vec{r}_{mr} \tag{20}$$

$$\dot{\vec{r}}_{ia} = \dot{\vec{r}}_{im} + \vec{\omega}_{F/I} \times \vec{r}_{ma} \tag{21}$$

$$\dot{\vec{r}}_{ic} = \dot{\vec{r}}_{im} + \vec{\omega}_{F/I} \times \vec{r}_{mc} \tag{22}$$

$$\dot{\vec{r}}_{iy_n} = \dot{\vec{r}}_{im} + \vec{\omega}_{F/I} \times \vec{r}_{my} \tag{23}$$

and the acclerations at selected points become

$$\ddot{\vec{r}}_{it} = \ddot{\vec{r}}_{im} + \vec{\omega}'_{F/I} \times \vec{r}_{mt} + \vec{\omega}_{F/I} \times (\vec{\omega}_{F/I} \times \vec{r}_{mt}) \tag{24}$$

$$\ddot{\vec{r}}_{ih} = \ddot{\vec{r}}_{it} + \vec{\omega}'_{H/I} \times \vec{r}_{th} + \vec{\omega}_{H/I} \times (\vec{\omega}_{H/I} \times \vec{r}_{th}) \tag{25}$$

$$\ddot{\vec{r}}_{ic} = \ddot{\vec{r}}_{im} + \vec{\omega}'_{F/I} \times \vec{r}_{mc} + \vec{\omega}_{F/I} \times (\vec{\omega}_{F/I} \times \vec{r}_{mc}) \tag{26}$$

$$\ddot{\vec{r}}_{iy_n} = \ddot{\vec{r}}_{im} + \vec{\omega}'_{F/I} \times \vec{r}_{my_n} + \vec{\omega}_{F/I} \times (\vec{\omega}_{F/I} \times \vec{r}_{my_n}) \tag{27}$$

The forces and moments of the fuselage are discussed separately, beginning with the inertial and gravity effects. At the fuselage center of gravity, the inertial force and moment vectors are

$$\vec{Q}_{IG} = M_F \left(-\ddot{\vec{r}}_{ic} + g\hat{Z}_I\right) \tag{28}$$

$$\vec{J}_I = -\overline{\overline{I}}_F \cdot \vec{\omega}'_{F/I} - \vec{\omega}_{F/I} \times (\overline{\overline{I}}_F \cdot \vec{\omega}_{F/I}) \tag{29}$$

where the inertia tensor is defined in the F system.

The fuselage aerodynamic effects are based in the wind-axis coordinate frame W defined in figure 4. The velocity of the air relative to point a is

$$\vec{V}_a = \vec{V}_G - \dot{\vec{r}}_{ia} \tag{30}$$

which also defines the direction of the $\hat{x}_W$ component of the wind-axis frame. The angles α_f and β_f are defined from the relative velocity as

$$\alpha_f = \tan^{-1}\left(\frac{-\vec{V}_a \cdot \hat{z}_F}{-\vec{V}_a \cdot \hat{x}_F}\right) \qquad -\pi \le \alpha_F \le \pi \tag{31}$$

$$\beta_f = \tan^{-1}\left(\frac{-\vec{V}_a \cdot \hat{y}_F}{\sqrt{\left(\vec{V}_a \cdot \hat{x}_F\right)^2 + \left(\vec{V}_a \cdot \hat{z}_F\right)^2}}\right) \tag{32}$$

The fuselage aerodynamic force and moment are

$$\vec{Q}_A = D\hat{x}_W + Y\hat{y}_W + L\hat{z}_W = \frac{1}{2}\rho\|V_a\|^2 S_f \left(C_{D_f}\hat{x}_W + C_{Y_f}\hat{y}_W + C_{L_f}\hat{z}_W\right) \tag{33}$$

$$\vec{J}_A = -R\hat{x}_W + M\hat{y}_W - N\hat{z}_W = \frac{1}{2}\rho\|V_a\|^2 S_f^{3/2} \left(-C_{R_f}\hat{x}_W + C_{M_f}\hat{y}_W - C_{N_f}\hat{z}_W\right) \tag{34}$$

which can be converted to the F frame via the transformation T_{FW}, which is defined in figure 4. The force and moment coefficients are functions of α_f and β_f, but the default fuselage-aerodynamics sets all force coefficients to zero except C_{D_f}, which is set to unity, making the fuselage reference area S_f the equivalent drag area.

The fuselage mount moments are modeled as linear nonorthogonal springs, and the mount forces are treated as given quantities. These forces can be used during trim to satisfy a constraint condition, such as setting a certain amount of thrust. The parameters defining the mount effects can be set to zero for free-flight analysis. The force and moment expressions for the mount are given by

$$\vec{L}_M = \left(M_x - M_z S_{\theta_y}\right)\hat{x}_F + \left(M_y C_{\theta_x} + M_z S_{\theta_x} C_{\theta_y}\right)\hat{y}_F + \left(-M_y S_{\theta_x} + M_z C_{\theta_x} C_{\theta_y}\right)\hat{z}_F \tag{35}$$

where

$$M_x = -K_{F_x}\left(\theta_x - \theta_{x_0}\right) - C_{F_x}\dot{\theta}_x \tag{36}$$

$$M_y = -K_{F_y}\left(\theta_y - \theta_{y_0}\right) - C_{F_y}\dot{\theta}_y \tag{37}$$

$$M_z = -K_{F_z}\left(\theta_z - \theta_{z_0}\right) - C_{F_z}\dot{\theta}_z \tag{38}$$

$$\vec{Q}_M = F_x\hat{x}_I + F_y\hat{y}_I + F_z\hat{z}_I \tag{39}$$

The measurement outputs from the fuselage are acceleration, velocity, and angular rates. The $n_{A_{fus}}$ accelerometer outputs are expressed as

$$y(j) = \left(\ddot{\vec{r}}_{i_{y_j}} - g\hat{z}_I\right)\cdot\frac{\vec{f}_j}{\|\vec{f}_j\|} \qquad j = 1, 2, \ldots, n_{A_{fus}} \tag{40}$$

$$\vec{f}_j = f_{x_j}\hat{x}_F + f_{y_j}\hat{y}_F + f_{z_j}\hat{z}_F \tag{41}$$

where the direction of the measurement is selected through the components of $\vec{f}_j$. The velocity of the fuselage center of mass is resolved in the fuselage fixed frame and is available as a measurement, as are the fuselage angular rates. The components of the velocity and angular rate vectors are stored in y according to

$$y\left(n_{A_{fus}} + 1\right) = \dot{\vec{r}}_{ic}\cdot\hat{x}_F \tag{42}$$

$$y\left(n_{A_{fus}} + 2\right) = \dot{\vec{r}}_{ic}\cdot\hat{y}_F \tag{43}$$

$$y\left(n_{A_{fus}} + 3\right) = \dot{\vec{r}}_{ic}\cdot\hat{z}_F \tag{44}$$

$$y\left(n_{A_{fus}} + 4\right) = \vec{\omega}_{F/I}\cdot\hat{x}_F \tag{45}$$

$$y\left(n_{A_{fus}} + 5\right) = \vec{\omega}_{F/I}\cdot\hat{y}_F \tag{46}$$

$$y\left(n_{A_{fus}} + 6\right) = \vec{\omega}_{F/I}\cdot\hat{z}_F \tag{47}$$

Main Rotor

Fixed to the main rotor are n_b coordinate frames, one for each blade. Figure 5 shows the rotor coordinate frame R for the kth blade, in which several additional blade coordinate frames are defined. The additional frames are shown in figure 6. The first hinge is offset a distance e from the hub center, and point e corresponds to the origin of the link coordinate frame L. The second hinge is offset a distance f from point e. The origin of blade coordinate frame B is at point f and is fixed to the blade. The significant points on the blade are b, at the blade center of gravity, and x, at a distance x along the $\hat{x}_B$ axis. Also on the blade are $n_{A_{bld}}$ points designated w_n, which locate the blade accelerometer measurements.

The hinge sequences that define the orientation of the blade coordinate frames can be divided into two groups . The first group is flap-lag-pitch-torsion (flpt), flap-pitch-lag-torsion (fplt), and pitch-flap-lag-torsion (pflt), in all of which the flap motion precedes the lag. The second group places lag before flap in lag-flap-pitch-torsion (lfpt), lag-pitch-flap-torsion (lpft), and pitch-lag-flap-torsion (plft) hinge sequences. Only the flpt and lfpt sequences are available; they are defined in figures 7 and 8. An intermediate coordinate frame P, which is not shown in figure 6, is included in these figures. Frame P allows the introduction of hinge effects such as precone and δ_3. The angle β_p in figures 7 and 8 is the precone angle, and ζ_p is a cant in the flap hinge that geometrically introduces the δ_3 effect. By definition, the variable δ_3 is not an Euler angle (ref. 13), but it is related to the cant Euler angle by $\tan\delta_3 = -\tan\zeta_p \cos\beta_p$ for the flpt system and $\tan\delta_3 = -\tan\left(\zeta_p + \zeta_k\right)\cos\beta_p$ for the lfpt system. The remaining hinge sequences are defined such that for the flap-before-lag sequences, $\dot{\beta}_k$ rotates about the coordinates axis $-\hat{y}_P$; $\dot{\zeta}_k$, about $\hat{z}_L$; and $\dot{\phi}_k$, about $\hat{x}_B$. For the lag-before-flap sequences, $\dot{\zeta}_k$ rotates about the axis $\hat{z}_P$; $\dot{\beta}_k$, about $-\hat{y}_L$; and $\dot{\phi}_k$, about $\hat{x}_B$. The sequence of rotations of the blade angles is summarized in table 1. The items in the flpt row and R to P column are read as follows: starting in frame R, rotate through an angle of β_p about the negative $\hat{y}_R$ axis; then rotate through an angle of ζ_p about the $\hat{z}_{\beta_p}$ axis, to the P system. Each element of the table is read similarly.

The forces on the main rotor are shown in figure 9 with only the kth blade depicted. A rigid body representing the rotor hub mass contributes only inertia to the system. The link between points e and f is massless, contributing no inertial forces to the system. Each blade contributes inertial, gravitational, and aerodynamic forces and moments, which are related to the loads at hinges f and e by

$$\vec{F}_f = -\left(\vec{F}_{IG} + \vec{F}_A\right) = -\vec{F}_T \tag{48}$$

$$\vec{M}_f = -\left(\vec{M}_{IG} + \vec{M}_A\right) = -\vec{M}_T \tag{49}$$

$$\vec{F}_e = \vec{F}_f \tag{50}$$

$$\vec{M}_e = \vec{M}_f + \vec{r}_{ef} \times \vec{F}_f \tag{51}$$

The vectors $\vec{F}_T$ and $\vec{M}_T$ are the sums of the blade inertial, gravitational, and aerodynamic forces and moments at point f. The hub forces and moments of equations (1) and (2) for the main rotor are then

$$\vec{Q}_H = \vec{P}_{IG} + \sum_{k=1}^{n_b}\left(\vec{F}_T\right)_k \tag{52}$$

$$\vec{J}_H = \vec{R}_I + \sum_{k=1}^{n_b} \left[\left(\vec{r}_{he} + \vec{r}_{ef} \right) \times \vec{F}_T + \vec{M}_T \right]_k \tag{53}$$

This gives the rotor equation

$$f_{eq}(7) = T_q + \vec{J}_H \cdot \hat{z}_R = \text{moment about } \hat{z}_R \tag{54}$$

where T_q is the main-rotor torque. For the flpt, fplt, and pflt systems, the flap, lag, and torsion equations are

$$r_{eq}(k,1) = -\left[\vec{M}_e + \vec{M}_T + \vec{r}_{e_f} \times \vec{F}_T \right] \cdot \hat{y}_P \tag{55}$$

$$r_{eq}(k,2) = \left[\vec{M}_f + \vec{M}_T \right] \cdot \hat{z}_L \tag{56}$$

$$r_{eq}(k,3) = \left[\vec{M}_f + \vec{M}_T \right] \cdot \hat{x}_B \tag{57}$$

For the lfpt, lpft, and plft systems, these equations are

$$r_{eq}(k,1) = -\left[\vec{M}_f + \vec{M}_T \right] \cdot \hat{y}_L \tag{58}$$

$$r_{eq}(k,2) = \left[\vec{M}_e + \vec{M}_T + \vec{r}_{e_f} \times \vec{F}_T \right] \cdot \hat{z}_P \tag{59}$$

$$r_{eq}(k,3) = \left[\vec{M}_f + \vec{M}_T \right] \cdot \hat{x}_B \tag{60}$$

These rotor blade equations have been written such that they are equal to the β_k, ζ_k, and ϕ_k equations that would result from using a Lagrangian approach. The total aerodynamic forces and moments at the hub center are

$$\vec{S}_{F_A} = \sum_{k=1}^{n_b} \left(\vec{F}_A \right)_k \tag{61}$$

$$\vec{S}_{M_A} = \sum_{k=1}^{n_b} \left[\vec{M}_A + \left(\vec{r}_{he} + \vec{r}_{ef} \right) \times \vec{F}_A \right]_k \tag{62}$$

The angular velocities and accelerations are

$$\vec{\omega}_{R/I} = \vec{\omega}_{R/H} + \vec{\omega}_{H/I} \tag{63}$$

$$\vec{\omega}_{P/I} = \vec{\omega}_{P/R} + \vec{\omega}_{R/I} \tag{64}$$

$$\vec{\omega}_{L/I} = \vec{\omega}_{L/P} + \vec{\omega}_{P/I} \tag{65}$$

$$\vec{\omega}_{B/I} = \vec{\omega}_{B/L} + \vec{\omega}_{L/I} \tag{66}$$

$$\dot{\vec{\omega}}_{R/I} = \vec{\omega}'_{R/I} = \vec{\omega}'_{R/H} + \vec{\omega}_{R/I} \times \vec{\omega}_{R/H} + \dot{\vec{\omega}}_{H/I} \tag{67}$$

$$\dot{\vec{\omega}}_{P/I} = \vec{\omega}'_{P/I} = \vec{\omega}'_{P/R} + \vec{\omega}_{P/I} \times \vec{\omega}_{P/R} + \dot{\vec{\omega}}_{R/I} \tag{68}$$

$$\dot{\vec{\omega}}_{L/I} = \vec{\omega}'_{L/I} = \vec{\omega}'_{L/P} + \vec{\omega}_{L/I} \times \vec{\omega}_{L/P} + \dot{\vec{\omega}}_{P/I} \tag{69}$$

$$\dot{\vec{\omega}}_{B/I} = \vec{\omega}'_{B/I} = \vec{\omega}'_{B/L} + \vec{\omega}_{B/I} \times \vec{\omega}_{B/L} + \dot{\vec{\omega}}_{L/I} \tag{70}$$

For the blade aerodynamic calculations, the velocity of point x results from

$$\dot{\vec{r}}_{ie} = \dot{\vec{r}}_{ih} + \vec{\omega}_{R/I} \times \vec{r}_{he} \tag{71}$$

$$\dot{\vec{r}}_{if} = \dot{\vec{r}}_{ie} + \vec{\omega}_{L/I} \times \vec{r}_{ef} \tag{72}$$

$$\dot{\vec{r}}_{ix} = \dot{\vec{r}}_{if} + \vec{\omega}_{B/I} \times \vec{r}_{fx} \tag{73}$$

For the mass matrix calculation, the velocity of the blade center of mass is

$$\dot{\vec{r}}_{ib} = \dot{\vec{r}}_{if} + \vec{\omega}_{B/I} \times \vec{r}_{fb} \tag{74}$$

The accelerations of the blade center of mass, the points w_n, and the point x along $\hat{x}_B$ result from

$$\ddot{\vec{r}}_{ie} = \ddot{\vec{r}}_{ih} + \vec{\omega}'_{R/I} \times \vec{r}_{he} + \vec{\omega}_{R/I} \times \left(\vec{\omega}_{R/I} \times \vec{r}_{he}\right) \tag{75}$$

$$\ddot{\vec{r}}_{if} = \ddot{\vec{r}}_{ie} + \vec{\omega}'_{L/I} \times \vec{r}_{ef} + \vec{\omega}_{L/I} \times \left(\vec{\omega}_{L/I} \times \vec{r}_{ef}\right) \tag{76}$$

$$\ddot{\vec{r}}_{ib} = \ddot{\vec{r}}_{if} + \vec{\omega}'_{B/I} \times \vec{r}_{fb} + \vec{\omega}_{B/I} \times \left(\vec{\omega}_{B/I} \times \vec{r}_{fb}\right) \tag{77}$$

$$\ddot{\vec{r}}_{iw_n} = \ddot{\vec{r}}_{if} + \vec{\omega}'_{B/I} \times \vec{r}_{fw} + \vec{\omega}_{B/I} \times \left(\vec{\omega}_{B/I} \times \vec{r}_{fw}\right) \tag{78}$$

$$\ddot{\vec{r}}_{ix} = \ddot{\vec{r}}_{if} + \vec{\omega}'_{B/I} \times \vec{r}_{fx} + \vec{\omega}_{B/I} \times \left(\vec{\omega}_{B/I} \times \vec{r}_{fx}\right) \tag{79}$$

The rotor hub center of mass is at point h, and the rotor hub orientation is referenced to the $k = 1$ rotor coordinate system. The inertial and gravitational effect of the rotor hub is

$$\vec{P}_{IG} = M_R \left(-\ddot{\vec{r}}_{ih} + g\hat{z}_I\right) \tag{80}$$

and the inertial moment is

$$\vec{R}_I = -\left[\overline{\overline{I}}_R \cdot \vec{\omega}'_{R/I} + \vec{\omega}_{R/I} \times \left(\overline{\overline{I}}_R \cdot \vec{\omega}_{R/I}\right)\right] \tag{81}$$

Likewise, for each blade, the inertial and gravitational force and moment are

$$\vec{F}_{IG} = M_B \left(-\ddot{\vec{r}}_{ib} + g\hat{z}_I\right) \tag{82}$$

$$\vec{M}_{IG} = -\left[\overline{\overline{I}}_B \cdot \vec{\omega}'_{B/I} + \vec{\omega}_{B/I} \times \left(\overline{\overline{I}}_B \cdot \vec{\omega}_{B/I}\right)\right] + \vec{r}_{fb} \times \vec{F}_{IG} \tag{83}$$

where the moment is about point f.

Blade hinge-spring restraining moments are of two types. The first type is nonorthogonal, and for the flpt, fplt, and pflt sequences the moments are

$$-\vec{M}_e \cdot \hat{y}_P = -K_y\beta_k - C_y\dot{\beta}_k \tag{84}$$

$$\vec{M}_f \cdot \hat{z}_L = -K_z\zeta_k - C_z\dot{\zeta}_k \tag{85}$$

$$\vec{M}_f \cdot \hat{x}_B = -K_x\phi_k - C_x\dot{\phi}_k \tag{86}$$

For the lfpt, lpft, and plft sequences, the nonorthogonal moments are

$$-\vec{M}_f \cdot \hat{y}_L = -K_y \beta_k - C_y \dot{\beta}_k \tag{87}$$

$$\vec{M}_e \cdot \hat{z}_P = -K_z \zeta_k - C_z \dot{\zeta}_k \tag{88}$$

$$\vec{M}_f \cdot \hat{x}_B = -K_x \phi_k - C_x \dot{\phi}_k \tag{89}$$

The second type of spring restraint is orthogonal and is used to approximate hingeless rotor-blade systems. These orthogonal moments are valid only for (1) no second offset ($f = 0$), (2) no cant angle ($\zeta_p = 0$), and (3) with the pitch inboard or outboard of the flap and lag degrees of freedom. For the flpt and pflt sequences, the moments are

$$\begin{aligned}\vec{M}_f = \vec{M}_e = &\left[-K_x\left(-\zeta_k S_{\beta_k} + \phi_k C_{\zeta_k} C_{\beta_k}\right) - C_x\left(-\dot{\zeta}_k S_{\beta_k} + \dot{\phi}_k C_{\zeta_k} C_{\beta_k}\right)\right] \hat{x}_P \\ &+ \left[-K_y\left(-\beta_k + \phi_k S_{\zeta_k}\right) - C_y\left(-\dot{\beta}_k + \dot{\phi}_k S_{\zeta_k}\right)\right] \hat{y}_P \\ &+ \left[-K_z\left(\zeta_k C_{\beta_k} + \phi_k C_{\zeta_k} S_{\beta_k}\right) - C_z\left(\dot{\zeta}_k C_{\beta_k} + \dot{\phi}_k C_{\zeta_k} S_{\beta_k}\right)\right] \hat{z}_P\end{aligned} \tag{90}$$

For the lfpt and plft sequences, the moments are

$$\begin{aligned}\vec{M}_f = \vec{M}_e = &\left[-K_x\left(\beta_k S_{\zeta_k} + \phi_k C_{\beta_k} C_{\zeta_k}\right) - C_x\left(\dot{\beta}_k S_{\zeta_k} + \dot{\phi}_k C_{\beta_k} C_{\zeta_k}\right)\right] \hat{x}_P \\ &+ \left[-K_y\left(-\beta_k C_{\zeta_k} + \phi_k C_{\beta_k} S_{\zeta_k}\right) - C_y\left(-\dot{\beta}_k C_{\zeta_k} + \dot{\phi}_k C_{\beta_k} S_{\zeta_k}\right)\right] \hat{y}_P \\ &+ \left[-K_z\left(\zeta_k + \phi_k S_{\beta_k}\right) - C_z\left(\dot{\zeta}_k + \dot{\phi}_k S_{\beta_k}\right)\right] \hat{z}_P\end{aligned} \tag{91}$$

The total blade aerodynamic effects are found by integrating the sectional aerodynamic forces and moments along the span according to

$$\vec{F}_A = \int_{x_1}^{x_2} \vec{f}_A \, dx \tag{92}$$

$$\vec{M}_A = \int_{x_1}^{x_2} \left[(x\ \hat{x}_B) \times \vec{f}_A + \vec{m}_A\right] dx \tag{93}$$

where

$$\vec{f}_A = f_{\dot{y}_C} \hat{y}_C + f_{\dot{z}_C} \hat{z}_C \tag{94}$$

$$\vec{m}_A = m_{\dot{x}_C} \hat{x}_C \tag{95}$$

The integrations are carried out using Gaussian quadrature numerical integration. Blade-section forces are resolved in a chord coordinate frame C shown in figure 10, which is rotated from the blade coordinate frame B by a geometric twist. The linear twist function is defined by

$$\theta_T(x) = T_{wx} x + T_{wc} \tag{96}$$

The components of the sectional forces and moments are expressed in terms of the angular velocity and acceleration of the chord section and of the components of the relative velocity and acceleration of the air mass at the origin of the C frame. The latter two are

$$\vec{V}_c = \vec{V}_G + \vec{\lambda}_i - \dot{\vec{r}}_{ix} \tag{97}$$

$$\vec{A}_c = \dot{\vec{V}}_G - \ddot{\vec{r}}_{ix} \tag{98}$$

where the vector $\vec{\lambda}_i$ is the induced air velocity whose derivative has been ignored in the air-mass acceleration. The induced air velocity results from the dynamic inflow model, which is described in a subsequent section.

The sectional aerodynamic model is based on quasi-steady Greenberg theory, which is a Theodorsen theory modified to account for lead-lag motions (refs. 3,14). The lift and moment about the torsion axis are given by

$$L = \rho_A ab \left[VQ + P\frac{b}{2} i_{Aero} \right] \tag{99}$$

$$M = \rho_A ab \left[\left(x_{ab} + \frac{b}{2} \right) VQ + \left(x_{ab} P - V\frac{b}{2}\dot{\alpha} - \frac{b^2}{8}\ddot{\alpha} \right) \frac{b}{2} i_{Aero} \right] \tag{100}$$

where

$$Q = \left(\dot{h} + V\alpha \right) - \left(x_{ab} - \frac{b}{2} \right) \dot{\alpha} \tag{101}$$

$$P = \left(\dot{h} + V\alpha \right)^{\cdot} - x_{ab}\ddot{\alpha} \tag{102}$$

The variable i_{Aero} is a switch to remove the apparent mass effects, which can be ignored when the order of magnitude of the mass of the airfoil section is much greater than the order of magnitude of the mass of the air it occupies (ref. 14, chap. 5). Drag and additional moments due to camber are added by

$$D = d_0 + d_1\ \alpha_{eff} + d_2\ \alpha_{eff}^2 \tag{103}$$

$$M_{cam} = m_0 + m_1\ \alpha_{eff} \tag{104}$$

Figure 11 shows the application of the sectional aerodynamic model in forward and reverse flow conditions. The variables in the Greenberg theory are interpreted as in reference 15, where the quantity $\dot{h} + V\alpha$ is interpreted as the normal air velocity at the torsion axis. The derivative of this quantity is then the derivative of the $\hat{z}_c$ component of the air velocity $\vec{V}'_c$, which can be extracted from $\vec{A}_c = \vec{V}'_c + \vec{\omega}_{C/I} \times \vec{V}_C$.

Blade measurements are stored in $\underline{w}$ in the following manner. For the kth blade, the $n_{A_{bld}}$ acclerometer outputs are given by

$$w\left[k + n_b(n-1)\right] = \left(\ddot{\vec{r}}_{iw_n} - g\hat{z}_I \right) \cdot \frac{\vec{b}_n}{\| \vec{b}_n \|} \qquad n = 1, 2, \ldots, n_{A_{bld}} \tag{105}$$

$$\vec{b}_n = b_{x_n}\hat{x}_B + b_{y_n}\hat{y}_B + b_{z_n}\hat{z}_B \tag{106}$$

where the direction of the measurement is selected through the vector $\vec{b}_n$. Blade moments at the hinges are also in $\underline{w}$. They are given by the following expressions when flap is before lag:

$$w\left[k + n_b n_{A_{bld}}\right] = \left(\vec{M}_T + \vec{r}_{ef} \times \vec{F}_T\right) \cdot \hat{y}_P \tag{107}$$

$$w\left[k + n_b\left(n_{A_{bld}} + 1\right)\right] = \vec{M}_T \cdot \hat{z}_L \tag{108}$$

$$w\left[k + n_b\left(n_{A_{bld}} + 2\right)\right] = \vec{M}_T \cdot \hat{x}_B \tag{109}$$

and by the following expressions when lag is before flap:

$$w\left[k + n_b n_{A_{bld}}\right] = \vec{M}_T \cdot \hat{y}_L \tag{110}$$

$$w\left[k + n_b\left(n_{A_{bld}} + 1\right)\right] = \left(\vec{M}_T + \vec{r}_{ef} \times \vec{F}_T\right) \cdot \hat{z}_P \tag{111}$$

$$w\left[k + n_b\left(n_{A_{bld}} + 2\right)\right] = \vec{M}_T \cdot \hat{x}_B \tag{112}$$

Inflow

The rotor inflow is modeled using the three-state nonlinear Pitt/Peters model of reference 4, which is applied in the actuator-disk coordinate frame A shown in figure 12. This frame is tipped to the left by the sine of the flapping angle and tipped forward by the cosine of the flapping angle. The velocity and acceleration of the air relative to the hub center are

$$\vec{V}_h = \vec{V}_G - \dot{\vec{r}}_{ih} \tag{113}$$

$$\vec{A}_h = \dot{\vec{V}}_G - \ddot{\vec{r}}_{ih} \tag{114}$$

The advance ratio, the free-stream inflow, and the total average inflow can be found by using the velocity vectors; they are

$$\mu = \frac{\sqrt{\left(\vec{V}_h \cdot \hat{x}_A\right)^2 + \left(\vec{V}_h \cdot \hat{y}_A\right)^2}}{R\Omega} \tag{115}$$

$$\lambda_{fs} = \frac{\vec{V}_h \cdot \hat{z}_A}{R\Omega} \tag{116}$$

$$\lambda = \lambda_{fs} + \lambda_0 \tag{117}$$

where the total average inflow λ is the sum of the free-stream inflow plus the constant induced-inflow component, which is one state of the dynamic inflow model. The inflow vector for the blade aerodynamic calculation, in terms of the inflow states, is

$$\vec{\lambda}_i = \lambda_i \hat{z}_A = \left(\lambda_0 + \lambda_{1s}\frac{r}{R}S_{\psi_k} + \lambda_{1c}\frac{r}{R}C_{\psi_k}\right)\hat{z}_A \tag{118}$$

where λ_0, λ_{1s}, and λ_{1c} are the three inflow states that define the inflow in the A system. These inflow states are governed by the first-order inflow equations

$$\left\{ \begin{array}{c} x_{eq}(1) \\ x_{eq}(2) \\ x_{eq}(3) \end{array} \right\} = L_I M_I \left\{ \begin{array}{c} \overset{*}{\nu}_0 \\ \overset{*}{\nu}_{1s} \\ \overset{*}{\nu}_{1c} \end{array} \right\} + \left\{ \begin{array}{c} \nu_0 \\ \nu_{1s} \\ \nu_{1c} \end{array} \right\} - L_I \left\{ \begin{array}{c} C_T \\ C_L \\ C_M \end{array} \right\} \tag{119}$$

The ν's in equation (119) are coefficients that define the inflow in the same way that the λ's define the inflow in equation (118). However, the ν's define the inflow in the D system, which is aligned with the velocity in the disk plane. The ν coefficients and the λ coefficients are related by

$$\nu_0 = \lambda_0 \tag{120}$$

$$\nu_{1s} = \lambda_{1s} C_{\beta_h} + \lambda_{1c} S_{\beta_h} \tag{121}$$

$$\nu_{1c} = \lambda_{1c} C_{\beta_h} + \lambda_{1s} S_{\beta_h} \tag{122}$$

$$\overset{*}{\nu}_0 = \frac{\lambda_0}{\Omega} \tag{123}$$

$$\overset{*}{\nu}_{1s} = \frac{\dot{\lambda}_{1s}}{\Omega} C_{\beta_h} + \frac{\dot{\lambda}_{1c}}{\Omega} S_{\beta_h} + \frac{\dot{\beta}_h}{\Omega} \left(-\lambda_{1s} S_{\beta_h} + \lambda_{1c} C_{\beta_h} \right) \tag{124}$$

$$\overset{*}{\nu}_{1c} = \frac{\dot{\lambda}_{1c}}{\Omega} C_{\beta_h} - \frac{\dot{\lambda}_{1s}}{\Omega} S_{\beta_h} - \frac{\dot{\beta}_h}{\Omega} \left(\lambda_{1c} S_{\beta_h} + \lambda_{1s} C_{\beta_h} \right) \tag{125}$$

where the side-slip angle and rate are

$$\beta_h = \tan^{-1} \left(\frac{-\vec{V}_h \cdot \hat{y}_A}{-\vec{V}_h \cdot \hat{x}_A} \right) \tag{126}$$

$$\dot{\beta}_h = \frac{\left(\dot{\vec{V}}_h \cdot \hat{x}_A \right) \left(\vec{A}_h \cdot \hat{y}_A \right) - \left(\vec{A}_h \cdot \hat{x}_A \right) \left(\vec{V}_h \cdot \hat{y}_A \right)}{\left(\vec{V}_h \cdot \hat{x}_A \right)^2 + \left(\vec{V}_h \cdot \hat{y}_A \right)^2} \tag{127}$$

The thrust, roll, and pitch coefficients in equation (119) are given, in terms of the main-rotor aerodynamic forces and moments, by

$$C_T = -\frac{\vec{S}_{F_A} \cdot \hat{z}_A}{\pi \rho_A R^4 \Omega^2} \tag{128}$$

$$C_L = \frac{\left(\vec{S}_{M_A} \cdot \hat{y}_A \right) S_{\beta_h} + \left(\vec{S}_{M_A} \cdot \hat{x}_A \right) C_{\beta_h}}{\pi \rho_A R^5 \Omega^2} M_{off} \tag{129}$$

$$C_M = \frac{\left(\vec{S}_{M_A} \cdot \hat{y}_A \right) C_{\beta_h} - \left(\vec{S}_{M_A} \cdot \hat{x}_A \right) S_{\beta_h}}{\pi \rho_A R^5 \Omega^2} M_{off} \tag{130}$$

The matrices for the Pitt/Peters model are

$$L_I = \begin{bmatrix} \frac{1}{2\nu_T} & 0 & \frac{15\pi}{64\nu}\sqrt{\frac{1-S_{\alpha_s}}{1+S_{\alpha_s}}} \\ 0 & \frac{-4}{\nu(1+S_{\alpha_s})} & 0 \\ \frac{15\pi}{64\nu_T}\sqrt{\frac{1-S_{\alpha_s}}{1+S_{\alpha_s}}} & 0 & \frac{-4S_{\alpha_s}}{\nu(1+S_{\alpha_s})} \end{bmatrix} \tag{131}$$

$$M_I = \begin{bmatrix} m_0(mass) & 0 & 0 \\ 0 & \frac{-16}{45\pi} & 0 \\ 0 & 0 & \frac{-16}{45\pi} \end{bmatrix} \tag{132}$$

where

$$\nu = \frac{\mu^2 + \lambda(\lambda + \lambda_0)}{\sqrt{\mu^2 + \lambda^2}} \tag{133}$$

$$\nu_T = \sqrt{\mu^2 + \lambda^2} \tag{134}$$

$$\alpha_s = \tan^{-1}\left(\frac{\lambda}{\mu}\right) \tag{135}$$

The element m_0 takes on two possible values. One value corresponds to a zero-inflow boundary condition at the hub center, $m_0(0) = \frac{128}{75\pi}$; the other value, $m_0(1) = \frac{8}{3\pi}$, does not enforce this condition.

Tail Surfaces

Up to five tail surfaces are available (the subscript representing each surface will be omitted in the following discussion); they are oriented as in figure 13. Each surface can be tipped away from the horizontal by an angle σ_x, and the pitch incidence can be adjusted through σ_y to define the zero point of the input i_{TS}. The velocity of the air relative to the surface is

$$\vec{V}_s = \vec{V}_G + \vec{d}_{TS} - \dot{\vec{r}}_{is} \tag{136}$$

where $\vec{d}_{TS}$ is the downwash from the main rotor. Each tail surface has its own downwash table that is a function of the angles at which the air strikes the hub center, the magnitude of the air velocity, and the thrust coefficient (i.e., $\vec{d}_{TS} = C_T f_{DW_{TS}}(\alpha_v, \beta_v, V_v)\,\hat{z}_s$). The moment $\vec{J}_s$ at the surface is zero, but the force at the tail surface is

$$\begin{aligned} \vec{Q}_s = & \frac{1}{2}\rho_A \parallel \vec{V}_s \parallel^2 S_{TS}\Big\{\left[C_L(\alpha_z)\,S_{\alpha_s} - C_D(\alpha_z)\,C_{\alpha_s}\right]\hat{x}_s \\ & + \left[-C_L(\alpha_z)\,C_{\alpha_s} - C_D(\alpha_z)\,S_{\alpha_s}\right]\hat{z}_s\Big\} q_{loss} S_R \end{aligned} \tag{137}$$

where, for forward flow, α_z and S_R are defined by

$$\left.\begin{array}{rcl} \alpha_z &=& \alpha_s \\ S_R &=& 1 \end{array}\right\} \text{for } -\tfrac{\pi}{2} \le \alpha_s \le \tfrac{\pi}{2}$$

and, for reverse flow, they are defined by

$$\left.\begin{array}{rcl} \alpha_z &=& \alpha - \pi \\ S_R &=& 0.8 \end{array}\right\} \text{for } \tfrac{\pi}{2} \le \alpha_s \le \pi$$
$$\left.\begin{array}{rcl} \alpha_z &=& \alpha + \pi \\ S_R &=& 0.8 \end{array}\right\} \text{for } -\pi \le \alpha_s \le -\tfrac{\pi}{2} \tag{138}$$

where

$$\alpha_s = \tan^{-1}\left(\frac{-\vec{V}_s \cdot \hat{z}_s}{-\vec{V}_s \cdot \hat{x}_s}\right) \tag{139}$$

The lift and drag coefficients are functions of α_z and are defined by specifying the break points shown in figures 14 and 15. The dynamic pressure loss due to fuselage blockage is approximated by the functions

$$q_{loss} = 1 - \left(\frac{v_{loss}}{V_s}\right)^2 \tag{140}$$

$$\frac{v_{loss}}{V_s} = C_{TS}\exp\left\{-\frac{1}{2}\left[\left(\frac{\alpha_f - a_{0_{TS}}}{a_{TS}}\right)^2 + \left(\frac{\beta_f - b_{0_{TS}}}{b_{TS}}\right)^2\right]\right\} \tag{141}$$

When the angles α_f and β_f are at $a_{0_{TS}}$ and $b_{0_{TS}}$, respectively, the loss is a maximum.

Tail Rotor

The tail-rotor orientation is shown in figure 16; the Euler angles ρ_x and ρ_y have the same sequence as the tail-surface orientation. The relative velocity of the air is given by

$$\vec{V}_r = \vec{V}_G + \vec{d}_{TR} - \dot{\vec{r}}_{ir} \tag{142}$$

and the downwash $\vec{d}_{TR}$, like the tail surface downwash, is interpolated from a table. From the figure, the advance ratio and total inflow are

$$\mu_{TR} = \frac{\sqrt{\left(\vec{V}_r \cdot \hat{x}_T\right)^2 + \left(\vec{V}_r \cdot \hat{y}_T\right)^2}}{R_{TR}\Omega_{TR}} \tag{143}$$

$$\lambda_{TR} = \mu_{TR}\tan\alpha_r + \frac{C_{T_{TR}}}{2\sqrt{\mu_{TR}^2 + \lambda_{TR}^2}} = \lambda_{fs_{TR}} + \frac{C_{T_{TR}}}{2\sqrt{\mu_{TR}^2 + \lambda_{TR}^2}} \tag{144}$$

The wind orientation angles with respect to the hub are defined as

$$\beta_r = \tan^{-1}\left(\frac{-\vec{V}_r \cdot \hat{y}_T}{-\vec{V}_r \cdot \hat{x}_T}\right) \tag{145}$$

$$\alpha_r = \tan^{-1}\left[\frac{\vec{V}_r \cdot \hat{z}_T}{\sqrt{\left(\vec{V}_r \cdot \hat{x}_T\right)^2 + \left(\vec{V}_r \cdot \hat{y}_T\right)^2}}\right] \tag{146}$$

The force and moment for the hub from the tail rotor are

$$\vec{Q}_R = \left(-H_{TR}C_{\beta_r} - Y_{TR}S_{\beta_r}\right)\hat{x}_T + \left(-H_{TR}S_{\beta_r} + Y_{TR}C_{\beta_r}\right)\hat{y}_T - T_{TR}f_{blk}\hat{z}_T \tag{147}$$

$$\vec{J}_R = \left(L_{TR}C_{\beta_r} - M_{TR}S_{\beta_r}\right)\hat{x}_T + \left(L_{TR}S_{\beta_r} + M_{TR}C_{\beta_r}\right)\hat{y}_T + Q_{TR}\hat{z}_T \tag{148}$$

All components of the force and moment expressions result from the quasi-static flapping model of reference 6, and are functions of the total inflow and the blade harmonic components. The inflow comes from equation (144) and the blade harmonics result from

$$[\tilde{K}]\underline{a} - \tilde{f} = 0 \tag{149}$$

where $\underline{a}$ is a vector containing the collective, the first sine, and the first cosine components of the blade flapping motion. The precise definitions of the matrices and the rotor forces and moments are given in appendix C of reference 6. In the present report the total inflow is defined such that positive inflow is down through the rotor, whereas in reference 6 total inflow is defined such that positive inflow is up through the rotor. Both equations (144) and (149) are algebraic nonlinear equations and are solved using the Newton method. Once acceptable convergence is reached, the values of $\underline{a}$ and λ_{TR} can be used in the force and moment equations. The loss factor f_{blk} in equation (147) is included in order to model the interference effect between the rotor and the surface to which it is mounted. Loss factor f_{blk} is defined as follows:

$$f_{blk} = (TR_{loss} - 1)\sqrt{1 - \left(\frac{\mu_{TR}}{TR_{brk}}\right)^2} + 1 \qquad \mu_{TR} \le TR_{brk} \tag{150}$$

$$f_{blk} = 1 \qquad \mu_{TR} > TR_{brk} \tag{151}$$

The variable TR_{loss} is the percentage of thrust available at zero advance ratio, and TR_{brk} is the advance ratio at which f_{blk} becomes unity and remains unity at advance ratios above TR_{brk}.

Main-Rotor Downwash

The downwash of the main rotor on the tail surfaces and tail rotor is calculated using the flat-wake model described in detail in chapter 2 of reference 5. The wake model assumes a rotor in edgewise flow, as shown in figure 17; the coordinate frame is that of reference 5. The downwash velocity is determined using the Biot-Savart law, assuming cycloidal vortex filaments shedding from the disk plane. This flat-wake assumption is considered valid in forward flight when $V/R\Omega \ge 1.63\sqrt{C_T}$. The x, y, and z components of the velocity are calculated from

$$\overline{v}_j(\overline{x}_1, \overline{y}_1, \overline{z}_1) = \frac{1}{4\pi\overline{V}}\int_{\overline{r}_1}^{\overline{r}_2} \Delta\hat{v}_j \frac{d\overline{\Gamma}}{d\overline{\rho}} d\overline{\rho} \qquad j = x, y, z \tag{152}$$

where $\Delta\hat{v}_j$ results from

$$\Delta\hat{v}_x = \Delta\hat{v}_x(\tilde{x}_1, \tilde{y}_1, \tilde{z}_1) \tag{153}$$

$$\Delta\hat{v}_y = \Delta\hat{v}_{y_1}(\tilde{x}_1, \tilde{y}_1, \tilde{z}_1) - \frac{1}{2}\left\{\frac{\overline{V}}{\overline{\rho}}\left[\tilde{M}(\tilde{x}_1, \tilde{y}_1, \tilde{z}_1) + \tilde{M}(\infty, \tilde{y}_1, \tilde{z}_1)\right] + \left[\tilde{N}(\tilde{x}_1, \tilde{y}_1, \tilde{z}_1) + \tilde{N}(\infty, \tilde{y}_1, \tilde{z}_1)\right]\right\} \tag{154}$$

$$\Delta\hat{v}_z = -\frac{1}{2}\left\{\frac{\overline{V}}{\overline{\rho}}\left[\tilde{K}(\tilde{x}_1, \tilde{y}_1, \tilde{z}_1) + \tilde{K}(\infty, \tilde{y}_1, \tilde{z}_1)\right] + \left[\tilde{L}(\tilde{x}_1, \tilde{y}_1, \tilde{z}_1) + \tilde{L}(\infty, \tilde{y}_1, \tilde{z}_1)\right]\right\} \tag{155}$$

The functions in equations (153) through (155) are pretabulated and depend on the nondimensional distance from the hub center $\overline{\rho}$ and the components of the point of interest, through

$$\tilde{x}_1 = \frac{\overline{x}_1}{\overline{\rho}} \quad ; \quad \tilde{y}_1 = \frac{\overline{y}_1}{\overline{\rho}} \quad ; \quad \tilde{z}_1 = \frac{\overline{z}_1}{\overline{\rho}} \tag{156}$$

A typical example of each of these functions is shown in figure 18 for $\tilde{y}_1 = 0.6$. The functions need to be tabulated only at the positive values of $\tilde{x}_1$, $\tilde{y}_1$, and $\tilde{z}_1$ because of the symmetric and antisymmetric properties of the functions. A summary of the odd and even behavior of the functions is shown in table 2 along with the equation numbers and figure numbers that define the functions in reference 5. The downwash components are expressed in terms of the function $\overline{\Gamma}$, which is the average circulation over a rotor revolution at a radial distance from the center of the rotor. As in appendix C of reference 16, this function is approximated as

$$\overline{\Gamma}(\overline{\rho}) = \overline{\Gamma}_0(1 - \overline{\rho})\overline{\rho}^2 \tag{157}$$

$$\overline{\Gamma}_0 = \frac{20\pi C_T}{5\left(r_2^4 - r_1^4\right) - 4\left(r_2^5 - r_1^5\right)} \tag{158}$$

where the constant $\overline{\Gamma}_0$ is a function of the thrust coefficient. This relationship between the circulation and the thrust coefficient comes from evaluating

$$\overline{T} = \int_{r_1}^{r_2}\left[\frac{1}{2\pi}\int_0^{2\pi}\frac{d\overline{T}}{d\overline{\rho}}d\psi\right]d\overline{\rho} \tag{159}$$

where

$$\frac{1}{2\pi}\int_0^{2\pi}\frac{d\overline{T}}{d\overline{\rho}}d\psi = \overline{\rho}_A\overline{\Gamma}(\overline{\rho})\overline{\rho} \tag{160}$$

which results from the Joukowsky lifting law.

The wake model can be used to generate a downwash table for each tail surface and tail rotor. The wake is oriented along the relative air velocity vector in the $\hat{x}_V - \hat{y}_V$ plane, shown in figure 19. The S-frame is the tail-surface frame, but the tail-rotor frame T can be substituted for it. The velocity at the hub is

$$\vec{V}_v = \vec{V}_G + \lambda_0\hat{z}_A - \dot{\vec{r}}_{ih} \tag{161}$$

and the orientation angles are

$$\alpha_v = \tan^{-1} \frac{\vec{V}_v \cdot \hat{z}_H}{\sqrt{\left(\vec{V}_v \cdot \hat{x}_H\right)^2 + \left(\vec{V}_v \cdot \hat{y}_H\right)^2}} \tag{162}$$

$$\beta_v = \tan^{-1} \left(\frac{-\vec{V}_v \cdot \hat{y}_H}{-\vec{V}_v \cdot \hat{z}_H} \right) \tag{163}$$

For the given tail surface (tail rotor) fixed in the S (T) frame, downwash values $f_{DW_{TS}}$ ($f_{DW_{TR}}$) at different combinations of α_v, β_v, and $\|\vec{V}_v\|$ are calculated and stored in a table. These values are the downwash velocities in the $\hat{z}_S$ ($\hat{z}_T$) direction divided by C_T. This division of the downwash velocities by C_T is based on equations (152) through (158), from which the proportionality of C_T to the downwash velocity can be deduced. For the tail rotor, the downwash vector is

$$\vec{d}_{TR} = C_T f_{DW_{TR}} \left(\alpha_v, \beta_v, \|\vec{V}_v\|\right) \hat{z}_T \tag{164}$$

and for each tail surface the downwash vector is

$$\vec{d}_{TS} = C_T f_{DW_{TS}} \left(\alpha_v, \beta_v, \|\vec{V}_v\|\right) \hat{z}_S \tag{165}$$

The f_{DW} functions are linearly interpolated from values tabulated from a given set of α_v, β_v, and $\vec{V}_v$.

The points that make up the interpolation tables are selected in the following manner. The $\|\vec{V}_v\|$'s are chosen directly by selecting the number $n_{v_{DW}}$ and the particular values. The α_v's are chosen by selecting a set of points α_{PT} and defining $\alpha_v = \alpha_{PT} + \alpha_{v0}$; similarly, the β_v's are chosen by selecting a set of points β_{PT} and defining $\beta_v = \beta_{PT} + \beta_{v0}$. The quantities α_{v0} and β_{v0} are the orientation angles that center the wake on the given surface (i.e., when $\vec{V}_v$ is parallel to $\vec{r}_{hs}$). The points α_{PT} are chosen by setting the boundary angles $\alpha_{LO_{BND}} < \alpha_{LO} < -\Delta_{DW} < 0 < \Delta_{DW} < \alpha_{UP} < \alpha_{UP_{BND}}$, and the points β_{PT} are chosen by setting the boundary angles $\beta_{LO_{BND}} < \beta_{LO} < 0 < \beta_{UP} < \beta_{UP_{BND}}$. These boundary angles are defined for the condition in which the flat wake is centered on the given surface. For the α boundaries, the number of divisions in the end regions, $[\alpha_{LO_{BND}}, \alpha_{LO}]$ and $[\alpha_{UP}, \alpha_{UP_{BND}}]$, is selected through $n_{\alpha_{end}}$, and the number of divisions in the middle regions, $[\alpha_{LO}, -\Delta_{DW}]$ and $[\Delta_{DW}, \alpha_{UP}]$, is selected through $n_{\alpha_{mid}}$. The value Δ_{DW} is a small value and precludes evaluation of the downwash on the wake layer, where the vortex singularities are present. For the β boundaries, the number of divisions in the end regions, $[\beta_{LO_{BND}}, \beta_{LO}]$ and $[\beta_{UP}, \beta_{UP_{BND}}]$, is selected through $n_{\beta_{end}}$, and the number of divisions in the middle regions, $[\beta_{LO}, 0]$ and $[0, \beta_{UP}]$, is selected through $n_{\beta_{mid}}$.

Mass Matrix

The equations of motion are formed numerically, making the model described in this report implicit. Because of this, the system mass matrix is not readily available as it would be if the equations were derived explicitly. Allowing for different hinge sequences precludes the explicit calculation of the mass

matrix, since each of the many hinge sequences would require a separate calculation. To avoid this, the mass matrix is implicitly calculated with the condition that no acceleration-dependent applied forces, such as the apparent mass terms in blade-section aerodynamics, are present in the system. Such forces contribute to the mass matrix, making its extraction more difficult. It is well known from analytical dynamics that the form of the kinetic energy is

$$T_{kin} = T_2 + T_1 + T_0 = \frac{1}{2}\dot{\underline{q}}^T \left[M_{qq}(\underline{q},t)\right]\dot{\underline{q}} + C(\underline{q},t)^T\dot{\underline{q}} + r(\underline{q},t) \tag{166}$$

where $\left[M_{qq}\right]$ is the mass matrix of the system and $\underline{q}$ represents the system generalized coordinates. In the model presented,

$$\underline{q}^T = \left[\underbrace{\beta_1,\beta_2,\ldots,\beta_{n_b},\zeta_1,\zeta_2,\ldots,\zeta_{n_b},\phi_1,\phi_2,\ldots,\phi_{n_b}}_{\underline{r}^T},\underbrace{\theta_x,\theta_y,\theta_z,R_{m_x},R_{m_y},R_{m_z},\psi}_{\underline{f}^T}\right] \tag{167}$$

and the quadratic contribution T_2 to the kinetic energy is given by

$$T_2 = T_{2_{fuselage}} + T_{2_{rotor}} + \sum_{k=1}^{n_b}\left(T_{2_{blade}}\right)_k \tag{168}$$

For the fuselage, the velocity and angular rate are given by

$$\underline{\omega}_{F/I}^{(F)} = W_{F/I}\,\dot{\underline{\Theta}} = \overbrace{\left[\breve{\omega}_{F/I}\,\vdots\,0\right]}^{W_F}\left\{\begin{array}{c}\dot{\underline{\Theta}}\\ \dot{\underline{R}}\end{array}\right\} \tag{169}$$

$$\dot{\underline{r}}_{ic}^{(F)} = T_{FI}\dot{\underline{R}} + \breve{r}_{mc}^{(F)}\breve{\omega}_{F/I}\dot{\underline{\Theta}} = \underbrace{\left[\breve{r}_{mc}^{(F)}\omega_{F/I}\,\vdots\,T_{FI}\right]}_{R_F}\left\{\begin{array}{c}\dot{\underline{\Theta}}\\ \dot{\underline{R}}\end{array}\right\} \tag{170}$$

which is a re-expression of equation (22) using matrix notation instead of vector notation. The elements of the column matrix $\dot{\underline{R}}$ are the time-derivatives of the three translational degrees of freedom describing the motion of point m on the fuselage; the elements of $\dot{\underline{\Theta}}$ are the time-derivatives of the three Euler angles of the fuselage. For the coordinate system F defining the fuselage motion,

$$\breve{\omega}_{F/I} = \left[\begin{array}{ccc}1 & 0 & -S_{\theta_y}\\ 0 & C_{\theta_x} & S_{\theta_x}C_{\theta_y}\\ 0 & -S_{\theta_x} & C_{\theta_x}C_{\theta_y}\end{array}\right] \tag{171}$$

The velocity and angular rate give the T_2 contribution to the kinetic energy from the fuselage

$$T_{2fuselage} = \frac{1}{2}\left\{\begin{array}{c}\dot{\underline{\Theta}}\\ \dot{\underline{R}}\end{array}\right\}^T\left[M_F R_F^T R_F + W_F^T I_F W_F\right]\left\{\begin{array}{c}\dot{\underline{\Theta}}\\ \dot{\underline{R}}\end{array}\right\} \tag{172}$$

Likewise, for the rotor hub mass, the matrix representation of the velocity and angular rate is

$$\underline{\omega}_{R/I}^{(R)} = \underline{\omega}_{F/I}^{(R)} + \underline{\omega}_{H/F}^{(R)} + \underline{\omega}_{R/H} = T_{RF}\breve{\omega}_{F/I}\dot{\underline{\Theta}} + \breve{\omega}_{R/F}\dot{\psi} = \underbrace{\left[T_{RF}\breve{\omega}_{F/I} \vdots 0 \vdots \breve{\omega}_{R/F}\right]}_{W_R} \left\{ \begin{array}{c} \dot{\Theta} \\ \dot{\underline{R}} \\ \dot{\psi} \end{array} \right\} \quad (173)$$

$$\dot{\underline{r}}_{ih}^{(F)} = T_{F/I}\dot{\underline{R}} + \breve{r}_{mh}^{(F)}\breve{\omega}_{F/I}\dot{\underline{\Theta}} = \underbrace{\left[\breve{r}_{mh}^{(F)}\breve{\omega}_{F/I} \vdots T_{F/I} \vdots 0\right]}_{R_R} \left\{ \begin{array}{c} \dot{\Theta} \\ \dot{\underline{R}} \\ \dot{\psi} \end{array} \right\} \quad (174)$$

where

$$\underline{\omega}_{R/F} = \left[\begin{array}{c} 0 \\ 0 \\ 1 \end{array} \right] \dot{\psi} = \breve{\omega}_{R/F}\dot{\psi} \quad (175)$$

Equations (173) and (174) arise from equations (14), (18), and (63). As with the fuselage, the T_2 contribution to the kinetic energy from the rotor hub is

$$T_{2_{rotor}} = \frac{1}{2} \left\{ \begin{array}{c} \dot{\Theta} \\ \dot{\underline{R}} \\ \dot{\psi} \end{array} \right\}^T \left[M_R R_R^T R_R + W_R^T I_R W_R\right] \left[\begin{array}{c} \dot{\Theta} \\ \dot{\underline{R}} \\ \dot{\psi} \end{array} \right] \quad (176)$$

The same approach is used to find the kinetic energy for the kth blade. For the kth blade the angular rate is

$$\underline{\omega}_{B/I}^{(B)} = \underline{\omega}_{R/I}^{(B)} + \underline{\omega}_{L/R}^{(B)} + \underline{\omega}_{B/L} = T_{BF}\breve{\omega}_{F/I}\dot{\Theta} + T_{BR}\breve{\omega}_{R/F}\dot{\psi} + T_{BL}\breve{\omega}_{L/R}\dot{\underline{a}}_{L/R} + \breve{\omega}_{B/L}\dot{\underline{a}}_{B/L}$$

$$= \underbrace{\left[T_{BF}\breve{\omega}_{F/I} \vdots 0 \vdots T_{BR}\breve{\omega}_{R/F} \vdots T_{BL}\breve{\omega}_{L/R} \vdots \breve{\omega}_{B/L}\right]}_{W_{B_k}} \left\{ \begin{array}{c} \dot{\Theta} \\ \dot{\underline{R}} \\ \dot{\psi} \\ \dot{\underline{a}}_{L/R} \\ \dot{\underline{a}}_{B/L} \end{array} \right\} \quad (177)$$

and from equation (74) the velocity of the center of mass becomes

$$\begin{aligned} \dot{\underline{r}}_{ie}^{(R)} &= \dot{\underline{r}}_{ih}^{(R)} + \breve{\underline{r}}_{he}^{(R)}\underline{\omega}_{R/I} \\ \dot{\underline{r}}_{if}^{(L)} &= \dot{\underline{r}}_{ie}^{(L)} + \breve{\underline{r}}_{ef}^{(L)}\underline{\omega}_{L/I} \end{aligned} \quad (178)$$

$$\dot{\underline{r}}_{ib}^{(B)} = \dot{\underline{r}}_{if}^{(B)} + \breve{\underline{r}}_{fb}^{(B)}\underline{\omega}_{B/I} = \underbrace{\left[M_3\breve{\omega}_{F/I} \vdots T_{BI} \vdots M_2\breve{\omega}_{R/F} \vdots M_1\breve{\omega}_{L/R} \vdots \breve{r}_{fb}^{(B)}\breve{\omega}_{B/L}\right]}_{R_{B_k}} \left\{ \begin{array}{c} \dot{\Theta} \\ \dot{\underline{R}} \\ \dot{\psi} \\ \dot{\underline{a}}_{L/R} \\ \dot{\underline{a}}_{B/L} \end{array} \right\}$$

where

$$M_1 = T_{BL}\check{r}_{ef}^{(L)} + \check{r}_{fb}^{(B)}T_{BL}$$

$$M_2 = M_1 T_{LR} + T_{BR}\check{r}_{he}^{(R)}$$

$$M_3 = M_2 T_{RF} + T_{BF}\check{r}_{mh}^{(F)}$$

Since no particular hinge sequence has been stipulated, the $\underline{\dot{a}}_{L/R}$ and $\underline{\dot{a}}_{B/L}$ are generic, representing the generalized coordinates in the transformation indicated in the subscripts. For the flpt, fplt, and pflt hinge sequences, the terms are defined as

$$\underline{\omega}_{L/R} = \begin{bmatrix} S_{\zeta_P} \\ -C_{\zeta_P} \\ 0 \end{bmatrix} \dot{\beta}_k = \check{\omega}_{L/R}\underline{\dot{a}}_{L/R} \tag{179}$$

$$\underline{\omega}_{B/L} = \begin{bmatrix} 0 & 1 \\ S_{\theta_k+\phi_k} & 0 \\ C_{\theta_k+\phi_k} & 0 \end{bmatrix} \begin{Bmatrix} \dot{\zeta}_k \\ \dot{\phi}_k \end{Bmatrix} = \check{\omega}_{B/L}\underline{\dot{a}}_{B/R} \tag{180}$$

and for the lfpt, lpft, and plft hinge sequences, the terms are defined as

$$\underline{\omega}_{L/R} = \begin{bmatrix} 0 \\ 0 \\ 1 \end{bmatrix} \dot{\zeta}_k = \check{\omega}_{L/R}\underline{\dot{a}}_{L/R} \tag{181}$$

$$\underline{\omega}_{B/L} \begin{bmatrix} S_{\zeta_P} & 1 \\ C_{\theta_k+\phi_k C_{\zeta_P}} & 0 \\ S_{\theta_k+\phi_k C_{\zeta_P}} & 0 \end{bmatrix} \begin{Bmatrix} \dot{\beta}_k \\ \dot{\phi}_k \end{Bmatrix} = \check{\omega}_{L/R}\underline{\dot{a}}_{B/R} \tag{182}$$

Using the velocity and angular rate, the T_2 contribution to the kinetic energy from the kth blade becomes

$$\left(T_{2_{blade}}\right)_k = \frac{1}{2} \begin{Bmatrix} \dot{\Theta} \\ \dot{R} \\ \dot{\psi} \\ \underline{\dot{a}}_{L/R} \\ \underline{\dot{a}}_{B/L} \end{Bmatrix}^T \left[M_B R_{B_k}^T R_{B_k} + W_{B_k} I_B W_{B_k}\right] \begin{Bmatrix} \dot{\Theta} \\ \dot{R} \\ \dot{\psi} \\ \underline{\dot{a}}_{L/R} \\ \underline{\dot{a}}_{B/L} \end{Bmatrix} \tag{183}$$

For the inflow model, the mass matrix associated with the first-order states $\underline{x}^T = [\lambda_0, \lambda_{1s}, \lambda_{1c}]$ can be easily extracted using equation (119) and equations (123) through (125). The mass matrix for the inflow model is

$$M_{DI} = \frac{1}{\Omega} L_I M_I \begin{bmatrix} 1 & 0 & 0 \\ 0 & C_{\beta_h} & S_{\beta_h} \\ 0 & -S_{\beta_h} & C_{\beta_h} \end{bmatrix} \tag{184}$$

If there are no acceleration-dependent applied forces, the total mass matrix of the system can then be related to the equations of motion by

$$-\begin{bmatrix} M_{qq} & 0 \\ 0 & M_{DI} \end{bmatrix} \begin{Bmatrix} \ddot{q} \\ \dot{\underline{x}} \end{Bmatrix} + \underline{g} = \begin{Bmatrix} \underline{r}_{eq}\left(\ddot{q}, \dot{\underline{x}}, \dot{q}, \underline{x}, q\right) \\ \underline{f}_{eq}\left(\ddot{q}, \dot{\underline{x}}, \dot{q}, \underline{x}, q\right) \\ \underline{x}_{eq}\left(\ddot{q}, \dot{\underline{x}}, \dot{q}, \underline{x}, q\right) \end{Bmatrix} \tag{185}$$

The matrix M_{qq} is formed using the T_2 terms in equation (168), by adding the contributions of the corresponding fuselage, rotor hub, and blade elements. The equations included in $\underline{r}_{eq}$ are the rotor-blade equations, equations (55) through (57) or equations (58) through (60); the equations included in $\underline{f}_{eq}$ are the fuselage equations, equations (8) through (13) and equation (54). Finally, the equations included in $\underline{x}_{eq}$ are the inflow equations, equations (119). The reader will note that these equations have been cast such that they are identical to equations that would result from a Lagrangian formulation. Thus, the mass matrix calculation is compatible with the equations of motion and allows the relationships

$$-M_{qq} = \frac{\partial}{\partial \ddot{q}} \begin{bmatrix} \underline{r}_{eq} \\ \underline{f}_{eq} \end{bmatrix} \tag{186}$$

$$-M_{DI} = \frac{\partial}{\partial \dot{\underline{x}}} \left[\underline{x}_{eq}\right] \tag{187}$$

$$\underline{g} = \begin{Bmatrix} \underline{r}_{eq}\left(0, 0, \dot{q}, \underline{x}, q\right) \\ \underline{f}_{eq}\left(0, 0, \dot{q}, \underline{x}, q\right) \\ \underline{x}_{eq}\left(0, 0, \dot{q}, \underline{x}, q\right) \end{Bmatrix} \tag{188}$$

Multiblade Coordinate Transformation

For rotor systems with three or more blades, a multiblade coordinate transformation (MBCT) is available to transform the rotor rotating coordinates to nonrotating coordinates (ref. 7). For a set of rotating variables, each of which represents the same physical quantity for each blade,

$$\underline{x}_R^T = [x_1, x_2, x_3, \ldots] \tag{189}$$

The nonrotating representation for an even number of blades is

$$\underline{x}_N^T = [x_0, x_d, x_{1s}, x_{1c}, x_{2s}, \ldots] \tag{190}$$

The generic variable x_0 is the collective, while x_d is the differential, which is not present if the number of blades is odd. The x_{ns} terms are the nth sine variables, while the x_{nc} terms are the nth cosine variables. An example is the flap degree of freedom, for which $\underline{x}_R$ is a vector whose components are flapping angles. The transformation between variables is linear and time-varying, so the transformation from rotating to nonrotating systems is given by

$$\underline{x}_N = T_{NR}\underline{x}_R \tag{191}$$

$$\dot{\underline{x}}_N = T_{NR}\dot{\underline{x}}_R + \dot{T}_{NR}\underline{x}_R \tag{192}$$

$$\ddot{\underline{x}}_N = T_{NR}\ddot{\underline{x}}_R + 2\dot{T}_{NR}\dot{\underline{x}}_R + \ddot{T}_{NR}\underline{x}_R \tag{193}$$

and the transformation from nonrotating to rotating systems is

$$\underline{x}_R = T_{RN}\underline{x}_N \tag{194}$$

$$\dot{\underline{x}}_R = T_{RN}\dot{\underline{x}}_N + \dot{T}_{RN}\underline{x}_N \tag{195}$$

$$\ddot{\underline{x}}_R = T_{RN}\ddot{\underline{x}}_N + 2\dot{T}_{NR}\dot{\underline{x}}_N + \ddot{T}_{NR}\underline{x}_N \tag{196}$$

The form of the transformation matrix for models with an even number of blades is

$$T_{RN} = \begin{bmatrix} 1 & -1 & S_{\psi_1} & C_{\psi_1} & S_{2\psi_1} & C_{2\psi_1} & \cdots \\ 1 & 1 & S_{\psi_2} & C_{\psi_2} & S_{2\psi_2} & & \\ 1 & -1 & S_{\psi_3} & C_{\psi_3} & \ddots & & \\ 1 & 1 & S_{\psi_4} & & & & \\ \vdots & & & & & & \end{bmatrix} \tag{197}$$

and its inverse is given by

$$T_{RN}^{-1} = T_{NR} = \frac{1}{n_b}\begin{bmatrix} 1 & 1 & 1 & 1 & \cdots \\ -1 & 1 & -1 & 1 & \\ 2S_{\psi_1} & 2S_{\psi_2} & 2S_{\psi_3} & & \\ 2C_{\psi_1} & 2C_{\psi_2} & 2C_{\psi_3} & & \\ 2S_{2\psi_1} & 2S_{2\psi_2} & \ddots & & \\ 2C_{2\psi_1} & & & & \\ \vdots & & & & \end{bmatrix} \tag{198}$$

The ψ_k terms are the azimuth positions of the blades:

$$\psi_k = \psi_1 + (k-1)\frac{2\pi}{n_b} \qquad k = 1, 2, \ldots, n_b \tag{199}$$

These positions all have the same time derivatives. For models with odd numbers of blades, the second column of equation (197) and the second row of equation (198) are not present.

OPERATIONS

Basic Setup

A driving routine performs four basic operations on the helicopter mathematical model: initialization, trim, linearization, and integration (fig. 20). Initialization sets the basic data that define the helicopter configuration and conveys to the driving routine all the data necessary to operate on the model. The trim operation sets the helicopter configuration into some prescribed steady condition. A harmonic balance technique is used, which simultaneously balances the fuselage forces and moments and finds the rotor-blade equilibrium solution. Once the model is trimmed, two possibilities are available. One is linearization, in which a two-point difference formula is used to linearize the model about

the trim condition. The other possibility is time integration, which gives the system time response, initialized in trim condition, for given control inputs.

Each operation uses a subset of the model, whose general structure is shown in figure 21 and represented in equation form as follows:

$$\underline{F}(\mathrm{X}) = \begin{Bmatrix} \underline{r}_{eq} \\ \underline{f}_{eq} \\ \underline{x}_{eq} \end{Bmatrix} = -\left[M\left(\underline{r}, \underline{f}, \underline{x}, \underline{r}, \underline{f}, \underline{\theta}, \underline{u}\right)\right] \begin{bmatrix} \ddot{r} \\ \ddot{f} \\ \dot{x} \end{bmatrix} + \underline{G}\left(\underline{r}, \underline{f}, \underline{x}, \underline{r}, \underline{f}, \underline{\theta}, \underline{u}\right) = 0 \tag{200}$$

$$\underline{Y} = \begin{Bmatrix} \underline{w} \\ \underline{y} \\ \mathrm{X} \end{Bmatrix} \tag{201}$$

$$\mathrm{X}^T = \left[\underline{\ddot{r}}^T, \underline{\ddot{f}}^T, \underline{\dot{x}}^T, \underline{r}^T, \underline{f}^T, \underline{x}^T, \underline{r}^T, \underline{f}^T, \underline{\theta}^T, \underline{u}^T\right] \tag{202}$$

Variables and controls are represented in a single vector $\underline{X}$, which acts as the input to the model, whereas the equations and measured quantities are represented in a single vector $\underline{F}_{eq}^T = [\underline{F}^T \underline{Y}^T]$, which acts as the output. Both the inputs and the outputs can be categorized into three types: rotor-blade, fixed, and augmented. The rotor-blade inputs/outputs are items associated with the rotating coordinate system, such as the flap degrees of freedom or the blade pitch; the fixed inputs/outputs are items associated with the nonrotating system, such as fuselage degrees of freedom or fuselage acceleration measurements. The augmented inputs/outputs are associated with any additional first-order equations necessary to complete the model. The structure in figure 21 allows the use of rotating or nonrotating inputs and outputs. The variables are transformed by the multiblade coordinate transformation; the choice of the coordinate system depends on the particular operation. This basic setup is general and the operations can work on any model set up in this manner.

For the model described in the Helicopter Equations of Motion section, the rotor-blade degrees of freedom in the rotating system are

$$\underline{r}^T = [\beta_1, \beta_2, \ldots, \zeta_1, \zeta_2, \ldots, \phi_1, \phi_2, \ldots] \tag{203}$$

When using nonrotating coordinates, the vector $\underline{r}$ is defined according to equation (190) for each degree of freedom. For a model with an even number of blades the rotor degrees of freedom in the nonrotating system are

$$\underline{r}^T = [\beta_0, \beta_d, \beta_{1s}, \beta_{1c}, \ldots, \zeta_0, \zeta_d, \zeta_{1s}, \zeta_{1c}, \ldots, \phi_0, \phi_d, \phi_{1s}, \phi_{1c}, \ldots] \tag{204}$$

For a model with an odd number of blades, the differential coordinates are not present. Using nonrotating coordinates for the input variables requires that the flag ISNROT = 1, which transforms the nonrotating coordinates to the rotating system via equations (194) through (196).

The rotor-blade controls in the rotating system are

$$\underline{\theta}^T = \left[\ddot{\theta}_1, \ddot{\theta}_2, \ldots, \dot{\theta}_1, \upsilon_2, \ldots, \theta_1, \theta_2, \ldots\right] \tag{205}$$

and as with the rotor-blade variables, the function of the flag IINROT is to transform $\underline{\theta}$ to the rotating system if these inputs are given in the nonrotating system. For a model with an even number of blades, the rotor-blade controls in the nonrotating system are

$$\underline{\theta}^T = \left[\ddot{\theta}_0, \ddot{\theta}_d, \ddot{\theta}_{1s}, \ddot{\theta}_{1c}, \ldots, \dot{\theta}_0, \dot{\theta}_d, \dot{\theta}_{1s}, \dot{\theta}_{1c}, \ldots, \theta_0, \theta_d, \theta_{1s}, \theta_{1c}, \ldots\right] \tag{206}$$

For a model with an odd number of blades, the differential coordinates are not present. The fixed variables are the fuselage degrees of freedom and the rotor azimuth angle

$$\underline{f}^T = \left[\theta_x, \theta_y, \theta_z, R_{m_x}, R_{m_y}, R_{m_z}, \psi\right] \tag{207}$$

and the augmented variables are the three dynamic inflow coefficients

$$\underline{x}^T = [\lambda_0, \lambda_{1s}, \lambda_{1c}] \tag{208}$$

The fixed controls $\underline{u}$ are

$$\underline{u}^T = \left[\theta_{0_{TR}}, T_q, v_{g_x}, v_{g_y}, v_{g_z}, i_{TS_1}, i_{TS_2}, \ldots, i_{TS_{n_s}}\right] \tag{209}$$

The center block of figure 21 is the model, described in the previous section, that calculates the helicopter equations of motion. The equations in $\underline{r}_{eq}$ are the rotor-blade equations, equations (55) through (57) or equations (58) through (60), and the equations in $\underline{f}_{eq}$ are the fuselage equations, equations (8) through (13) and equation (54). The equations in $\underline{x}_{eq}$ are the inflow equations, equations (119). The vector $\underline{y}$ is defined by equations (40) through (47), and $\underline{w}$ is defined by equation (105) and equations (107) through (112). The vector $\underline{w}$ is in the rotating frame but can be transformed to the nonrotating frame by using the flag IONROT.

Initialization

Initialization performs two basic functions, one of which is to set up any data not given in $\underline{X}$ that define the model. These data are the physical parameters defining the model that was previously described; they are summarized in table 3. The main-rotor downwash tables are either generated and stored in files or read in from previously generated files. The second function of initialization is to transfer basic system data to the driver so that subsequent operations can be carried out on the model. These data, summarized in table 4, are primarily size data of the full model. Included in the table are the current values of these data for the model described in the Helicopter Equations of Motion section of this report.

Trim

The trim operation places the helicopter in the desired flight configuration by using a harmonic balance technique that is described in reference 8, chapter 3. The method casts the helicopter equations in an algebraic form by defining the rotor-blade variables as a Fourier series. The coefficients of this series expansion, along with the fixed and augmented state variables and inputs, are adjusted to force the rotor-blade, fuselage, and augmented state equations to zero. The rotor-blade equations are also expressed as a Fourier series, so that forcing the rotor blade equations to zero means forcing the coefficients of this

series expansion to zero. It is assumed that the helicopter main rotor has a constant rotation rate $\dot{\psi} = \Omega$ and that the rotor-blade controls are expressed in the nonrotating frame (i.e., IINROT = 1). All blades are assumed identical, and information from only one blade, expressed in terms of rotating coordinates (i.e., ISNROT = 0), is needed in the trim. An IMSL nonlinear algebraic equation solver, ZSPOW, is used to find the solution to the following equation (ref. 17):

$$\underline{F}(\underline{V}) = \underline{0} \tag{210}$$

The vector of inputs, $\underline{V}$, is defined as

$$\underline{V} = \begin{Bmatrix} \underline{\ddot{f}}\left[i_{\ddot{f}}(n)\right] & n = 1,2,\ldots,n_{i_{\ddot{f}}} \\ \underline{\dot{f}}\left[i_{\dot{f}}(n)\right] & n = 1,2,\ldots,n_{i_{\dot{f}}} \\ \underline{f}\left[i_f(n)\right] & n = 1,2,\ldots,n_{i_f} \\ \underline{x}\left[i_1(n)\right] & n = 1,2,\ldots,n_{i_1} \\ \underline{\theta}\left\{K(n) + n_b\left[j_\theta(1) - 1\right]\right\} & n = 1,2,\ldots,n_K \\ \quad\vdots & \quad\vdots \\ \underline{\theta}\left\{K(n) + n_b\left[j_\theta(n_{j_\theta}) - 1\right]\right\} & n = 1,2,\ldots,n_K \\ \underline{u}\left[i_u(n)\right] & n = 1,2,\ldots,n_{i_u} \\ r_{co}\left[n, j_r(1)\right] & n = 1,2,\ldots,(2n_{h_{TRM}} + 1) \\ \quad\vdots & \quad\vdots \\ r_{co}\left[n, j_r(n_{j_r})\right] & n = 1,2,\ldots,(2n_{h_{TRM}} + 1) \end{Bmatrix} \tag{211}$$

which is composed of fixed, augmented, and rotor-blade inputs. (Matrices are stacked by columns when represented in column vectors.) The blade variables are represented as coefficients of the Fourier expansion,

$$\underline{r}\left[k + n_b(j-1)\right] = r_{co}(1,j) + \sum_{n=1}^{n_{h_{TRM}}} r_{co}(2n,j)\cos(n\psi_k) + r_{co}(2n+1,j)\sin(n\psi_k) \tag{212}$$

The variable k is the blade number, and j is the blade degree of freedom (e.g., $j = 2$ is the lead-lag; see eq. (203)). For the model of this report, the coefficients are represented in matrix form as

$$r_{co} = \begin{bmatrix} \beta_0 & \zeta_0 & \phi_0 \\ \beta_{1c} & \zeta_{1c} & \phi_{1c} \\ \beta_{1s} & \zeta_{1s} & \phi_{1s} \\ \beta_{2c} & \vdots & \vdots \\ \vdots & \ddots & \\ \beta_{n_{h_{TRM}}c} & & \\ \beta_{n_{h_{TRM}}s} & & \end{bmatrix} \tag{213}$$

The elements of $\underline{V}$ are adjusted by the equation solver after the user chooses determining indices. For example, the choice of $n_{i_f} = 2$ with $i_f(1) = 2$ and $i_f(2) = 3$ directs the solver to adjust angles θ_y and θ_z to find the trim. Given the information in $\underline{V}$, the input vector $\underline{X}$ can be formed and the model can be evaluated. The resulting equations can then be used to form $\underline{F}$, which is defined as

$$\underline{F}(\underline{V}) = \left\{ \begin{array}{ll} r_{fo}[n, j_r(1)] & n = 1, 2, \ldots, (2n_{h_{TRM}} + 1) \\ \vdots & \vdots \\ r_{fo}\left[n, j_r(n_{j_r})\right] & n = 1, 2, \ldots, (2n_{h_{TRM}} + 1) \\ \frac{\Omega}{2\pi} \int_0^{2\pi/\Omega} \underline{f}_{eq}\left[i_{feq}(n)\right] dt & n = 1, 2, \ldots, n_{feq} \\ \frac{\Omega}{2\pi} \int_0^{2\pi/\Omega} \underline{x}_{eq}\left[i_1(n)\right] w_1(n) dt & n = 1, 2, \ldots, n_{i_1} \end{array} \right\} \tag{214}$$

where

$$\begin{aligned} r_{fo}(1, j) &= \frac{\Omega}{2\pi} \int_0^{2\pi/\Omega} \underline{r}_{eq}\left[1 + n_b(j-1)\right] dt \\ r_{fo}(2, j) &= \frac{\Omega}{\pi} \int_0^{2\pi/\Omega} \underline{r}_{eq}\left[1 + n_b(j-1)\right] \cos(\Omega t) dt \\ r_{fo}(3, j) &= \frac{\Omega}{\pi} \int_0^{2\pi/\Omega} \underline{r}_{eq}\left[1 + n_b(j-1)\right] \sin(\Omega t) dt \\ &\vdots \qquad\qquad\qquad \vdots \\ r_{fo}(2n_{h_{TRM}}, j) &= \frac{\Omega}{\pi} \int_0^{2\pi/\Omega} \underline{r}_{eq}\left[1 + n_b(j-1)\right] \cos(n_{h_{TRM}} \Omega t) dt \\ r_{fo}(2n_{h_{TRM}} + 1, j) &= \frac{\Omega}{\pi} \int_0^{2\pi/\Omega} \underline{r}_{eq}\left[1 + n_b(j-1)\right] \sin(n_{h_{TRM}} \Omega t) dt \end{aligned} \tag{215}$$

These equation are the Fourier coefficients of the first blade equation, where

$$r_{eq}\left[k + n_b(j-1)\right] = r_{fo}(1, j) + \sum_{n=1}^{n_{h_{TRM}}} r_{fo}(2n, j) \cos(n\psi_k) + r_{fo}(2n+1, j) \sin(n\psi_k) \tag{216}$$

The choice of $n_{h_{TRM}}$ determines the number of rotor coefficients that are adjusted to force the same number of coefficients of the blade equations to zero. The fixed and augmented equations are averaged over one rotor revolution in equation (214) to zero only the constant harmonics of these equations. A summary of the inputs that control the trim procedure is shown in table 5. Indices and their number (in parentheses) are selected to choose the adjustable variables and the equations that are to be satisfied. If an adjustable variable is set to a value, the value acts as an initial condition to the solver. If the variable is not adjusted by the solver, it remains at the set value throughout the trim. An example of the use of this feature would be to trim the model at a constant climb rate.

Integration

The time response of the system shown in figure 22 to given inputs $\underline{u}_p$ can be obtained by numerical integration. Since it is difficult to generalize helicopter control/actuator models, these systems have

been broadly defined as first-order equations that can be defined by the user. The P block in figure 22 represents precompensation, and the A block is any actuator/mixer dynamics; feedback dynamics are represented in the C block and sensor dynamics are represented in the S block, which has the restriction that the output of S cannot explicitly depend on $\underline{u}_s$. The helicopter model is represented in block G with nonrotating rotor inputs (IINROT = 1) and rotating-blade degrees of freedom and outputs (ISNROT = 0, IONROT = 0). By default, P and A are identity feedthrough and C and S are zero, giving the response of the open-loop helicopter model G. Any subset of the model represented by equation (200) can be integrated, where the state of G is defined by

$$\underline{x}_G = \left\{ \begin{array}{ll} \dot{\underline{r}}\{n + n_b[j_{\dot{r}}(m) - 1]\} & n = 1,2,\ldots,n_b;\ m = 1,2,\ldots,n_{j_{\dot{r}}} \\ \dot{\underline{f}}\left[i_{\dot{f}}(m)\right] & m = 1,2,\ldots,n_{i_{\dot{f}}} \\ \underline{x}\left[i_1(m)\right] & m = 1,2,\ldots,n_{i_1} \\ \underline{r}\{n + n_b[j_r(m) - 1]\} & n = 1,2,\ldots,n_b;\ m = 1,2,\ldots,n_{j_r} \\ \underline{f}\left[i_f(n_i)\right] & m = 1,2,\ldots,n_{i_f} \end{array} \right\} \tag{217}$$

As in the the trim procedure, the selection of the variables and equations is done by choosing indices. If the rotor degree of freedom is not selected, a constant rotor rate is used, by default, in the integration of the model (i.e., $\dot{\psi} = \Omega$). The inputs are defined as

$$\underline{u}_G = \left\{ \begin{array}{ll} \underline{\theta}\{K(n) + n_b[j_\theta(m) - 1]\} & n = 1,2,\ldots,n_b;\ m = 1,2,\ldots,n_{j_\theta} \\ \underline{u}\left[i_u(m)\right] & m = 1,2,\ldots,n_{i_u} \end{array} \right\} \tag{218}$$

The feedback outputs are

$$\underline{y}_G = \left\{ \begin{array}{ll} \underline{w}\{n + n_b[j_w(m) - 1]\} & n = 1,2,\ldots,n_b;\ m = 1,2,\ldots,n_{i_w} \\ \underline{y}\left[i_y(m)\right] & m = 1,2,\ldots,n_{i_y} \\ \underline{\mathrm{X}}\left[i_{\mathrm{X}}(m)\right] & m = 1,2,\ldots,n_{\mathrm{X}} \end{array} \right\} \tag{219}$$

and the auxilary outputs are

$$\underline{z}_G = \left\{ \begin{array}{ll} \underline{w}\{n + n_b[j_{\tilde{w}}(m) - 1]\} & n = 1,2,\ldots,n_b;\ m = 1,2,\ldots,n_{i_{\tilde{w}}} \\ \underline{y}\left[i_{\tilde{y}}(m)\right] & m = 1,2,\ldots,n_{i_{\tilde{y}}} \\ \underline{\mathrm{X}}\left[i_{\tilde{\mathrm{X}}}(m)\right] & m = 1,2,\ldots,n_{\tilde{\mathrm{X}}} \end{array} \right\} \tag{220}$$

The equations integrated are

$$\underline{F}_G = \left\{ \begin{array}{ll} \underline{r}_{eq}\{n + n_b[j_{\dot{r}}(m) - 1]\} & n = 1,2,\ldots,n_b;\ m = 1,\ldots,n_{j_{\dot{r}}} \\ \underline{f}_{eq}\left[i_{\dot{f}}(m)\right] & m = 1,2,\ldots,n_{i_{\dot{f}}} \\ \underline{x}_{eq}\left[i_1(m)\right] & m = 1,2,\ldots,n_{i_1} \end{array} \right\} \tag{221}$$

From equation (200) the form of the subsystem that is integrated is

$$-M_G(\underline{x}_G, \underline{u}_G)\underline{\dot{d}}_G + \underline{G}_G(\underline{x}_G, \underline{u}_G) = \underline{F}_G(\underline{d}_G, \underline{x}_G, \underline{u}_G) \tag{222}$$

where

$$\underline{d}_G = \left\{ \begin{array}{ll} \underline{\ddot{x}}\{n + n_b[j_{\dot{x}}(m) - 1]\} & n = 1, 2, \ldots, n_b;\ m = 1, 2, \ldots, n_{j_{\dot{x}}} \\ \underline{\ddot{f}}\left[i_{\dot{f}}(m)\right] & m = 1, 2, \ldots, n_{i_{\dot{f}}} \\ \underline{\dot{x}}\left[i_1(m)\right] & m = 1, 2, \ldots, n_{i_1} \end{array} \right\} \tag{223}$$

Two methods are available for extracting the mass matrix M_G. One method uses equation (222) directly, in which it is clear that the jth column of M_G is $\underline{F}_G$, with $\underline{d}_G$ equal to zero except for the jth element set to unity, minus $\underline{F}_G(\underline{0}, \underline{x}_G, \underline{u}_G)$. If M_G is of dimension $n_{M_G} = n_b n_{j_{\dot{x}}} + n_{i_{\dot{f}}} + n_{i_1}$, one evaluation of the model is necessary to get $\underline{F}_G(\underline{0}, \underline{x}_G, \underline{u}_G)$, and n_{M_G} additional evaluations of the model are necessary to get M_G. This approach always works; however, it requires many evaluations of the model and thus is inefficient. The other method is to use the corresponding elements from the mass matrix, which is calculated in and passed from the model, to form the submatrix M_G. Once M_G is available, the equation

$$\underline{\dot{x}}_G = \left\{ \begin{array}{ll} M_G^{-1}(\underline{x}_G, \underline{u}_G)\, \underline{G}_G(\underline{x}_G, \underline{u}_G) & \\ \underline{\dot{x}}[n + n_b j_{\dot{x}}(m) - 1] & n = 1, 2, \ldots, n_b;\ m = 1, 2, \ldots, n_{j_{\dot{x}}} \\ \underline{\dot{f}}\left[i_{\dot{f}}(m)\right] & m = 1, 2, \ldots, n_{i_{\dot{f}}} \end{array} \right\} \tag{224}$$

can be found; this is the expected form of block G in figure 22.

If the helicopter model is trimmed, the inputs and outputs of G are available at the initial time. The initial state x_{G_0}, initial input u_{G_0}, and initial output y_{G_0} can be used to extract the initial conditions of the blocks A, C, P, and S (fig. 22) as follows. It is assumed that $\dot{x}_A = \dot{x}_C = \dot{x}_P = \dot{x}_S = 0$ and it is required that $n_{u_G} = n_{u_P}$, which gives an equal number of equations and unknowns. With these conditions, a nonlinear equation $\underline{f}(\underline{v}) = 0$ can be set up, where $\underline{f}$ and $\underline{v}$ are defined as in figure 23. The variables on the left-hand side of the figure are adjusted until the variables on the right-hand side are forced to zero. The values at which this occurs are the initial conditions of the system of figure 22. The solution is extracted with the modified Newton method used in the trim procedure.

With the initial conditions available, the entire system of figure 22 is integrated according to the flow diagram in figure 24. The S block is evaluated to get its output $\underline{y}_S$ using $\underline{u}_S^*$, which is not necessarily the the correct value at the given time. However, the output of S is specified to be independent of $\underline{u}_S$, so the output value is correct. With this input to block C, the values on the right-hand side of the figure can be evaluated from the given information on the left-hand side of the figure. With this setup, and the input $\underline{u}_P$ defined by the user, the integration is carried out using the predictor-corrector method in the subroutine DVERK from the IMSL package (ref. 17). A summary of the integration inputs is shown in table 6. As in the trim, the variables to be integrated are selected through indices. The input is $\underline{Up} = \underline{Up}_0 + \Delta\underline{Up}$, where $\underline{Up}_0$ is determined in the trim. The term $\Delta\underline{Up}$ is the input perturbation about this trim.

Linearization

After trim, it is also possible to linearize a subset of the helicopter model (e.g., block G of fig. 22) in the nonrotating system (ISNROT = 1, IINROT = 1, and IONROT = 1). Linearization is done about

the trim solution using the two-point finite-difference formula,

$$\frac{\partial \underline{f}}{\partial x_j} \simeq \frac{\underline{f}\left(x_j + \Delta x_j\right) - \underline{f}\left(x_j - \Delta x_j\right)}{2\Delta x_j} \tag{225}$$

The partial-derivative matrix of the helicopter model is defined in figure 25; the rows and columns are selected in the same way as in the integration process. For any given time, the partial-derivative matrix can be calculated and the linear system can be evaluated according to the following equation:

$$S(t) = \begin{bmatrix} \begin{bmatrix} M_G^{-1}P \\ \cdots\cdots \\ I \vdots 0 \end{bmatrix} & \begin{bmatrix} M_G^{-1}Q \\ \cdots\cdots \\ 0 \end{bmatrix} \\ \left[EM_G^{-1}P + R\right] & \left[EM_G^{-1}Q + U\right] \end{bmatrix} = \begin{bmatrix} A(t) & B(t) \\ C(t) & D(t) \end{bmatrix} \tag{226}$$

The harmonics of the linear model matrix can be found using

$$S_0 = \frac{\omega_f}{2\pi}\int_0^{2\pi/\omega_f} S(t)dt \tag{227}$$

$$S_{nc} = \frac{\omega_f}{\pi}\int_0^{2\pi/\omega_f} S(t)\cos(n\omega_f t)dt \tag{228}$$

$$S_{ns} = \frac{\omega_f}{\pi}\int_0^{2\pi/\omega_f} S(t)\sin(n\omega_f t)dt \tag{229}$$

These integrals are evaluated numerically using a Gaussian quadrature procedure. The periodic model matrix is then expressible as

$$S(t) = \begin{bmatrix} A_0 & B_0 \\ C_0 & D_0 \end{bmatrix} + \sum_{n=1}^{n_{HLIN}} \begin{bmatrix} A_{nc} & B_{nc} \\ C_{nc} & D_{nc} \end{bmatrix} \cos(n\omega_f t) + \begin{bmatrix} A_{ns} & B_{ns} \\ C_{ns} & D_{ns} \end{bmatrix} \sin(n\omega_f t) \tag{230}$$

Since nonrotating coordinates are used, the helicopter model matrix will be constant when the model is in hover. In forward flight, the model matrix has periodic coefficients, which become more important as the forward flight speed is increased. The fundamental frequency ω_f depends on the number of blades in the helicopter system. If n_b is odd then $\omega_f = n_b\Omega$, whereas if it is even, $\omega_f = \frac{n_b}{2}\Omega$. A summary of the linearization procedure inputs is given in table 7.

RESULTS

The model results are compared with other experimental and analytical results as a preliminary validation. The first comparison is with blade-equilibrium responses in trim, of a flap-lag-torsion rotor model used in reference 8. Unlike the model described in the present report, the equations in reference 8 were symbolically generated out to their final form. An omission in the reverse-flow region was

discovered in the model of reference 8: the model did not account for the sign change in x_{ab} in its aerodynamic formulation (see fig. 11). This error is introduced into the model described herein so the comparison would be valid. The parameters of the model, presented in table 8, are of a four-bladed, soft in-plane rotor with a lead-lag frequency of 0.7/rev. The rotor trim is calculated with six harmonics ($n_{h_{TRM}} = 6$) in each blade degree of freedom, and the fuselage mass is chosen to give a weight coefficient of 0.005. The flap, lag, and torsion equations are satisfied for the blade equilibrium while simultaneously satisfying the roll-moment, pitch-moment, x-force, and z-force equations. The trimmed blade-equilibrium response in flap, lag, and torsion is shown in figure 26. Three response curves are presented for each blade degree of freedom: (1) a curve from the model from reference 8, which has an erroneous reverse-flow formulation; (2) a curve from the model of the present report, which uses the same reverse-flow formulation as that used in reference 8; and (3) a curve from the model of the present report, which uses what is believed to be the correct interpretation of the aerodynamic formulation in the reverse-flow region. The two models with the incorrect reverse-flow interpretation show close agreement, which serves to verify the analysis. The alternative reverse-flow interpretation greatly affects the torsion response of the system, although its effect on the flap and lag responses is still very small.

The results from the linearized helicopter model are compared with experimental hover results from reference 9. The experimental setup consisted of a three-bladed rotor mounted on a mast that allowed pitch and roll motions. Each blade had metal plates with notches, which acted as concentrated hinge springs to closely simulate the flap-lag rigid-blade approximation. Torsion springs on the body mount of the experimental rotor were adjusted to simulate an air-resonance condition. The parameters necessary to model this system are given in table 9. Measurements were made of the damping and frequencies of the system modes, and it is to these data that a correlation is made. Figure 27 shows the modal frequencies and the lead-lag regressing damping plotted against the rotor rotation rate, with zero blade pitch. The simulated air-resonance condition occurs when the body roll-mode frequency nears that of the lead-lag regressing mode, which is near a rotor rotational rate of 700 rpm. Excellent correlation with the experimental data is seen in this condition. The body pitch and roll damping at zero blade pitch is shown in figure 28. Good correlation between experiment and theory is also seen here, although the model tends to overpredict the damping at the higher rotor rates. The lead-lag regressing damping at 9° blade pitch is shown in figure 29; again, the model does a good job of predicting the damping in the resonance condition. Detailed cross-plots of the lead-lag regressing damping with respect to the blade pitch are shown in figure 30. Good agreement is seen between experiment and theory, although the damping tends to fall short at high and negative blade-pitch angles at the higher rotor rates. Figure 31 shows cross-plots of the body damping at 650 rpm; good agreement in pitch is seen at positive blade-pitch angles. The body roll damping tends to be overpredicted, getting worse at higher blade-pitch angles.

The main-rotor wake model used to calculate the downwash on the empennage surfaces is tested by correlating it with experimental results from reference 5, page 77. A correlation is done in the reference and is also done in the present report by using the flat-wake model described in the Main Rotor Downwash subsection. Unlike the model used in reference 5, the model described herein assumes a circulation distribution. In reference 5, a blade-element approach is used to find the circulation distribution. The integral in equation (152) is evaluated by using a Gaussian quadrature integration method along with linearly interpolated values from the pretabulated functions. Figure 32 shows the vertical nondimensional downwash at various azimuths at $0.1R$ below the rotor. The experimental rotor,

with 10° blade twist, is immersed in edgewise flow at $C_T = 0.006$. Using the flat-wake model gives good correlation results; the asymmetry of the downwash at the 90° and 270° azimuth positions is captured.

With the rotor and downwash models validated, it is now possible to validate the full helicopter model. The model is configured to simulate a UH-60A helicopter in order to compare model responses with the flight-test data that are available in references 10 and 18. Reference 10 presents a validation of the real-time model presented in reference 11, which is also known as the GEN HEL model. Reference 18 presents a validation of an updated version of the GEN HEL model, which is referred to as the Ames GEN HEL model. In the model of the UH-60A used in this report, all automatic controls are off (SAS, PBA, etc.). The fuselage aerodynamic representation in the model was generated from curve-fitted equations of the static aerodynamic characteristics. The exact equations are given in reference 19, pages 2-3, and are used in place of the equivalent-drag-area fuselage aerodynamic model. The lag damper is modeled according to reference 11, page 5.1.10, and this representation is substituted for the spring/damper model. The control mixer is modeled according to reference 11, pages 5.5.14 to 5.5.17, without the servo models. The tail-rotor parameters are extracted from reference 20, where a detailed description of the UH-60A tail rotor is given. References 11 and 12 are used to extract other physical parameters of the helicopter. Table 10 summarizes of all of the inputs to the model. The data followed by a question mark are specified for each of the following correlations. From table 10 it can be seen that the model has a flap-and-lag main rotor and a six-degree-of-freedom fuselage at constant rpm. The dynamic inflow model is included, and the collective pitch, sine pitch, cosine pitch, and tail-rotor collective pitch act as the inputs to the helicopter model. No feedback outputs are selected, and accelerometer outputs are taken from the fuselage at the positions corresponding to those on the flight-test vehicle.

Trim results calculated with and without the effect of the main-rotor wake in straight and level flight are compared with experimental results in figure 33. The trim data were calculated at 25-knot increments with the horizontal tail surface at the following settings: 40° for 0, 25, and 50 knots; 11.3° for 75 knots; and 4° for 100, 125, and 150 knots. The vehicle was trimmed by satisfying all six fuselage force and moment equations, the flap and lag rotor equations, and the inflow equations (see table 10). Between 0 and 50 knots, the angle θ_z was fixed, while the angle θ_x was adjusted (i.e., $i_f = 1, 2$ in table 10). Between 50 and 150 knots, the angle θ_x was fixed, while the angle θ_z was adjusted (i.e., $i_f = 2, 3$ in table 10). The collective, longitudinal, lateral, and pedal inputs are presented in percent of total motion; the total motion is 10 in. for the stick inputs and 5.38 in. for the pedals. The model tends to deviate significantly from the experimental data above 120 knots, where aerodynamic effects such as dynamic stall and radial flow, which are not accounted for in this model, can become important. Below 120 knots, good correlation is seen and the results are similar to those presented in reference 18, p. 28. The lateral and longitudinal stick positions are predicted more accurately by the Ames GEN HEL model, but the pedal position is closer for the model described herein. Overall, the results from the Ames GEN HEL model are slightly better, probably because that model used tabular data for blade-section aerodynamics, as well as other refinements particular to the UH-60A configuration. The flat-wake model enhances correlation in all but the collective and lateral stick positions. The collective stick position is hardly changed, whereas the lateral stick position is degraded by 1/4 in. at 150 knots.

Flight test time-histories from reference 10 are compared with the responses of the UH-60A model, at 1 knot (figs. 34-37) and at 100 knots (figs. 38-41). Four sets of time-responses are presented at each

flight speed; they correspond to 1 in. adjustments to the collective, longitudinal, lateral, and pedal inputs. The inputs to the model are those from the flight data, referenced about the trim of the model. The trim values generated by the model are indicated by points c, e, a, and p, corresponding to the collective, longitudinal, lateral, and pedal inputs, respectively. The angular rates of the fuselage (roll, pitch, and yaw) and the accelerometer outputs from the fuselage (longitudinal, lateral, and vertical) are also presented for each case. The accelerometer position corresponds to the approximate center of gravity of the helicopter; the precise center-of-gravity location is given as POSFUS in table 10. Each plot has three curves: the test data, the model response, and the linearized model response. The test data are from reference 10 and the test numbers are identical to the numbers used in the reference. The model responses come from integration of the full nonlinear system, and the linearized model responses come from integration of the linearized model. The responses of the linearized model are added to the trim values to give the total responses presented. Since the helicopter is in straight and level flight, the angular rates are zero at trim, and the linearized responses are identical to the total responses. The accelerometer responses contain gravity effects, and the nonzero trim values of the accelerometers must be added to the linearized accelerometer outputs.

At 1 knot (figs. 34-37), the on-axis angular rates agree well with the test results. The off-axis responses of the model do not correlate as well, with the pitch axis being the most troublesome by diverging from the test data in tests 212, 203, and 209. However, this is no worse than the results from the GEN HEL model, which is refined specifically to the UH-60A configuration and includes an engine model with a rotor rpm degree of freedom and actuator dynamics. At 100 knots (figs. 38-41) the on-axis responses have fair agreement with experimental results, and again, these results are consistent with results from the GEN HEL model. Other tests were run at 60 knots and 140 knots, and the results show a strong similarity to the results from the GEN HEL model. Another source for comparison is reference 16, in which the results of a linearized model are compared with the same flight data. The results from reference 16 are also similar to results obtained with the model of this report. Taking all these results together, it is concluded that the present model gives results that are consistent with those obtained from the GEN HEL program and the linearized model of reference 16.

A final comparison is made of the linearized model with the eight-state quasi-static model generated from the Ames GEN HEL program. The linearized GEN HEL model is generated with $\Omega = 27$ rad/sec, $ST_m = ST_c = ST_a = 29.583$ ft, $WL_m = WL_c = WL_a = 20.683$ ft, $M_F = 492.13$ slugs, $i_{aero} = 0$, and $\sigma_y = [0, 0, 0]$ rad. The linearized model of this report is generated and arranged according to

$$\begin{Bmatrix} \dot{\underline{x}}_r \\ \dot{\underline{x}}_f \end{Bmatrix} = \begin{bmatrix} A_{rr} & A_{rf} \\ A_{fr} & A_{ff} \end{bmatrix} \begin{Bmatrix} \underline{x}_r \\ \underline{x}_f \end{Bmatrix} + \begin{bmatrix} B_r \\ B_f \end{bmatrix} \underline{u}_\delta \tag{231}$$

$$\underline{y} = \begin{bmatrix} C_r & C_f \end{bmatrix} \begin{pmatrix} \underline{x}_r \\ \underline{x}_f \end{pmatrix} + D\, \underline{u}_\delta \tag{232}$$

The vector $\underline{x}_r$ contains all rotor states and inflow states, and the vector $\underline{x}_f$ contains all fuselage states. The inputs are the longitudinal, collective, lateral, and pedal positions ($\underline{u}_\delta^T = [\delta_e, \delta_c, \delta_a, \delta_p]^T$). The outputs $\underline{y}$ are chosen to correspond to the states of the GEN HEL model ($\underline{y}^T = [u, w, q, \Delta\theta, v, p, \Delta\phi, r, \Delta\psi]$). For comparison with the GEN HEL model, the derivatives of the rotor and inflow states $\dot{x}_r$ are set to

zero, yielding

$$\dot{\underline{x}}_f = A_{red}\underline{x}_f + B_{red}\underline{u} \tag{233}$$

$$\underline{y} = C_{red}\underline{x}_f + D_{red}\underline{u} \tag{234}$$

$$A_{red} = A_{ff} - A_{fr}A_{rr}^{-1}A_{rf} \tag{235}$$

$$B_{red} = B_f - A_{fr}A_{rr}^{-1}B_r \tag{236}$$

$$C_{red} = C_f - C_rA_{rr}^{-1}A_{rf} \tag{237}$$

$$D_{red} = D - C_rA_{rr}^{-1}B_r \tag{238}$$

The state variables used to describe the fuselage motions are not precisely those used in the GEN HEL model; however, the information needed to make the transformation to the GEN HEL states is found in the equation

$$y = \begin{Bmatrix} u \\ w \\ q \\ \Delta\theta \\ v \\ p \\ \Delta\phi \\ r \\ \Delta\psi \end{Bmatrix} = [C_{red}] \begin{Bmatrix} \dot{\theta}_x \\ \dot{\theta}_y \\ \dot{\theta}_z \\ \dot{R}_{mx} \\ \dot{R}_{my} \\ \dot{R}_{mz} \\ \theta_x \\ \theta_y \\ \theta_z \end{Bmatrix} \tag{239}$$

The quantities u, v, and w are the velocities along the fuselage, and p, q, and r are the body angular rates. The quantities $\Delta\theta$, $\Delta\phi$, and $\Delta\psi$ are the pitch, roll, and yaw angular perturbations. With this choice of output quantities, it is clear that $D_{red} = 0$, and thus equation (239) holds. Equation (239) is then used to transform the model to the final form

$$\frac{d}{dt}\begin{Bmatrix} u \\ w \\ q \\ \Delta\theta \\ v \\ p \\ \Delta\phi \\ r \end{Bmatrix} = F\begin{Bmatrix} u \\ w \\ q \\ \Delta\theta \\ v \\ p \\ \Delta\phi \\ r \end{Bmatrix} + G\begin{Bmatrix} \delta_e \\ \delta_c \\ \delta_a \\ \delta_p \end{Bmatrix} \tag{240}$$

where $\Delta\psi$ has been removed from the system.

This operation was carried out on a linearized model at 1 knot; the resulting F and G matrices are presented in table 11 along with the system matrices from the Ames GEN HEL program. The

eigenvalues and normalized eigenvectors are shown in figure 42 for both models. The calculations are based on the F matrix represented in dimensions of feet, seconds and degrees so as to scale the angular rates to an order of magnitude comparable to the velocities. Real eigenvalues have real eigenvectors (figs. 42(d) and 42(e)); complex eigenvalues have complex eigenvectors composed of a real part and an imaginary part. The eigenvector corresponding to the complex conjugate of the eigenvalue is the complex conjugate of the eigenvector. The greatest difference between models arises in the higher frequency modes, shown in figures 42(a) and 42(b). The model of this report tends to introduce more coupling between roll and pitch than the Ames GEN HEL model. The mode in figure 42(c) is dominated by w and r in both models, although the content differs. In figures 42(d) and 42(e) the two modes are very close, although the damping is much higher in the model of this report. Differences in the damping and frequencies of the eigenvalues are also noted; they are likely caused by the different inflow models used in the two analyses. Selected Bode plots of the system are shown in figure 43. The δ_c/w plot shows good agreement and the δ_p/r gain agrees well with the Ames GEN HEL model. The 360° phase shift in the δ_p/r plot is due to a zero in the right half of the s-plane that is not unstable in the model of this report. The sharp peak in the δ_a/p plot is due to the light damping that is predicted by the Ames GEN HEL model.

The entire process is repeated at 100 knots, resulting in the F and G matrices given in table 12. The eigenvalues and eigenvectors are presented in figure 44; the eigenvectors agree more closely between models in this case than in the 1-knot case. The on-axis Bode plots of the 100-knot case are given in figure 45. The two models do not agree closely, but the general trends in the models are similar.

CONCLUDING REMARKS

A single-rotor helicopter mathematical model for the design of high-bandwidth flight control systems has been described. The flap, lag, and torsion rotor model allows the approximate modeling of hingeless rotor systems, and the various hinge sequences that are available allow the modeling of many different articulated rotors. Quasi-steady Greenberg aerodynamics are used in conjunction with the nonlinear Pitt/Peters dynamic inflow model to calculate the blade aerodynamic forces. An rpm degree of freedom of the main rotor is available, along with a six-degree-of-freedom rigid fuselage. The tail surfaces have main-rotor downwash effects that arise from the flat-wake simulation. Operations on the model include trim, linearization, and time-integration, which have been formulated so that they may be applied to any consistently cast rotorcraft mathematical model. This features allows for modification of the helicopter model without requiring significant changes in the operations. Preliminary validation of the model showed reasonable correlation with experimental and analytical results.

Further validation of the model is necessary. The higher order linearized models need to be compared to experimental results, and flap-lag-torsion experimental data are needed to validate the torsional effects of the rotor model. Also, additional work is necessary to extend the range of valid flight conditions, which are currently limited to low-speed, lightly loaded helicopter systems. The limiting factor is the blade-section aerodynamic model, which should be improved to account for dynamic stall, radial-flow effects, and compressibility effects. Finally, the linearization process is limited to the helicopter model itself. A useful additional operation would be the linearization of the remaining blocks of the system and the combination of these linearized blocks into a single set of system matrices.

REFERENCES

1. Chen, R. T. N.; and Hindson, W. S.: Influence of High Order Dynamics on Helicopter Flight Control System Bandwidth. J. Guidance, Control, and Dynamics, vol. 9, no. 2, Mar./Apr. 1986.

2. Curtiss, Howard C.: Modeling Effects of Blade Torsional Flexibility in Helicopter Stability and Control. Forum of the Amer. Hel. Soc., St. Louis, MO, May 1983.

3. Greenberg, J. M.: Airfoil in Sinusoidal Motion in a Pulsating Stream. NACA TN-1326, 1947.

4. Gaonkar, G. H.; and Peters, D. A.: Review of Dynamic Inflow Modeling for Rotorcraft Flight Dynamics. AIAA Paper 86-0845, 1986.

5. Baskin, V. E.; Vil'dgrube, L. S.; Vozhdayev, Ye. S.; and Maykapar, G. I.: Theory of the Lifting Airscrew. NASA TT-F 823, 1976.

6. Talbot, P. D.; Tinling, B. E.; Decker, W. A.; and Chen, R. T. N.: A Mathematical Model of a Single Main Rotor Helicopter for Piloted Simulation. NASA TM-84281, 1982.

7. Hohenemeser, K. H.; and Yin, S. K.: Some Applications of the Method of Multi-Blade Coordinates. J. Amer. Hel. Soc., vol. 17, no. 4, 1972, pp. 1-12.

8. Takahashi, M. D.: Active Control of Helicopter Aeromechanical and Aeroelastic Instabilities. Ph.D. Dissertation, Dept. of Mechanical, Aerospace, and Nuclear Engineering, UCLA, Los Angeles, CA, 1988.

9. Bousman, W. G.: An Experimental Investigation of the Effects of Aeroelastic Coupling on Aeromechanical Stability of a Hingeless Rotor Helicopter. J. Amer. Hel. Soc., vol., 26, no. 1, Jan. 1981, pp. 46-54.

10. Kaplita, T. T.: UH-60A Black Hawk Engineering Simulation Model Validation Transient Response Comparison Data. United Technologies/Sikorsky Aircraft, SER-70983, Contract No. NAS2-11570, June 1984.

11. Howlett, J. J.: UH-60A Black Hawk Engineering Simulation Program. Vol. I. Mathematical Model. NASA CR-166309, 1981.

12. Howlett, J. J.: UH-60A Black Hawk Engineering Simulation Program. Vol. II. Background Report. NASA CR-166310, 1981.

13. Bramwell, A. R. S.: Helicopter Dynamics. John Wiley and Sons, 1976.

14. Bisplinghoff, R. L.; Ashley, H.; and Halfman, R. L.: Aeroelasticity. Addison-Wesley Pub. Co., Inc., 1955, pp. 251-281.

15. Johnson, Wayne: Application of Unsteady Airfoil Theory to Rotary Wings. AIAA J. Aircraft, vol. 17, no. 4, Apr. 1980.

16. Zhao, X.; and Curtiss, H. C., Jr.: A Study of Helicopter Stability and Control Including Blade Dynamics. TR 1823T, Dept. of Mech. Engr., Princeton U., Princeton, NJ, Oct. 1988.

17. IMSL Library Reference Manual, 9th edition. IMSL Inc., Houston,TX, 1982.

18. Ballin, M. G.: Validation of a Real-Time Engineering Simulation of the UH-60A Helicopter. NASA TM-88360, 1987.

19. Hilbert, K. B.: A Mathematical Model of the UH-60 Helicopter. NASA TM-85890, 1984.

20. Gerdes, W. H.; Jackson, M. E.; and Beno, E. A.: Directional Control Developmental Experiences Associated with the UH-60A Utility Helicopter. U.S. Army Research and Technology Laboratories Report No. USAAVRADCOM-TR-82-D-26, May 1983.

Table 1. Rotation sequences of blade coordinate systems

	R to P	P to L	L to B
flpt	$\beta_p : -\hat{y}_R$ $\zeta_p : \hat{z}_{\beta_p}$	$\beta_k : -\hat{y}_P$ $\zeta_p : -\hat{z}_\beta$	$\zeta_k : \hat{z}_L$ $\theta_k + \phi_k : \hat{x}_\zeta$
fplt	$\beta_p : -\hat{y}_R$ $\zeta_p : \hat{z}_{\beta_p}$	$\beta_k : -\hat{y}_P$ $\zeta_p : -\hat{z}_\beta$ $\theta_k : \hat{x}_{\zeta_p}$	$\zeta_k : \hat{z}_L$ $\phi_k : \hat{x}_\zeta$
pflt	$\beta_p : -\hat{y}_R$ $\theta_k : \hat{x}_{\beta_p}$ $\zeta_p : \hat{z}_\theta$	$\beta_k : -\hat{y}_P$ $\zeta_p : -\hat{z}_\beta$	$\zeta_k : \hat{z}_L$ $\theta_k : \hat{x}_\zeta$
lftp	$\beta_p : -\hat{y}_R$	$\zeta_k + \zeta_p : \hat{z}_P$	$\beta_k : -\hat{y}_L$ $\zeta_p : -\hat{z}_\beta$ $\theta_k + \phi_k : \hat{x}_{\zeta_p}$
lpft	$\beta_p : -\hat{y}_R$	$\zeta_k : \hat{z}_P$ $\theta_k : \hat{x}_{\zeta_k}$ $\zeta_p : \hat{z}_\theta$	$\beta_k : -\hat{y}_L$ $\zeta_p : -\hat{z}_\beta$ $\phi_k : \hat{x}_{\zeta_p}$
plft	$\beta_p : -\hat{y}_P$ $\theta_k : \hat{x}_{\beta_p}$	$\zeta_k + \zeta_p : -\hat{z}_P$	$\beta_k : -\hat{y}_L$ $\zeta_p : -\hat{z}_\beta$ $\theta_k : \hat{x}_{\zeta_p}$

Table 2. Function odd/even properties

Function	Even/odd ($\tilde{x}_1, \tilde{y}_1, \tilde{z}_1$)	Equation number	Figure number
Δv_x	(E,O,E)	2.10	2.15
Δv_y	(O,E,E)	2.9	2.14
$\tilde{M}$	(O,E,O)	2.37	2.25
$\tilde{N}$	(O,E,E)	2.40	2.26
$\tilde{L}$	(O,O,O)	2.38	2.28
$\tilde{K}$	(O,O,E)	2.39	2.27

Table 3. Summary of helicopter properties

Symbol	Computer mnemonic	Description	Dimensions[a]
		Blade	
n_b	NB	Number of blades	[ND]
M_B	MB	Blade mass	[M]
R	R	Rotor radius	[L]
Ω	OMEG	Nominal rotor rate	[rad/T]
$[I_B]$	IB(3,3)	Blade inertia matrix	[M*L**2]
e, f	E,F	First and second hinge offsets	[L]
β_p, ζ_p	BETP,ZETP	Hinge offset angles	[rad],[rad]
x_b, y_b, z_b	XB,YB,ZB	Blade cg position components in B system	[L]
x_1, x_2	X1,X2	Aerodynamic forces integrated from x_1 to x_2 along $\hat{x}_B$	[L]
	MPT	Number of integration points for blade aerodynamics	[ND]
b	B	Blade section semi chord	[L]
x_A	XA	Blade section torsion axis distance behind 1/4 chord	[L]
$T_{wc} T_{wx}$	TWC,TWX	Blade linear twist constants; $\theta_T = T_{wc} + T_{wx} X_k$	[rad],[rad/L]
a	A	Blade section lift curve slope	[1/rad]
d_0, d_1, d_2	D0,D1,D2	Blade section drag function constants; $C_d = d_0 + d_1\alpha_z + d_2\alpha_z^2$	[ND],[1/rad],[1/rad**2]
m_0, m_1	M0,M1	Blade section moment function constants; $C_m = m_0 + m_1\alpha_z$	[ND]
K_x, K_y, K_z	KX,KY,KZ	Hinge spring constants	[M*L**2/rad*T**2]
C_x, C_y, C_z	CX,CY,CZ	Hinge damping constants	[M*L**2/rad*T]
i_{Aero}	IAERO	Apparent mass terms? (1 = yes, 0 = no)	[ND]
	IOPT1	Hinge sequence selection	[ND]
		1 - Flap-lag-torsion-pitch	
		2 - Flap-pitch-lag-torsion	
		3 - Pitch-flap-lag-torsion	
		4 - Lag-flap-torsion-pitch	
		5 - Lag-pitch-flap-torsion	
		6 - Pitch-lag-flap-torsion	
	IOPT2	Spring type selection	[ND]
		1 - Non-orthogonal (FLPT,FPLT,PFLT)	
		2 - Non-orthogonal (LFPT,LPFT,PLFT)	
		3 - Orthogonal (hingeless FLPT,PFLT)	
		4 - Orthogonal (hingeless LFPT,PLFT)	
		5 - Program EOM_SPRING_DAMP	

Table 3. Continued

Symbol	Computer mnemonic	Description	Dimensions[a]
		Rotor hub and fuselage	
θ_s, ϕ_s	THES,PHIS	Shaft tilt back, right	[rad]
h	H	Shaft length	[L]
ST_t, BL_t, WL_t	ST_T,BL_T,WL_T	Shaft tilt position	[L]
M_R	MR	Rotor hub mass	[M]
$[I_R]$	IR	Rotor hub inertia matrix	[M*L**2]
M_F	MF	Fuselage mass	[M]
$[I_F]$	IF	Fuselage inertia matrix	[M*L**2]
ST_m, BL_m, WL_m	ST_M,BL_M,WL_M	Translational DOF position m	[L]
ST_c, BL_c, WL_c	ST_C,BL_C,WL_C	Fuselage center of mass position c	[L]
ST_a, BL_a, WL_a	ST_A,BL_A,WL_A	Aerodynamic force position a	[L]
S_f	SF	Reference area of fuselage aerodynamic forces	[L**2]
$K_{f_x}, K_{f_y}, K_{f_z}$	KFX,KFY,KFZ	Mount spring constants	[M*L**2/rad*T**2]
$C_{f_x}, C_{f_y}, C_{f_z}$	CFX,CFY,CFZ	Mount damping constants	[M*L**2/rad*T]
$\theta_{x_0}, \theta_{y_0}, \theta_{z_0}$	THEX0,THEY0,THEZ0	Zero moment angles at mount	[rad]
F_x, F_y, F_z	FX,FY,FZ	Applied forces at mount	[M*L/T**2]

Table 3. Continued

Symbol	Computer mnemonic	Description	Dimensions[a]
		Tail rotor (TR)	
ρ_x, ρ_y	RHOX,RHOY	Orientation angles	[rad]
ST_r, BL_r, WL_r	ST_R,BL_R,WL_R	Position	[L]
$M_{B_{TR}}$	MBTR	Blade mass	[M]
Ω_{TR}	OMEGTR	Rotation rate	[rad/T]
$I_{b_{TR}}$	IBTR	Flap inertia about hinge offset	[M*L**2]
R_{TR}	RTR	Radius	[L]
$k_{1_{TR}}$	K1TR	Tangent of δ_3	[ND]
e_{TR}	EETR	Hinge offset	[L]
$x_{b_{TR}}$	XBTR	Center of mass from hinge offset	[L]
$K_{b_{TR}}$	KBTR	Flap spring constant	[M*L**2/rad*T**2]
$N_{b_{TR}}$	NBTR	Number of blades in TR	[ND]
a_{TR}	ATR	Lift curve slope	[1/rad]
b_{TR}	BTR	Semi-chord	[L]
$\theta_{t_{TR}}$	TTTR	Twist per unit length	[rad/L]
$C_{0_{TR}} C_{1_{TR}}$	C0TR,C1TR	Drag function constants; $\delta = C_{0_{TR}} + C_{1_{TR}} \left(\frac{6C_{T_{TR}}}{a_{TR}\sigma_{TR}} \right)^2$	[ND]
TR_{BRK}, TR_{LOSS}	TBRKTR,TLSSTR	Loss function constants	[ND]
	EPSTR	Solution accuracy of inflow and flap states	[ND]
	MAXTR	Maximum number of iterations of inflow and flap states	[ND]
	IOPT4	Main rotor downwash	
		1 - null	
		2 - null	
		3 - null	
		4 - Generate flat wake table for TR	
		5 - Read in flat wake table for TR	

Table 3. Continued

Symbol	Computer mnemonic	Description	Dimensions[a]
		Tail surface (TS)	
n_s	NS	Number of tail surfaces	[ND]
σ_x, σ_y	SIGXTS(5),SIGYTS(5)	Orientation angles	[rad]
ST_s, BL_s, WL_s	ST_S(5),BL_S(5),WL_S(5)	Position	[L]
S_{TS}	STS(5)	Reference area	[L**2]
$\alpha_{L_s}, \alpha_{L_1}, \alpha_{L_2}$	ALS(5),AL1(5),AL2(5)	CL angles	[rad]
$C_{L_s}, C_{L_1}, C_{L_2}$	CLS(5),CL1(5),CL2(5)	CL values at angles	[ND]
$\alpha_{D_1}, \alpha_{D_2}$, $\alpha_{D_3}, \alpha_{D_4}$	AD1(5),AD2(5), AD3(5),AD4(5)	CD angles	[rad]
$C_{D_0}, C_{D_1}, C_{D_2}$, $C_{D_3}, C_{D_4}, C_{D_5}$	CD0(5),CD1(5),CD2(5), CD3(5),CD4(5),CD5(5)	CD angles at angles	[ND]
$a_{0_{TS}}, b_{0_{TS}}$, a_{TS}, b_{TS}	A0TS(5),B0TS(5), ATS(5),BTS(5)	Dynamic pressure loss parameter angles	[rad]
C_{TS}	CTS(5)	Dynamic pressure loss factor	[ND]
	IOPT5(5)	Main-rotor downwash options 1 - null 2 - null 3 - null 4 - Generate flat wake table for TS 5 - Read in flat wake table for TS	
		Downwash (DW) table generation	
$\alpha_{LO_{BND}}, \alpha_{LO}$, $\alpha_{UP}, \alpha_{UP_{BND}}$	ALOBND,ALO, AUP,AUPBND	Relative alpha ranges	[rad]
$n_{\alpha_{mid}}, n_{\alpha_{end}}$	NAMID,NAEND	Number of divisions in mid/end region of alpha	
Δ_{DW}	DELDW	Nearest alpha to wake layer	[rad]
$\beta_{LO_{BND}}, \beta_{LO}$, $\beta_{UP}, \beta_{UP_{BND}}$	BLOBND,BLO, BUP,BUPBND	Relative beta ranges	[rad]
$n_{\beta_{mid}}, n_{\beta_{end}}$	NBMID,NBEND	Number of divisions in mid/end region of beta	
	MPTDW	Number integration points in DW calculation	
r_1, r_2	R1DW,R2DW	Integration limits in DW calculation	[L]
$V_v(n_{VEL})$	VELOPT(NVDW)	ND evaluation velocities of DW tables	

Table 3. Concluded

Symbol	Computer mnemonic	Description	Dimensions[a]
		Miscellaneous	
g	G	Gravity constant	[L/T**2]
a_{snd}	ASND	Speed of sound	[L/T]
ρ_A	RHO	Air density	[M/L**3]
$mass$	MASS	Collective inflow mass element selection flag	[ND]
		0 - M(1,1) = 128/75*PI	
		1 - M(1,1) = 8/3*PI	
M_{off}	MOFF	Decouple CL and CM from col inflow?	[ND]
		0 - Decouple CL,CM in Pitt model for uniform inflow	
		1 - Normal Pitt inflow model	
$n_{A_{fus}}$	NAFUS	Number of fuselage accelerometer measurements	
	POSFUS(6,3)	Fuselage accelerometer data, for the jth accelerometer	
		POSFUS(1,j) = ST_{y_j}	
		POSFUS(2,j) = BL_{y_j}	
		POSFUS(3,j) = WL_{y_j}	
		POSFUS(4,j) = f_{x_j}	
		POSFUS(5,j) = f_{y_j}	
		POSFUS(6,j) = f_{z_j}	
$n_{A_{BLD}}$	NABLD	Number of blade accelerometer measurements	
	POSBLD(6,3)	Blade accelerometer data, for the nth accelerometer	
		POSBLD(1,n) = ST_{w_n}	
		POSBLD(2,n) = BL_{w_n}	
		POSBLD(3,n) = WL_{w_n}	
		POSBLD(4,n) = b_{x_n}	
		POSBLD(5,n) = b_{y_n}	
		POSBLD(6,n) = b_{z_n}	

[a]ND = nondimensional, M = mass, L = length, rad = radians, T = time.

Table 4. Information passed to driver from model

Symbol	Computer mnemonic	Description	Value for model
		Information required by driver	
n_b	NB	Number of blades	NB
n_r	NR	Number of rotor blade DOF[a]	3
n_f	NF	Number of fixed DOF	7
n_l	NI	Number of augmented states	3
n_θ	NT	Number of rotor blade inputs	3
n_u	NU	Number of fixed inputs	9+NS
n_w	NW	Number of rotor outputs	NABLD+3
n_y	NY	Number of fixed outputs	NAFUS+3+3
w_f	WF	Rotor frequency	OMEG
	IP1_PSI	Position in $\underline{f}$ of first rotor DOF	7
	IP2_PSI	Position in $\underline{f}$ of second rotor DOF	0

[a]DOF = degrees of freedom.

Table 5. Summary of trim variables—namelist TRMDAT

Symbol	Computer mnemonic	Description
$j_r(n_{j_r})$	JR(NJR)	Rotor DOF indices and equation indices[a]
$i_{\bar{f}}(n_{i_{\bar{f}}})$	IDDF(NIDDF)	Second derivative fixed DOF indices
$i_{\dot{f}}(n_{i_{\dot{f}}})$	IDF(NIDF)	First derivative fixed DOF indices
$i_f(n_{i_f})$	IF(NIF)	Fixed DOF indices
$i_1(n_{i_1})$	II(NII)	First order variable indices and equation indices
$j_\theta(n_{j_\theta})$	JT(NJT)	Rotor control indices
$K(N_K)$	K(NK)	Rotor control indices
$i_u(n_{i_u})$	IU(NIU)	Fixed control indices
$i_{feq}(n_{feq})$	IFEQ(NFEQ)	Fixed equations indices
r_{co}	RCO (2*NHTRM+1,NR)	Fourier coefficients matrix of the blade DOF
$\bar{f}$	DDF (NF)	Second derivatives of fixed DOF array
$\dot{f}$	DF (NF)	First derivatives of fixed DOF array
f	F (NF)	Fixed DOF array
$\dot{x}$	DX (NI)	First derivative of first order augmented state array
x	X (NI)	First order augmented state array
θ	TH (NB,NT)	Rotor input matrix
U	U (NU)	Fixed input array
	MPTTRM	Number of points in gaussian quadriture integration of equation fourier coefficients
	NSGTRM	Significant figure accuracy of roots. See NSIG in IMSL subroutine ZSPOW
	IMXTRM	Max number of iteration. See ITMAX in IMSL subroutine ZSPOW
$n_{h_{TRM}}$	NHTRM	Number of harmonics in blade equilibrium solution
	NEVLPT	Blade equilibrium response data? (0 = no, 1 = yes)
	NEXT_TRM	1 - Linearization 2 - Integration

[a]DOF = degrees of freedom.

Table 6. Summary of integration variables—namelist INTDAT

Symbol	Computer mnemonic	Description
$j_{\dot{r}}(n_{j_r})$	JDR(NJDR)	First and second derivative rotor DOF indices and equation indices[a]
$j_r(n_{j_r})$	JR(NJR)	Rotor DOF indices
$i_{\dot{f}}(n_{i_f})$	IDF(NIDF)	First and second derivative fixed DOF indices and equation indices
$i_f(n_{i_f})$	IF(NIF)	Fixed DOF indices
$i_1(n_{i_1})$	II(NII)	First order variable indices and equation indices
$j_\theta(n_{j_\theta})$	JT(NJT)	Rotor control indices
$K(N_K)$	K(NK)	Rotor control indices
$i_u(n_{i_u})$	IU(NIU)	Fixed control indices
$j_w(n_{j_w})$	JW(NJW)	Feedback rotor output indices
$i_y(n_{i_y})$	IY(NIY)	Feedback fixed output indices
$i_X(n_{i_X})$	IX(NIX)	Feedback X output indices
$j_{\tilde{w}}(n_{j_{\tilde{w}}})$	JW_AUX(NJW_AUX)	Auxiliary rotor output indices
$i_{\tilde{y}}(n_{i_{\tilde{y}}})$	IY_AUX(NIY_AUX)	Auxiliary fixed output indices
$i_{\tilde{X}}(n_{i_{\tilde{X}}})$	IX_AUX(NIX_AUX)	Auxiliary X output indices
	NSGTRM,IMXTRM	Initial condition solver parameters. See NSIG and ITMAX in IMSL subroutine ZSPOW
	NPTINT	Number of evaluation point in integration time segment
$t_{f_{int}}$	TFINT	Final time of response
	TOLINT	Integration error control. See TOL in IMSL subroutine DVERK
$n_{x_A}, n_{x_C}, n_{x_P}, n_{x_S}$	NXA,NXC,NXP,NXS	Number of states in block A, C, P, and S
n_{u_C}, n_{u_A}	NUC,NUA	Number of inputs to block C and A
	IDUP	Read in $\Delta \underline{u}_p$? (0 = no, 1 = yes)
	INT_OPT	Use mass matrix from model subroutine in integration? (0 = no, 1 = yes)

[a]DOF = degrees of freedom.

Table 7. Summary of linearization variables—namelist LINDAT

Symbol	Computer mnemonic	Description
$j_{\dot{r}}(n_{j_r})$	JDR(NJDR)	First and second derivative rotor DOF indices and equation indices[a]
$j_r(n_{j_r})$	JR(NJR)	Rotor DOF indices
$i_{\dot{f}}(n_{i_f})$	IDF(NIDF)	First and second drivative fixed DOF indices and equation indices
$i_f(n_{i_f})$	IF(NIF)	Fixed DOF indices
$i_1(n_{i_1})$	II(NII)	First order variable indices and equation indices
$j_\theta(n_{j_\theta})$	JT(NJT)	Rotor control indices
$K(n_K)$	K(NK)	Rotor control indices
$i_u(n_{i_u})$	IU(NIU)	Fixed control indices
$j_w(n_{j_w})$	JW(NJW)	Feedback rotor output indices
$i_y(n_{i_y})$	IY(NIY)	Feedback fixed output indices
$i_X(n_{i_X})$	IX(NIX)	Feedback X output indices
$j_{\tilde{w}}(n_{j_{\tilde{w}}})$	JW_AUX(NJW_AUX)	Auxiliary rotor output indices
$i_{\tilde{y}}(n_{i_{\tilde{y}}})$	IY_AUX(NIY_AUX)	Auxiliary fixed output indices
$i_{\tilde{X}}(n_{i_{\tilde{X}}})$	IX_AUX(NIXAUX)	Auxiliary X output indices
$\Delta_{\dot{r}}$	DEL_DR(NJDR)	Finite difference delta for first derivative rotor DOF
Δ_r	DEL_R(NJR)	Finite difference delta for rotor DOF
$\Delta_{\dot{f}}$	DEL_DF(NIDF)	Finite difference delta for first derivative fixed DOF
Δ_f	DEL_F(NIF)	Finite difference delta for fixed DOF
Δ_x	DEL_X(NII)	Finite difference delta for augmented states
Δ_θ	DEL_T(NJT)	Finite difference delta for rotor blade inputs
Δ_u	DEL_U(NIU)	Finite difference delta for fixed inputs
Δ	DELTA	Finite difference delta for all. All other Δ inputs are ignored if this is greater than zero
	MPTLIN	Number of points in Gaussian quadrature integration of linear system coefficient matrices
$n_{h_{LIN}}$	NHLIN	Number of harmonics in periodic system linear coefficient matrices
	IOLWRT	Write out coefficient matrices in readable format? (0 = no, 1 = yes)

[a]DOF = degrees of freedom.

Table 8. Flap-lag-torsion rotor nondimensional data

Variable	Value	Variable	Value
Rotor		Trim	
n_b	4	$n_{H_{TRM}}$	6
mass	1	MPTTRM	30
I_B	$\begin{bmatrix} 0.0001 & 0 & 0 \\ 0 & 0.083333 & 0 \\ 0 & 0 & 0.083433 \end{bmatrix}$	n_{j_r}	3
M_{off}	1	$\dot{f}(4)$	μ
i_{Aero}	1	n_{i_f}	1
M_B	1	n_{i_1}	3
R	1	n_{j_θ}	1
Ω	1	n_K	3
x_b	0.5	n_{feq}	4
x_1	0	j_r	[1,2,3]
x_2	1	i_f	[2]
a	2π	i_1	[1,2,3]
ρ_A	4.8248	j_θ	[3]
d_0	0.01	K	[1,3,4]
K_x	0.0024	i_{feq}	[1,2,4,6]
K_y	0.088542		
K_z	0.16333		
M_f	38.1045		
h	0.2		
s_f	$\frac{\pi}{100}$		

Table 9. Flap-lag rotor/fuselage data

Variable	Value	Variable	Value
Rotor/fuselage		Trim	
n_b	3	$n_{H_{TRM}}$	2
M_b	0.209 kg	MPTTRM	30
R	0.811 m	n_{j_r}	2
Ω	? rad/sec	$j_r(4)$	0.01 m/sec
I_B	$\begin{bmatrix} 0 & 0 & 0 \\ 0 & 0.010069 & 0 \\ 0 & 0 & 0.010069 \end{bmatrix}$ kg m^2	n_{i_1}	3
mass	0	$\theta(1,3)$	θ_0 rad
M_{off}	1	n_{j_θ}	1
e	0.0851 m	n_K	2
g	9.81 m/sec^2	n_{feq}	2
i_{Aero}	1	j_r	[1,2]
x_b	0.186 m	i_1	[1,2,3]
x_2	0.726 m	j_θ	[3]
b	0.02095 m	K	[2,3]
MPT	10	i_{feq}	[1,2]
a	5.73 1/rad	Linearization	
ρ_A	1.2761 kg/m^3	$n_{H_{LIN}}$	0
T_{w^-}	0.02618 rad	MPTLIN	10
IOPT1	1	$n_{j_{\dot{r}}}$	2
d_0	0.0079	$j_{\dot{r}}$	[1,2]
IOPT2	3	n_{j_r}	2
K_y	6.691 kg m^2/rad sec^2	j_r	[1,2]
K_z	30.659 kg m^2/rad sec^2	n_{i_f}	2
C_y	0.003538 kg m^2/rad sec	i_f	[1,2]
C_z	0.007574 kg m^2/rad sec	n_{i_f}	2
K_{fx}	68.03 kg m^2/rad sec^2	i_f	[1,2]
K_{fy}	104.3 kg m^2/rad sec^2	n_{i_1}	3
C_{fx}	0.08117 kg m^2/rad sec	i_1	[1,2,3]
C_{fy}	0.4200 kg m^2/rad sec	$\Delta\dot{r}$	$[10^{-5}, 10^{-5}]$ rad/sec
I_F	$\begin{bmatrix} 0.183 & 0 & 0 \\ 0 & 0.633 & 0 \\ 0 & 0 & 0 \end{bmatrix}$ kg m^2	Δr	$[10^{-6}, 10^{-6}]$ rad
M_F	20.83 kg	$\Delta\dot{f}$	$[10^{-5}, 10^{-5}]$ rad/sec
h	0.241 m	Δf	$[10^{-6}, 10^{-6}]$ rad
		Δx	$[10^{-6}, 10^{-6}, 10^{-6}]$

Table 10. UH-60A configuration data

Variable	Value	Variable	Value
	UH-60A		
n_b	4	M_b	8.003 slug
R	26.83 ft	Ω	? rad/sec
x_b	10.833 ft	x_1	4.12 ft
x_2	24.78 ft	e	1.25 ft
a	5.73 1/rad	b	0.865 ft
d_0	0.01	d_2	1.2
T_{w_c}	0.043595 rad	T_{w_x}	−0.011258 rad/ft
g	32.1 ft/sec^2	ρ_A	0.002030 slug/ft^3
mass	0	M_{off}	1
MPT	10	i_{Aero}	?
IOPT1	4	IOPT2	5
I_B	$\begin{bmatrix} 0 & 0 & 0 \\ 0 & 573.42 & 0 \\ 0 & 0 & 573.42 \end{bmatrix}$ slug ft^2	M_F	? slug
ST_t	28.433 ft	S_f	1 ft^2
WL_t	26.250 ft	ST_m	? ft
θ_s	−0.05236 rad	WL_m	? ft
ST_c	? ft	I_F	[?] slug ft^2
WL_c	? ft	ST_a	? ft
MAXTR	40	WL_a	? ft
ρ_x	1.22173 rad	Ω_{TR}	124.62 rad/sec
R_{TR}	5.5 ft	$M_{B_{TR}}$	0.467 slug
EPSTR	0.1D−3	$C_{0_{TR}}$	0.01
b_{TR}	0.40625 ft	$K_{b_{TR}}$	−9920.8 slug ft^2/rad sec^2
$N_{b_{TR}}$	4	$k_{1_{TR}}$	0.7002
a_{TR}	5.73 1/rad	$\theta_{t_{TR}}$	−0.05458 rad/ft
ϵ_{TR}	1 ft	$x_{b_{TR}}$	2 ft
$I_{b_{TR}}$	3.0 slug ft^2	TR_{Brk}	0.8
WL_r	27.058 ft	TR_{LOSS}	0.7
ST_r	61.000 ft	IOPT4	1
σ_x	[0,0,−1.5708] rad	n_s	3
σ_y	[?,?,0] rad	ST_s	[58.367,58.367,57.917] ft
CL_s	[1.025,1.025,0.820]	BL_s	[−3.5,3.5,0] ft
CL_1	[0.75,0.75,0.890]	WL_s	[20.367,20.367,22.750] ft
CL_2	[0.85,0.85,0.800]	S_{TS}	[22.5,22.5,32.3] ft^2
α_{D_1}	[0.262,0.262,0.175] rad	IOPT5	[?,?,?]
α_{D_2}	[0.349,0.349,0.524] rad	$a_{0_{TS}}$	[0,0,0.08] rad
α_{D_3}	[0.524,0.524,0.698] rad	$b_{0_{TS}}$	[0.12,−0.12,0] rad
α_{D_4}	[1.047,1.047,1.047] rad	a_{TS}	[0.12,0.12,0.12] rad

Table 10. Continued

Variable	Value	Variable	Value
	UH-60A		
C_{D_0}	[0.01,0.01,0.02]	b_{TS}	[0.12,0.12,0.12] rad
C_{D_1}	[0.1875,0.1875,0.043]	C_{TS}	[0.5,0.5,0.5]
C_{D_2}	[0.3625,0.3625,0.360]	α_{L_s}	[0.262,0.262,0.349] rad
C_{D_3}	[0.4250,0.4250,0.580]	α_{L_1}	[0.524,0.524,0.436] rad
C_{D_4}	[0.9000,0.9000,0.875]	α_{L_2}	[0.786,0.786,0.698] rad
C_{D_5}	[1.200,1.200,1.100]	$\alpha_{LO_{BND}}$	−1.4 rad
α_{LO}	−0.4 rad	α_{UP}	0.4 rad
$\alpha_{UP_{BND}}$	1.4 rad	$\beta_{LO_{BND}}$	−1.4 rad
β_{LO}	−0.4 rad	β_{UP}	0.4 rad
$\beta_{UP_{BND}}$	1.4 rad	$n_{\alpha_{end}}$	3
$n_{\alpha_{mid}}$	8	$n_{\beta_{end}}$	3
$n_{\beta_{mid}}$	8	MPTDW	20
r_1	1.25 ft	r_2	26.83 ft
Δ_{DW}	0.08 rad	V_v	[20,60,100,140,180,220] ft/sec
$n_{v_{DW}}$	6	$n_{A_{fus}}$	3
POSFUS	$\begin{bmatrix} 32.417 & 32.417 & 32.417 \\ -2.5800 & -2.5800 & -2.5800 \\ 17.308 & 17.308 & 17.308 \\ 1 & 0 & 0 \\ 0 & 1 & 0 \\ 0 & 0 & 1 \end{bmatrix}$		
	Trim		
$n_{H_{TRM}}$	3	$f(4)$	groundspeed = ? ft/sec
i_r	[1,2]	n_{j_r}	2
i_f	[?,?]	n_{i_f}	2
i_1	[1,2,3]	n_{i_1}	3
j_θ	3	n_{j_θ}	3
K	[1,3,4]	n_K	3
i_u	[1,2]	n_{i_u}	2
i_{feq}	[1,2,3,4,5,6,7]	n_{feq}	7
	Linearization		
Δ	10^{-5}	MPTLIN	20
n_{j_r}	2	j_r	[1,2]
n_{j_r}	2	j_r	[1,2]
n_{i_f}	6	i_f	[1,2,3,4,5,6]
n_{i_f}	3	i_f	[1,2,3]
n_{i_1}	3	i_1	[1,2,3]
n_{j_θ}	1	j_θ	3
n_K	3	K	[1,3,4]
n_{i_u}	1	i_u	[1]
n_{i_y}	6	i_y	[1,2,3,7,8,9]

Table 10. Concluded

Variable	Value	Variable	Value
Integration			
t_{fint}	8	n_{u_A}	4
TOLINT	0.001	NPTINT	401
n_{j_r}	2	j_r	[1,2]
n_{j_r}	2	j_r	[1,2]
n_{i_f}	6	i_f	[1,2,3,4,5,6]
n_{i_f}	3	i_f	[1,2,3]
n_{i_1}	3	i_1	[1,2,3]
n_{j_θ}	1	j_θ	3
n_K	3	K	[1,3,4]
n_{i_u}	1	i_u	[1]
$n_{i_{\tilde{y}}}$	6	$i_{\tilde{y}}$	[1,2,3,7,8,9]

Table 11. System matrices from GEN HEL program and model of this report at 1 knot

	u(ft/sec)	w(ft/sec)	q(rad/sec)	$\Delta\theta$(rad)	v(ft/sec)	p(rad/sec)	$\Delta\phi$(rad)	r(rad/sec)
	−0.0211	0.0123	2.0151	−32.0656	−0.0132	−1.2081	−0.0365	−0.2816
	−0.0005	−0.2356	1.9317	−1.4828	−0.0005	−0.0977	1.6168	2.2755
	0.0038	0.0011	−0.9094	0.0000	0.0067	0.1532	0.0130	−0.0185
F_{model}	0.0000	0.0000	0.9987	0.0000	0.0000	0.0000	0.0000	0.0505
	0.0048	0.0000	−0.8659	0.0750	−0.0207	−0.2552	32.0278	−1.3799
	0.0368	0.0023	−1.6579	0.0000	−0.0312	−5.7728	0.0455	0.1431
	0.0000	0.0000	−0.0023	0.0000	0.0000	1.0000	0.0000	0.0462
	0.0006	0.0000	−0.1125	0.0000	0.0041	−0.0638	0.0010	−0.2238

	δe(in.)	δc(in.)	δa(in.)	δp(in.)
	−1.4993	0.5859	−0.0716	0.9537
	−0.0659	−6.4483	−0.0228	0.4332
	0.3483	−0.0377	0.0228	−0.0094
G_{model}	0.0000	0.0000	0.0000	0.0000
	−0.0374	0.1098	0.4170	−0.8778
	−0.0098	−0.2145	1.3989	−0.5988
	0.0000	0.0000	0.0000	0.0000
	0.0132	0.1090	0.0233	0.3998

	u(ft/sec)	w(ft/sec)	q(rad/sec)	$\Delta\theta$(rad)	v(ft/sec)	p(rad/sec)	$\Delta\phi$(rad)	r(rad/sec)
	−0.0006	0.0059	0.3396	−32.1130	0.0028	−1.0697	0.0000	−0.2459
	−0.0336	−0.1748	2.1064	−1.9851	−0.0028	−0.1569	1.6573	1.9794
	0.0066	0.0007	−0.5668	0.0000	0.0020	0.2193	0.0000	−0.0941
$F_{AMES\ GEN\ HEL}$	0.0000	0.0000	0.9987	0.0000	0.0000	0.0000	0.0000	0.0516
	−0.0034	−0.0009	−0.7403	0.1026	−0.0550	0.0830	32.0700	−1.1742
	0.0022	−0.0004	−1.5799	0.0000	−0.0432	−3.4710	0.0000	0.1147
	0.0000	0.0000	−0.0032	0.0000	0.0000	1.0000	0.0000	0.0618
	0.0020	−0.0015	−0.0899	0.0000	0.0037	−0.1745	0.0000	−0.3045

	δe(in.)	δc(in.)	δa(in.)	δp(in.)
	−1.5578	0.6415	−0.0747	1.0110
	−0.0824	−5.7034	0.0000	0.4423
	0.3730	−0.0426	0.0053	−0.0843
$G_{AMES\ GEN\ HEL}$	0.0000	0.0000	0.0000	0.0000
	−0.1064	0.1066	0.4950	−0.8769
	0.0595	−0.1700	1.4011	−0.4950
	0.0000	0.0000	0.0000	0.0000
	−0.0071	0.0950	0.0850	0.3894

Table 12. System matrices from GEN HEL program and model of this report at 100 knots

	u(ft/sec)	w(ft/sec)	q(rad/sec)	$\Delta\theta$(rad)	v(ft/sec)	p(rad/sec)	$\Delta\phi$(rad)	r(rad/sec)
	−0.0302	0.0286	−5.1818	−32.0649	0.0119	−0.9532	−0.0029	8.2478
	0.0049	−0.6470	169.4875	−1.5042	0.0075	−7.4070	−0.0112	1.8589
	−0.0004	−0.0008	−1.7096	0.0001	0.0132	0.1513	0.0016	−0.2108
F_{model}	0.0000	0.0000	1.0000	0.0000	0.0000	0.0000	0.0000	0.0000
	−0.0012	0.0037	−0.1804	0.0000	−0.1245	6.6971	32.0639	−166.8141
	−0.0017	0.0218	−1.2334	0.0000	−0.0386	−5.1197	−0.0002	0.5293
	0.0000	0.0000	0.0000	0.0000	0.0000	1.0000	0.0000	0.0469
	−0.0021	−0.0092	−0.1247	0.0000	0.0182	−0.0670	0.0000	−0.7404

	δe(in.)	δc(in.)	δa(in.)	δp(in.)
	−1.1791	0.4970	−0.0933	0.9139
	−4.5956	−7.3153	0.2426	3.3744
	0.4707	0.1184	0.0149	0.0364
G_{model}	0.0000	0.0000	0.0000	0.0000
	−0.1779	0.1072	0.4503	−1.3378
	0.2235	0.2176	1.3165	−1.0575
	0.0000	0.0000	0.0000	0.0000
	0.0141	0.0025	0.0245	0.6182

	u(ft/sec)	w(ft/sec)	q(rad/sec)	$\Delta\theta$(rad)	v(ft/sec)	p(rad/sec)	$\Delta\phi$(rad)	r(rad/sec)
	−0.0373	0.0492	−5.7918	−32.1430	0.0058	−0.1890	0.0000	0.6816
	0.0119	−0.6095	166.3600	−1.4053	−0.0113	−3.0689	0.0000	1.5562
	0.0002	−0.0022	−1.2337	0.0000	0.0164	0.2169	0.0000	−0.1516
$F_{AMES\ GEN\ HEL}$	0.0000	0.0000	1.0000	0.0000	0.0000	0.0000	0.0000	0.0000
	−0.0080	0.0009	−0.3770	0.0000	−0.1003	6.4911	32.1430	−167.0100
	−0.0067	0.0160	−1.0765	0.0000	−0.0378	−3.6998	0.0000	0.940
	0.0000	0.0060	1.0000	0.0000	0.0000	1.0000	0.0000	0.0437
	−0.0024	−0.0064	−0.1392	0.0000	0.0065	−0.3132	0.0000	−0.6739

	δe(in.)	δc(in.)	δa(in.)	δp(in.)
	−1.0684	0.5719	−0.1310	0.7649
	−4.7944	−6.8998	0.2911	3.4576
	0.4852	0.1303	−0.0014	−0.0994
$G_{AMES\ GEN\ HEL}$	0.0000	0.0000	0.0000	0.0000
	−0.1319	0.2227	0.4273	−1.1865
	0.1438	0.1778	1.3290	−0.7434
	0.0000	0.0000	0.0000	0.0000
	−0.0213	−0.0266	0.0908	0.4989

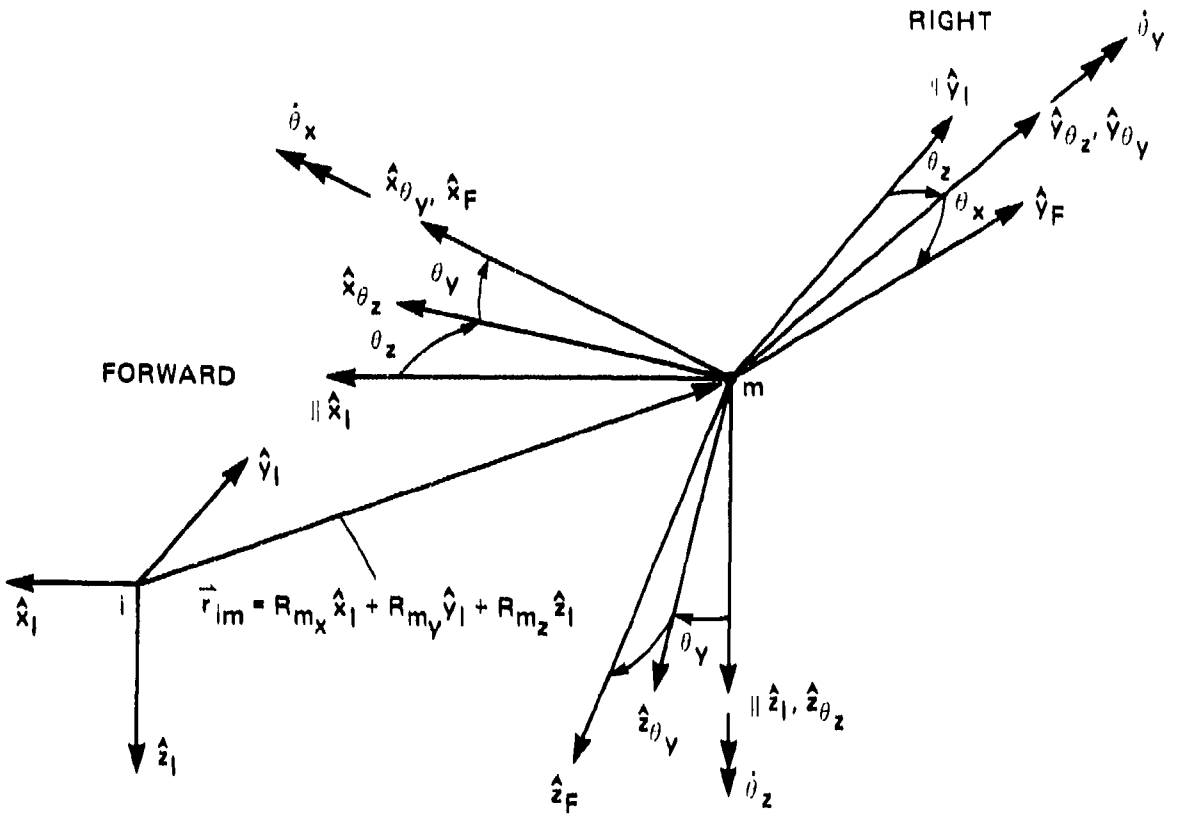

$$[T_{FI}] = \begin{bmatrix} C_{\theta_y}C_{\theta_z} & C_{\theta_y}S_{\theta_z} & -S_{\theta_y} \\ S_{\theta_x}S_{\theta_y}C_{\theta_z} - C_{\theta_x}S_{\theta_z} & S_{\theta_x}S_{\theta_y}S_{\theta_z} + C_{\theta_x}C_{\theta_z} & S_{\theta_x}C_{\theta_y} \\ C_{\theta_x}S_{\theta_y}C_{\theta_z} + S_{\theta_x}S_{\theta_z} & C_{\theta_x}S_{\theta_y}S_{\theta_z} - S_{\theta_x}C_{\theta_z} & C_{\theta_x}C_{\theta_y} \end{bmatrix}$$

$$\vec{\omega}_{F/I} = (\dot{\theta}_x - \dot{\theta}_z S_{\theta_y})\hat{x}_F + (\dot{\theta}_y C_{\theta_x} + \dot{\theta}_z S_{\theta_x} C_{\theta_y})\hat{y}_F + (\dot{\theta}_z C_{\theta_x} C_{\theta_y} - \dot{\theta}_y S_{\theta_x})\hat{z}_F$$

$$\vec{\omega}'_{F/I} = (\ddot{\theta}_x - \dot{\theta}_y\dot{\theta}_z C_{\theta_y} - \ddot{\theta}_z S_{\theta_y})\hat{x}_F$$
$$+(\ddot{\theta}_y C_{\theta_x} - \dot{\theta}_x\dot{\theta}_y S_{\theta_x} + \ddot{\theta}_z S_{\theta_x} C_{\theta_y} + \dot{\theta}_z\dot{\theta}_x C_{\theta_x} C_{\theta_y} - \dot{\theta}_z\dot{\theta}_y S_{\theta_x} S_{\theta_y})\hat{y}_F$$
$$+(\ddot{\theta}_z C_{\theta_x} C_{\theta_y} - \dot{\theta}_x\dot{\theta}_z S_{\theta_x} C_{\theta_y} - \dot{\theta}_z\dot{\theta}_y C_{\theta_x} S_{\theta_y} - \ddot{\theta}_y S_{\theta_x} - \dot{\theta}_y\dot{\theta}_x C_{\theta_x})\hat{z}_F$$

Figure 1. Fuselage-fixed coordinate frame (F).

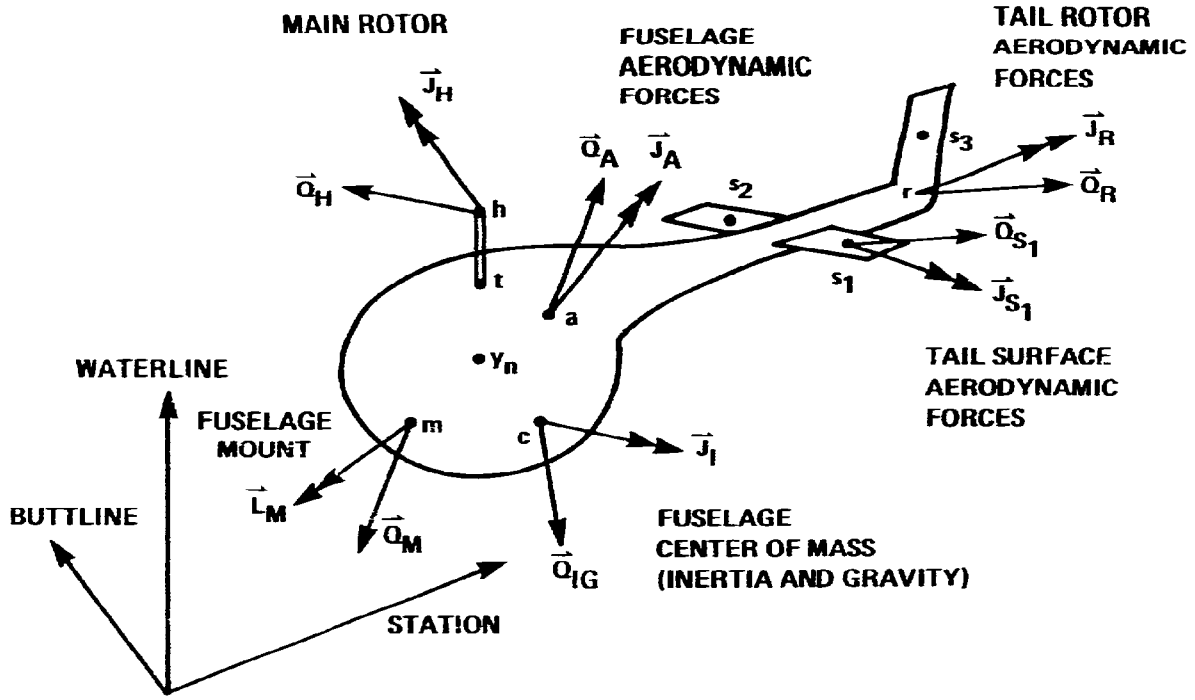

$$\vec{r}_{mt} = X_{mt}\hat{x}_F + Y_{mt}\hat{y}_F + Z_{mt}\hat{z}_F = -(ST_t - ST_m)\hat{x}_F + (BL_t - BL_m)\hat{y}_F - (WL_t - WL_m)\hat{z}_F$$

$$\vec{r}_{mc} = X_{mc}\hat{x}_F + Y_{mc}\hat{y}_F + Z_{mc}\hat{z}_F = -(ST_c - ST_m)\hat{x}_F + (BL_c - BL_m)\hat{y}_F - (WL_c - WL_m)\hat{z}_F$$

$$\vec{r}_{ma} = X_{ma}\hat{x}_F + Y_{ma}\hat{y}_F + Z_{ma}\hat{z}_F = -(ST_a - ST_m)\hat{x}_F + (BL_a - BL_m)\hat{y}_F - (WL_a - WL_m)\hat{z}_F$$

$$\vec{r}_{mr} = X_{mr}\hat{x}_F + Y_{mr}\hat{y}_F + Z_{mr}\hat{z}_F = -(ST_r - ST_m)\hat{x}_F + (BL_r - BL_m)\hat{y}_F - (WL_r - WL_m)\hat{z}_F$$

$$\vec{r}_{ms_j} = X_{ms_j}\hat{x}_F + Y_{ms_j}\hat{y}_F + Z_{ms_j}\hat{z}_F = -(ST_{s_j} - ST_m)\hat{x}_F + (BL_{s_j} - BL_m)\hat{y}_F - (WL_{s_j} - WL_m)\hat{z}_F$$
$$j = 1, 2, \ldots, n_s$$

$$\vec{r}_{th} = -h\hat{z}_H \text{ (see fig. 3)}$$

$$\vec{r}_{my_n} = X_{my_n}\hat{x}_F + Y_{my_n}\hat{y}_F + Z_{my_n}\hat{z}_F = -(ST_{y_n} - ST_m)\hat{x}_F + (BL_{y_n} - BL_m)\hat{y}_F - (WL_{y_n} - WL_m)\hat{z}_F$$
$$n = 1, 2, \ldots, n_{A_{fus}}$$

Figure 2. Free-body diagram of fuselage.

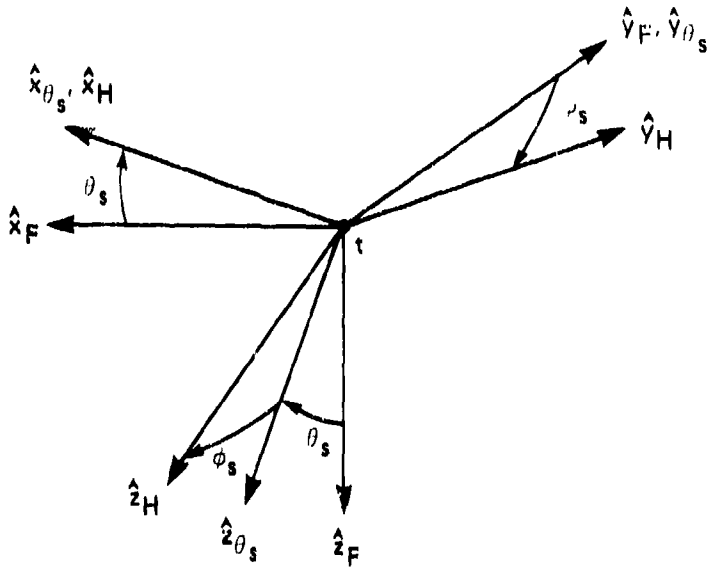

$$[T_{HF}] = \begin{bmatrix} C_{\theta_s} & 0 & -S_{\theta_s} \\ S_{\phi_s} S_{\theta_s} & C_{\phi_s} & S_{\phi_s} C_{\theta_s} \\ C_{\phi_s} S_{\theta_s} & -S_{\phi_s} & C_{\phi_s} C_{\theta_s} \end{bmatrix}$$

$$\vec{\omega}_{H/F} = 0$$

$$\dot{\vec{\omega}}_{H/F} = 0$$

Figure 3. Rotor-hub-axis coordinate frame (H) and its transformation from the F frame.

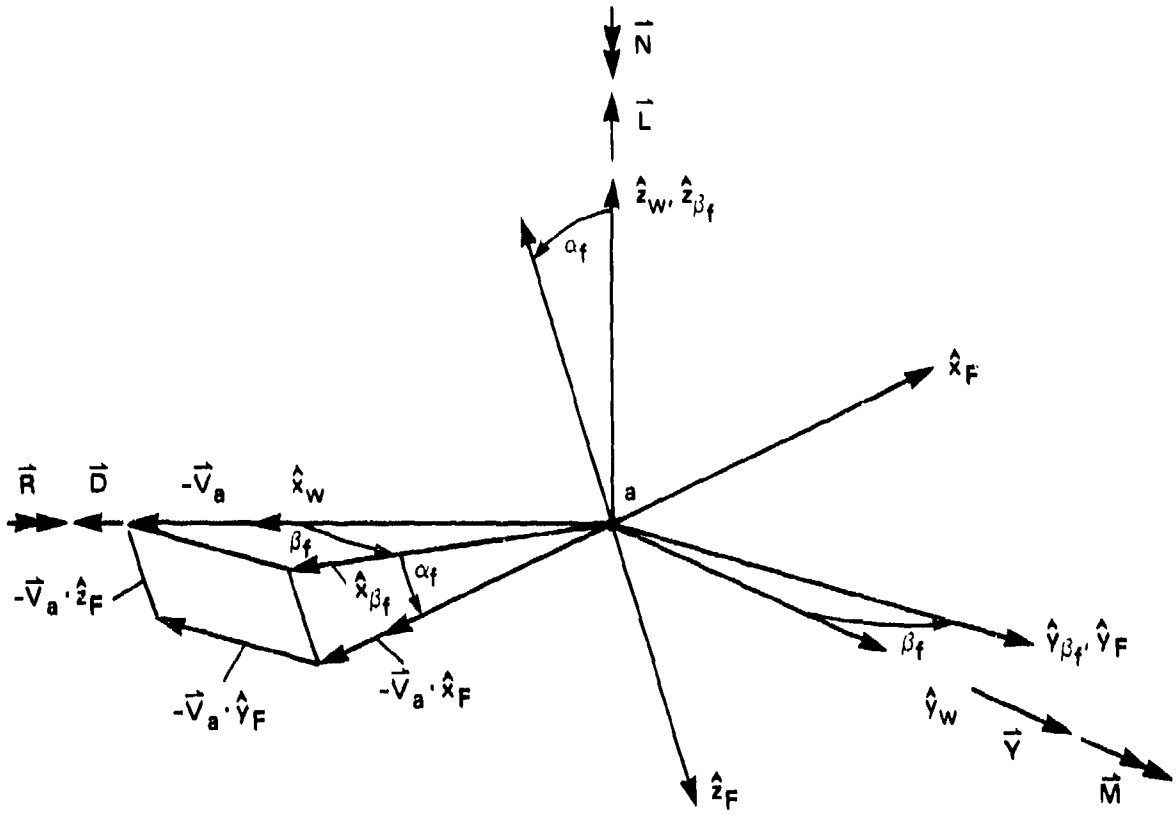

$\vec{V}_a$ = VELOCITY OF THE AIR RELATIVE TO POINT a

$$T_{FW} = \begin{bmatrix} -C_{\alpha_f} C_{\beta_f} & -C_{\alpha_f} S_{\beta_f} & S_{\alpha_f} \\ -S_{\beta_f} & C_{\beta_f} & 0 \\ -S_{\alpha_f} C_{\beta_f} & -S_{\alpha_f} S_{\beta_f} & -C_{\alpha_f} \end{bmatrix}$$

Figure 4. Fuselage wind-axis coordinate frame (W) and its transformation to the F frame.

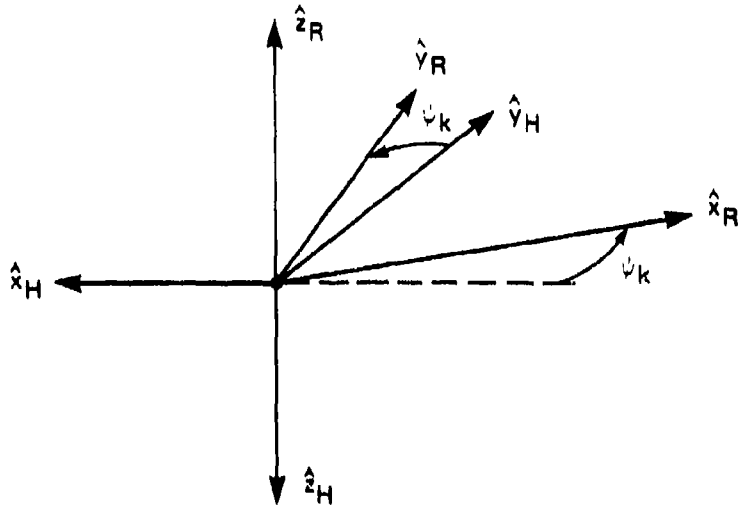

$$[T_{RH}] = \begin{bmatrix} -C_{\psi_k} & S_{\psi_k} & 0 \\ S_{\psi_k} & C_{\psi_k} & 0 \\ 0 & 0 & -1 \end{bmatrix}$$

$$\vec{\omega}_{R/H} = \dot{\psi}\,\hat{z}_R$$
$$\dot{\vec{\omega}}_{R/H} = \ddot{\psi}\,\hat{z}_R$$

Figure 5. Main-rotor coordinate frame (R) and its transformation from the H frame.

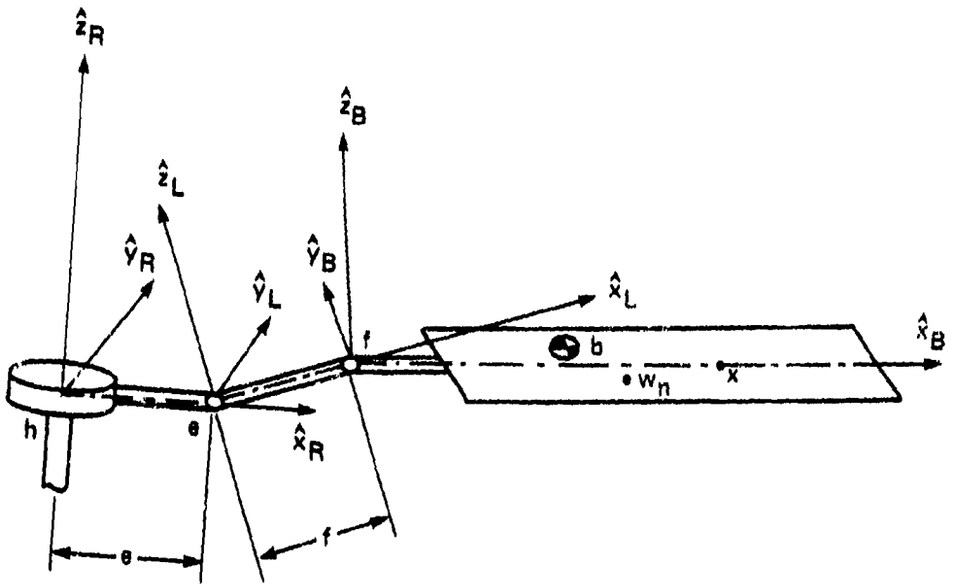

$$\vec{r}_{he} = e\,\hat{x}_R$$
$$\vec{r}_{ef} = f\,\hat{x}_L$$
$$\vec{r}_{fb} = x_b\,\hat{x}_B + y_b\,\hat{y}_B + z_b\,\hat{z}_B$$
$$\vec{r}_{fx} = x\,\hat{x}_B$$
$$\vec{r}_{fw_n} = x_{w_n}\,\hat{x}_B + y_{w_n}\,\hat{y}_B + z_{w_n}\,\hat{z}_B \quad n = 1, 2, \ldots n_{A_{bld}}$$

Figure 6. Main-rotor-blade coordinate frames.

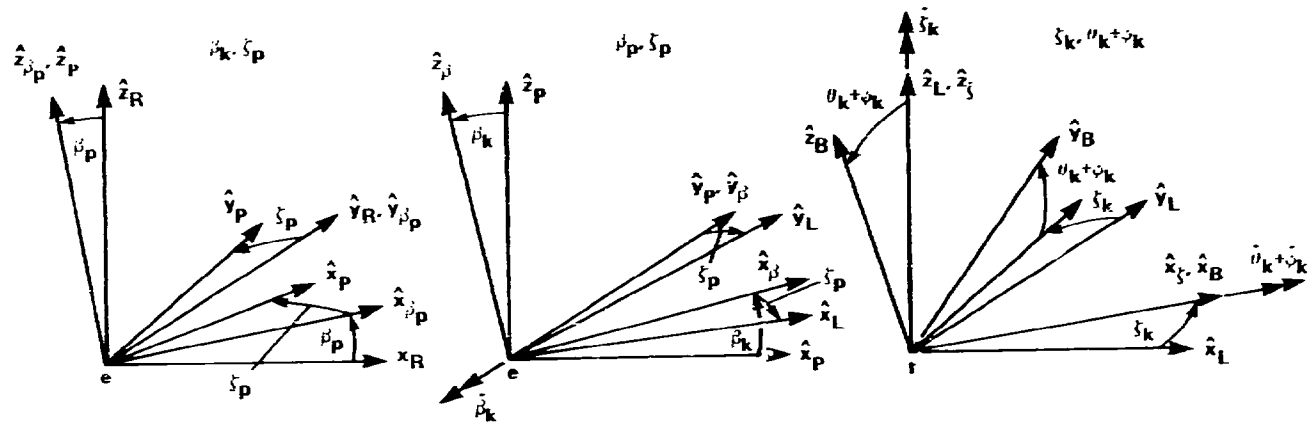

$$\begin{bmatrix} C_{\zeta_p}C_{\beta_p} & S_{\zeta_p} & C_{\zeta_p}S_{\beta_p} \\ -S_{\zeta_p}C_{\beta_p} & C_{\zeta_p} & -S_{\zeta_p}S_{\beta_p} \\ -S_{\beta_p} & 0 & C_{\beta_p} \end{bmatrix}_{T_{PR}} \begin{bmatrix} C_{\zeta_p}C_{\beta_k} & -S_{\zeta_p} & C_{\zeta_p}C_{\beta_k} \\ S_{\zeta_p}C_{\beta_k} & C_{\zeta_p} & S_{\zeta_p}S_{\beta_k} \\ -S_{\beta_k} & 0 & C_{\beta_k} \end{bmatrix}_{T_{LP}} \begin{bmatrix} C_{\zeta_k} & S_{\zeta_k} & 0 \\ -C_{\theta_k+\phi_k}S_{\zeta_k} & C_{\theta_k+\phi_k}C_{\zeta_k} & S_{\theta_k+\phi_k} \\ S_{\theta_k+\phi_k}S_{\zeta_k} & -S_{\theta_k+\phi_k}C_{\zeta_k} & C_{\theta_k+\phi_k} \end{bmatrix}_{T_{BL}}$$

$$\vec{\omega}_{P/R} = 0 \qquad \vec{\omega}_{L/P} = \dot{\beta}_k S_{\zeta_p}\hat{x}_L - \dot{\beta}_k C_{\zeta_p}\hat{y}_L \qquad \vec{\omega}_{B/L} = (\dot{\theta}_k + \dot{\phi}_k)\hat{x}_B + \dot{\zeta}_k S_{\theta_k+\phi_k}\hat{y}_B + \dot{\zeta}_k C_{\theta_k+\phi_k}\hat{z}_B$$

$$\vec{\omega}'_{P/R} = 0 \qquad \vec{\omega}'_{L/P} = \ddot{\beta}_k S_{\zeta_p}\hat{x}_L - \ddot{\beta}_k C_{\zeta_p}\hat{y}_L \qquad \vec{\omega}'_{B/L} = (\ddot{\theta}_k + \ddot{\phi}_k)\hat{x}_B + \left[\ddot{\zeta}_k S_{\theta_k+\phi_k} + \dot{\zeta}_k(\dot{\theta}_k + \dot{\phi}_k)C_{\theta_k+\phi_k}\right]\hat{y}_B + \left[\ddot{\zeta}_k C_{\theta_k+\phi_k} - \dot{\zeta}_k(\dot{\theta}_k + \dot{\phi}_k)S_{\theta_k+\phi_k}\right]\hat{z}_B$$

Figure 7. Flap-lag-pitch-torsion hinge sequence.

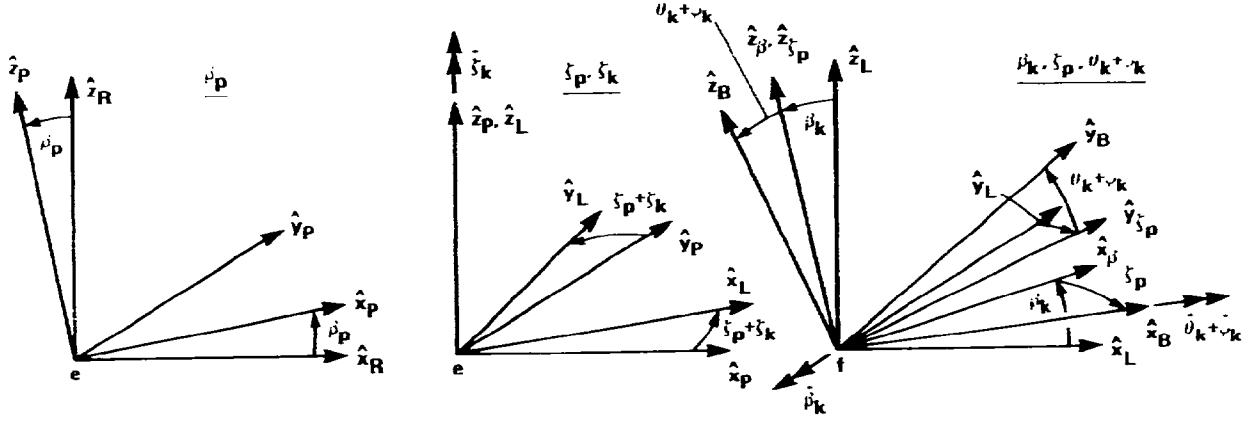

$$T_{PR} \qquad T_{LP} \qquad T_{BL}$$

$$\begin{bmatrix} C_{\beta_p} & 0 & S_{\beta_p} \\ 0 & 1 & 0 \\ -S_{\beta_p} & 0 & C_{\beta_p} \end{bmatrix} \begin{bmatrix} C_{\zeta_p+\zeta_k} & S_{\zeta_p+\zeta_k} & 0 \\ -S_{\zeta_p+\zeta_k} & C_{\zeta_p+\zeta_k} & 0 \\ 0 & 0 & 1 \end{bmatrix} \begin{bmatrix} C_{\zeta_p}C_{\beta_k} & -S_{\zeta_p} & C_{\zeta_p}S_{\beta_k} \\ C_{\theta_k+\phi_k}S_{\zeta_p}C_{\beta_k} - S_{\theta_k+\phi_k}S_{\beta_k} & C_{\theta_k+\phi_k}C_{\zeta_p} & C_{\theta_k+\phi_k}S_{\zeta_p}S_{\beta_k} + S_{\theta_k+\phi_k}C_{\beta_k} \\ -S_{\theta_k+\phi_k}S_{\zeta_p}C_{\beta_k} - C_{\theta_k+\phi_k}S_{\beta_k} & -S_{\theta_k+\phi_k}C_{\zeta_p} & -S_{\theta_k+\phi_k}S_{\zeta_p}S_{\beta_k} + C_{\theta_k+\phi_k}C_{\beta_k} \end{bmatrix}$$

$$\vec{\omega}_{P/R} = 0 \qquad \vec{\omega}_{L/P} = \dot{\zeta}_k \hat{z}_L \qquad \vec{\omega}_{B/L} = (\dot{\theta}_k + \dot{\phi}_k + \dot{\beta}_k S_{\zeta_p})\hat{x}_B - \dot{\beta}_k C_{\theta_k+\phi_k} C_{\zeta_p} \hat{y}_B + \dot{\beta}_k S_{\theta_k+\phi_k} C_{\zeta_p} \hat{z}_B$$

$$\vec{\omega}'_{P/R} = 0 \qquad \vec{\omega}'_{L/P} = \ddot{\zeta}_k \hat{z}_L \qquad \vec{\omega}'_{B/L} = (\ddot{\theta}_k + \ddot{\phi}_k + \ddot{\beta}_k S_{\zeta_p})\hat{x}_B + (-\ddot{\beta}_k C_{\theta_k+\phi_k} + \dot{\beta}_k(\dot{\theta}_k + \dot{\phi}_k) S_{\theta_k+\phi_k}) C_{\zeta_p} \hat{y}_B$$
$$+ (\ddot{\beta}_k S_{\theta_k+\phi_k} + \dot{\beta}_k(\dot{\theta}_k + \dot{\phi}_k) C_{\theta_k+\phi_k}) C_{\zeta_p} \hat{z}_B$$

Figure 8. Lag-flap-pitch-torsion hinge sequence.

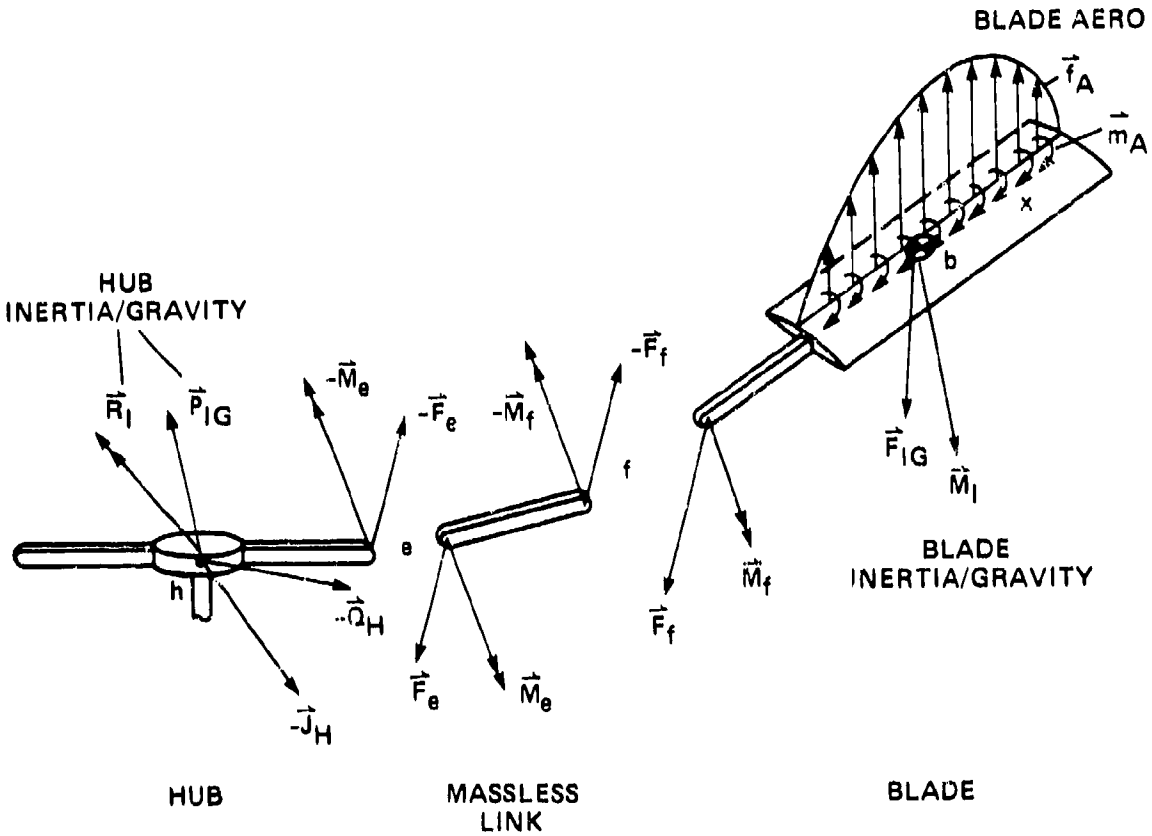

Figure 9. Main-rotor forces.

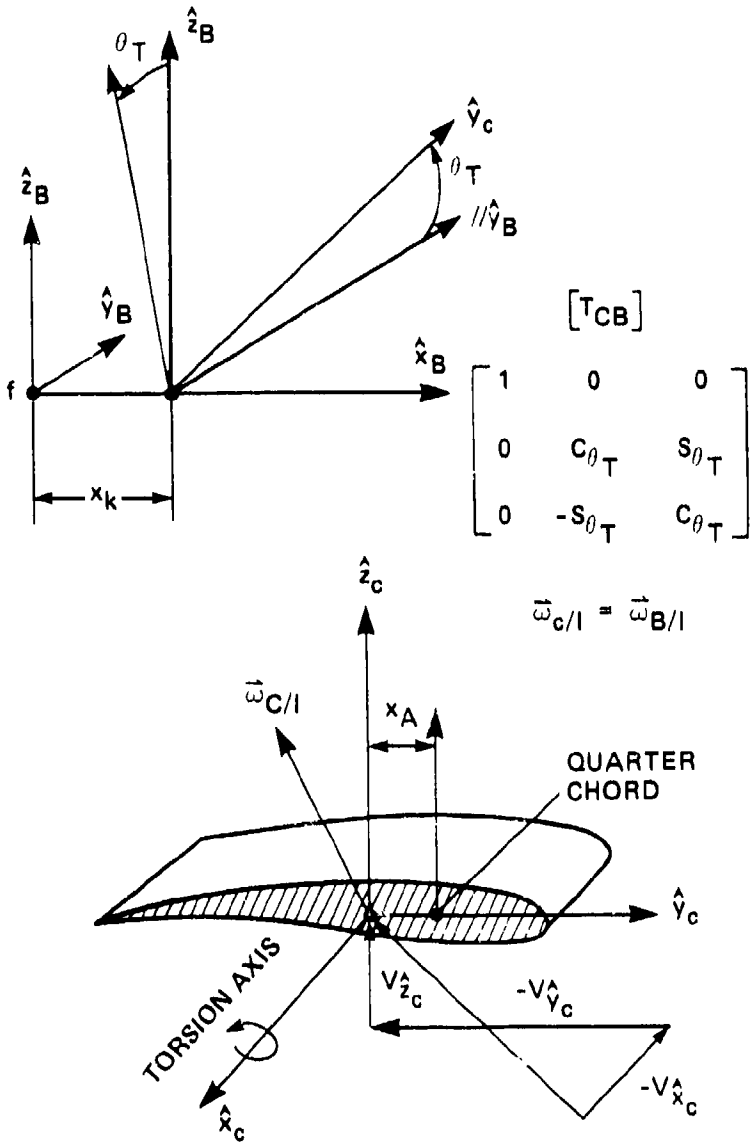

Figure 10. Blade-section chord coordinate frame (C).

FORWARD FLOW $V_{\hat{y}_c} < 0$	REVERSE FLOW $V_{\hat{y}_c} > 0$
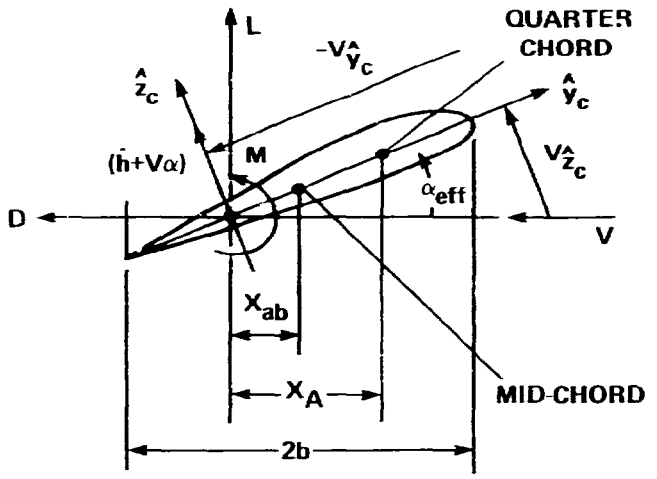	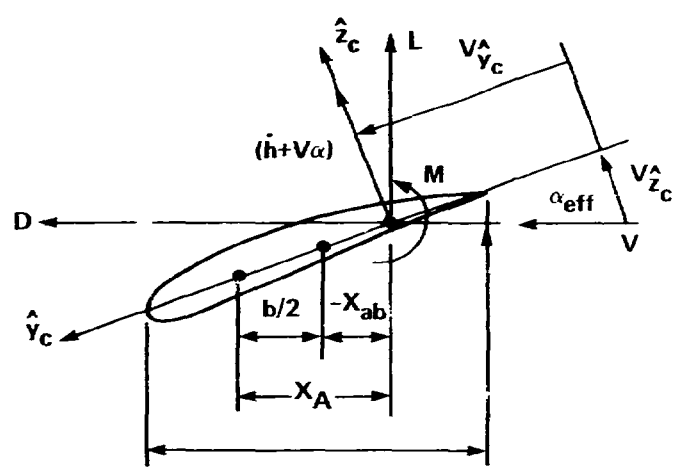
$\alpha_{eff} = \text{Tan}^{-1} \dfrac{V_{z_c}}{-V_{\hat{y}_c}}$	$\alpha_{eff} = \text{Tan}^{-1} \dfrac{V_{\hat{z}_c}}{V_{\hat{y}_c}}$
$\dot{\alpha} = \vec{\omega}_{C/I} \cdot \hat{x}_c$	$\dot{\alpha} = -\vec{\omega}_{C/I} \cdot \hat{x}_c$
$\ddot{\alpha} = \dot{\omega}_{C/I} \cdot \hat{x}_c$	$\ddot{\alpha} = -\dot{\omega}_{C/I} \cdot \hat{x}_c$
$V = \sqrt{V_{\hat{y}_c}^2 + V_{\hat{z}_c}^2}$	$V = \sqrt{V_{\hat{y}_c}^2 + V_{\hat{z}_c}^2}$
$(\dot{h}+V\alpha) = V_{\hat{z}_c}$	$(\dot{h}+V\alpha) = V_{\hat{z}_c}$
$X_{ab} = X_A - b/2$	$X_{ab} = b/2 - X_A$
$f_{\hat{y}_c} = \dfrac{L V_{\hat{z}_c} + D V_{\hat{y}_c}}{V}$	$f_{\hat{y}_c} = \dfrac{-L V_{\hat{z}_c} + D V_{\hat{y}_c}}{V}$
$f_{\hat{z}_c} = \dfrac{-L V_{\hat{y}_c} + D V_{\hat{z}_c}}{V}$	$f_{\hat{z}_c} = \dfrac{L V_{\hat{y}_c} + D V_{\hat{z}_c}}{V}$
$m_{\hat{x}_c} = M + M_{cam}$	$m_{\hat{x}_c} = -(M + M_{cam})$
$(\dot{h}+V\alpha)^{\cdot} = \dot{V}_{\hat{z}_c} = A_{\hat{z}_c} - (\omega_{C/I\,\hat{x}_c} V_{\hat{y}_c} - \omega_{C/I\,\hat{y}_c} V_{\hat{x}_c})$	$(\dot{h}+V\alpha)^{\cdot} = \dot{V}_{\hat{z}_c} = A_{\hat{z}_c} - (\omega_{I/C\,\hat{x}_c} V_{\hat{y}_c} - \omega_{C/I\,\hat{y}_c} V_{\hat{x}_c})$

Figure 11. Blade-section aerodynamics.

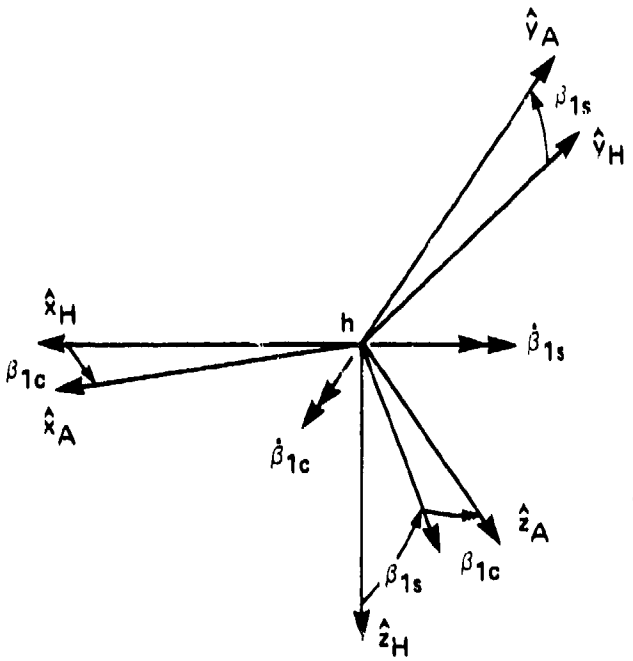

$$[T_{AH}]$$

$$\begin{bmatrix} C_{\beta_{1c}} & S_{\beta_{1s}} S_{\beta_{1c}} & S_{\beta_{1c}} C_{\beta_{1s}} \\ 0 & C_{\beta_{1s}} & -S_{\beta_{1s}} \\ -S_{\beta_{1c}} & S_{\beta_{1s}} C_{\beta_{1c}} & C_{\beta_{1s}} C_{\beta_{1c}} \end{bmatrix}$$

$$\vec{\omega}_{A/H} = -\dot{\beta}_{1s} C_{\beta_{1c}} \hat{X}_A - \dot{\beta}_{1c} \hat{Y}_A + \dot{\beta}_{1s} S_{\beta_{1c}} \hat{Z}_A$$

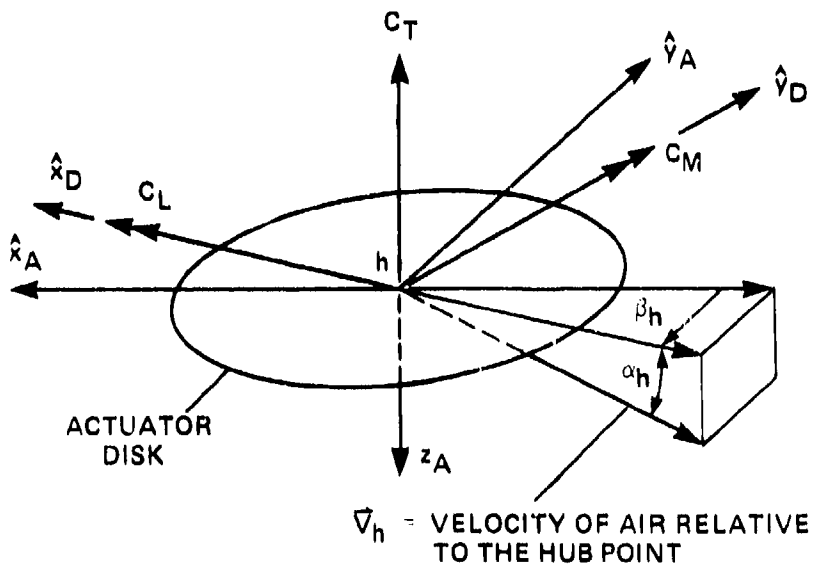

Figure 12. Actuator-disk coordinate frame (A).

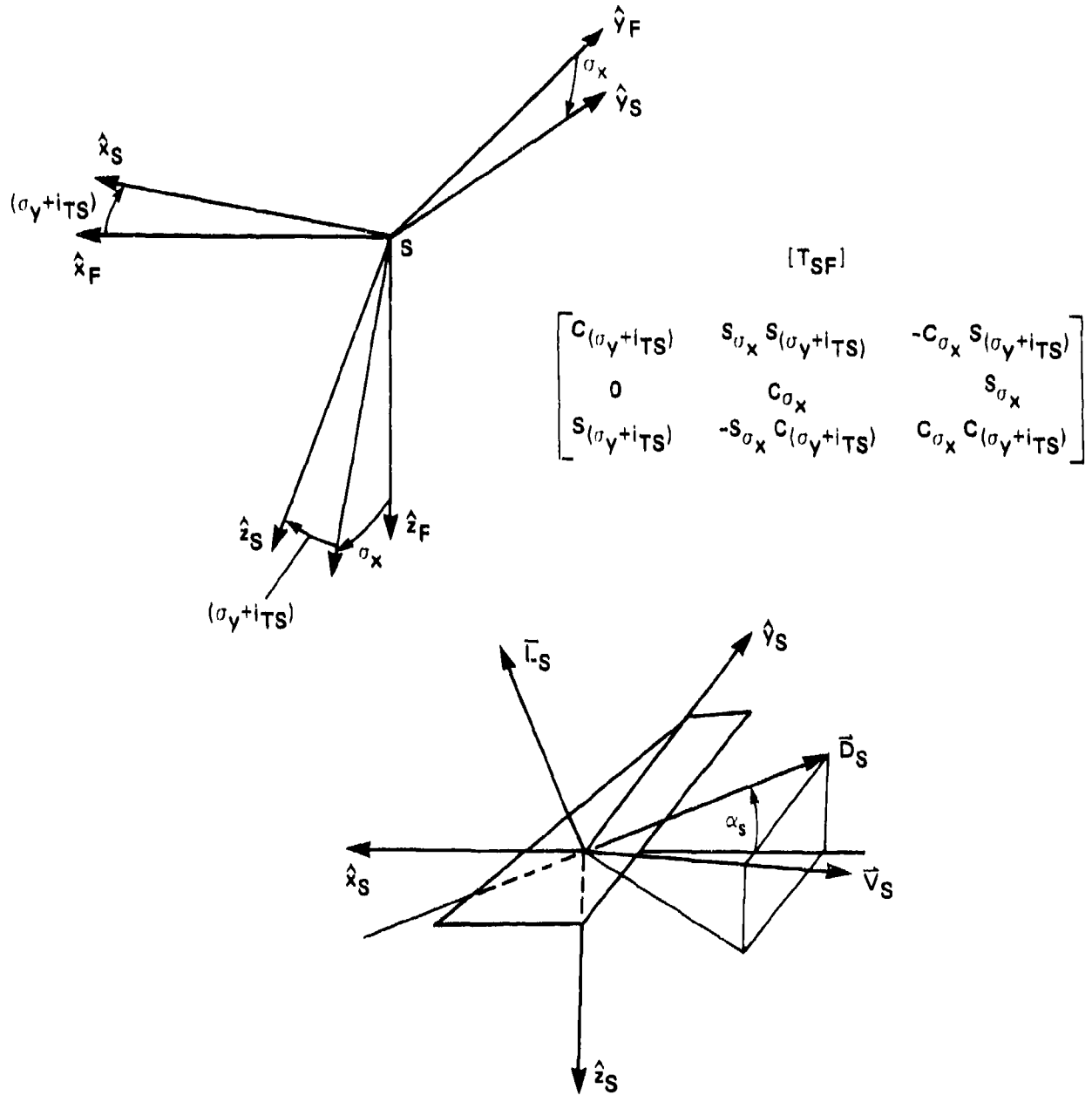

Figure 13. Tail-surface orientation and aerodynamic forces.

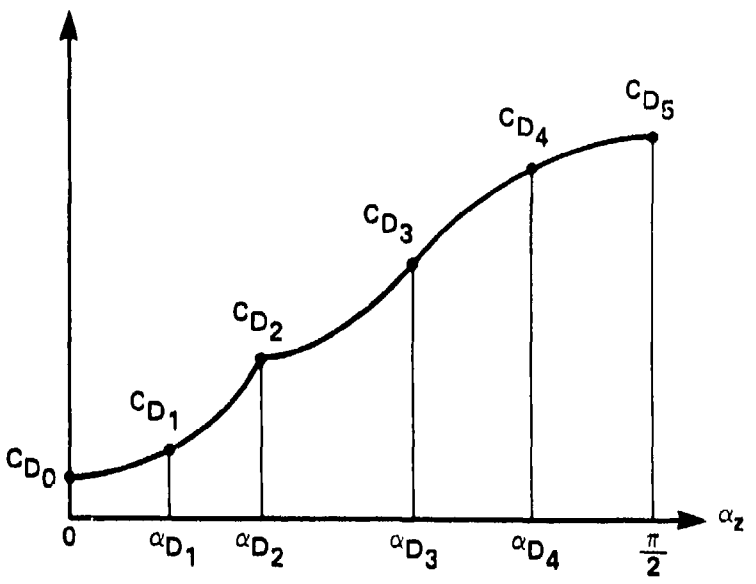

$$C'_D = \frac{\left(\alpha_z^2 - \alpha_{D_2}^2\right)\left(\alpha_z^2 - \alpha_{D_1}^2\right)}{\alpha_{D_1}^2 \alpha_{D_2}^2} C'_{D_0} + \frac{\left(\alpha_z^2 - \alpha_{D_2}^2\right)\alpha_z^2}{\left(\alpha_{D_1}^2 - \alpha_{D_2}^2\right)\alpha_{D_1}^2} C'_{D_1} + \frac{\left(\alpha_z^2 - \alpha_{D_1}^2\right)\alpha_z^2}{\left(\alpha_{D_2}^2 - \alpha_{D_1}^2\right)\alpha_{D_2}^2} C'_{D_2}$$

$$-\alpha_{D_2} \le \alpha_z \le \alpha_{D_2}$$

$$C'_D = \frac{\left(\alpha_z - \alpha_{D_3}\right)\left(\alpha_z - \alpha_{D_4}\right)\left(\alpha_z - \frac{\pi}{2}\right)}{\left(\alpha_{D_2} - \alpha_{D_3}\right)\left(\alpha_{D_2} - \alpha_{D_4}\right)\left(\alpha_{D_2} - \frac{\pi}{2}\right)} C'_{D_2} + \frac{\left(\alpha_z - \alpha_{D_2}\right)\left(\alpha_z - \alpha_{D_4}\right)\left(\alpha_z - \frac{\pi}{2}\right)}{\left(\alpha_{D_3} - \alpha_{D_2}\right)\left(\alpha_{D_3} - \alpha_{D_4}\right)\left(\alpha_{D_3} - \frac{\pi}{2}\right)} C'_{D_3}$$

$$+ \frac{\left(\alpha_z - \alpha_{D_2}\right)\left(\alpha_z - \alpha_{D_3}\right)\left(\alpha_z - \frac{\pi}{2}\right)}{\left(\alpha_{D_4} - \alpha_{D_2}\right)\left(\alpha_{D_4} - \alpha_{D_3}\right)\left(\alpha_{D_4} - \frac{\pi}{2}\right)} C'_{D_4} + \frac{\left(\alpha_z - \alpha_{D_2}\right)\left(\alpha_z - \alpha_{D_3}\right)\left(\alpha_z - \alpha_{D_4}\right)}{\left(\frac{\pi}{2} - \alpha_{D_2}\right)\left(\frac{\pi}{2} - \alpha_{D_3}\right)\left(\frac{\pi}{2} - \alpha_{D_4}\right)} C'_{D_5}$$

$$\alpha_{D_2} \le \alpha_z \le \frac{\pi}{2} \text{ and } \frac{-\pi}{2} \le \alpha_z \le -\alpha_{D_2}$$

Figure 14. Tail-surface drag coefficient break points.

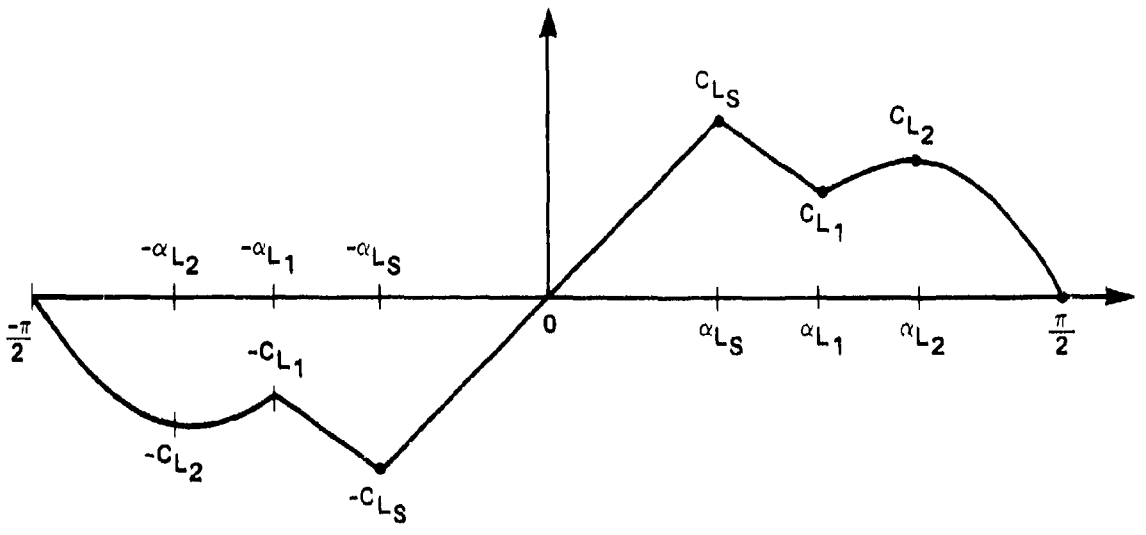

$$C_L = -\frac{\left(\alpha_z + \alpha_{L_2}\right)\left(\alpha_z + \frac{\pi}{2}\right)}{\left(\alpha_{L_1} - \alpha_{L_2}\right)\left(\alpha_{L_1} - \frac{\pi}{2}\right)} C_{L_1} - \frac{\left(\alpha_z + \alpha_{L_1}\right)\left(\alpha_z + \frac{\pi}{2}\right)}{\left(\alpha_{L_2} - \alpha_{L_1}\right)\left(\alpha_{L_2} - \frac{\pi}{2}\right)} C_{L_2} \quad \frac{-\pi}{2} \le \alpha_z \le -\alpha_{L_1}$$

$$C_L = \left(\frac{C_{L_1} - C_{L_s}}{\alpha_{L_1} - \alpha_{L_s}}\right)\left(\alpha_z + \alpha_{L_s}\right) - C_{L_s} \quad -\alpha_{L_1} \le \alpha_z \le -\alpha_{L_s}$$

$$C_L = \left(\frac{C_{L_s}}{\alpha_{L_s}}\right)\alpha_z \quad -\alpha_{L_s} < \alpha_z < \alpha_{L_s}$$

$$C_L = \left(\frac{C_{L_1} - C_{L_s}}{\alpha_{L_1} - \alpha_{L_s}}\right)\left(\alpha_z - \alpha_{L_s}\right) + C_{L_s} \quad \alpha_{L_s} < \alpha_z < \alpha_{L_1}$$

$$C_L = \frac{\left(\alpha_z - \alpha_{L_2}\right)\left(\alpha_z - \frac{\pi}{2}\right)}{\left(\alpha_{L_1} - \alpha_{L_2}\right)\left(\alpha_{L_1} - \frac{\pi}{2}\right)} C_{L_1} + \frac{\left(\alpha_z - \alpha_{L_1}\right)\left(\alpha_z - \frac{\pi}{2}\right)}{\left(\alpha_{L_2} - \alpha_{L_1}\right)\left(\alpha_{L_2} - \frac{\pi}{2}\right)} C_{L_2} \quad \alpha_{L_1} \le \alpha_z \le \frac{\pi}{2}$$

Figure 15. Tail-surface lift coefficient break points.

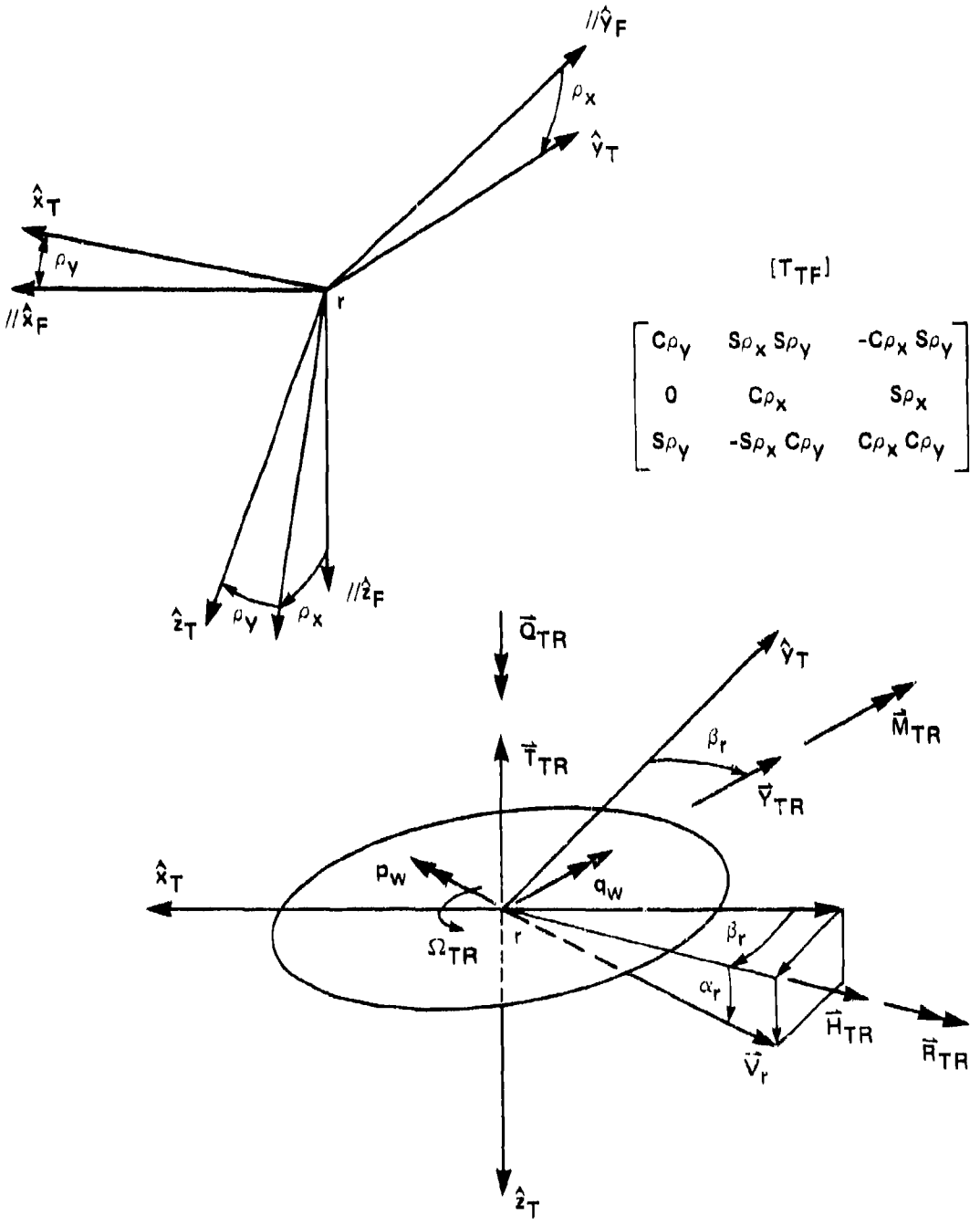

Figure 16. Tail-rotor orientation and aerodynamic forces.

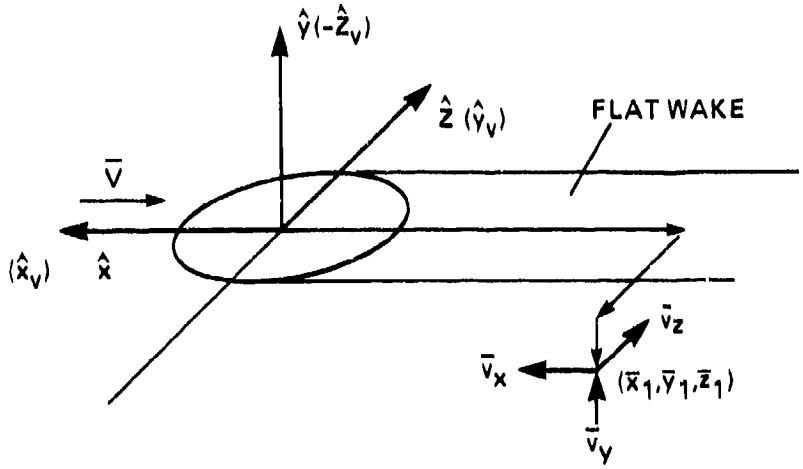

Figure 17. Flat-wake model coordinate system.

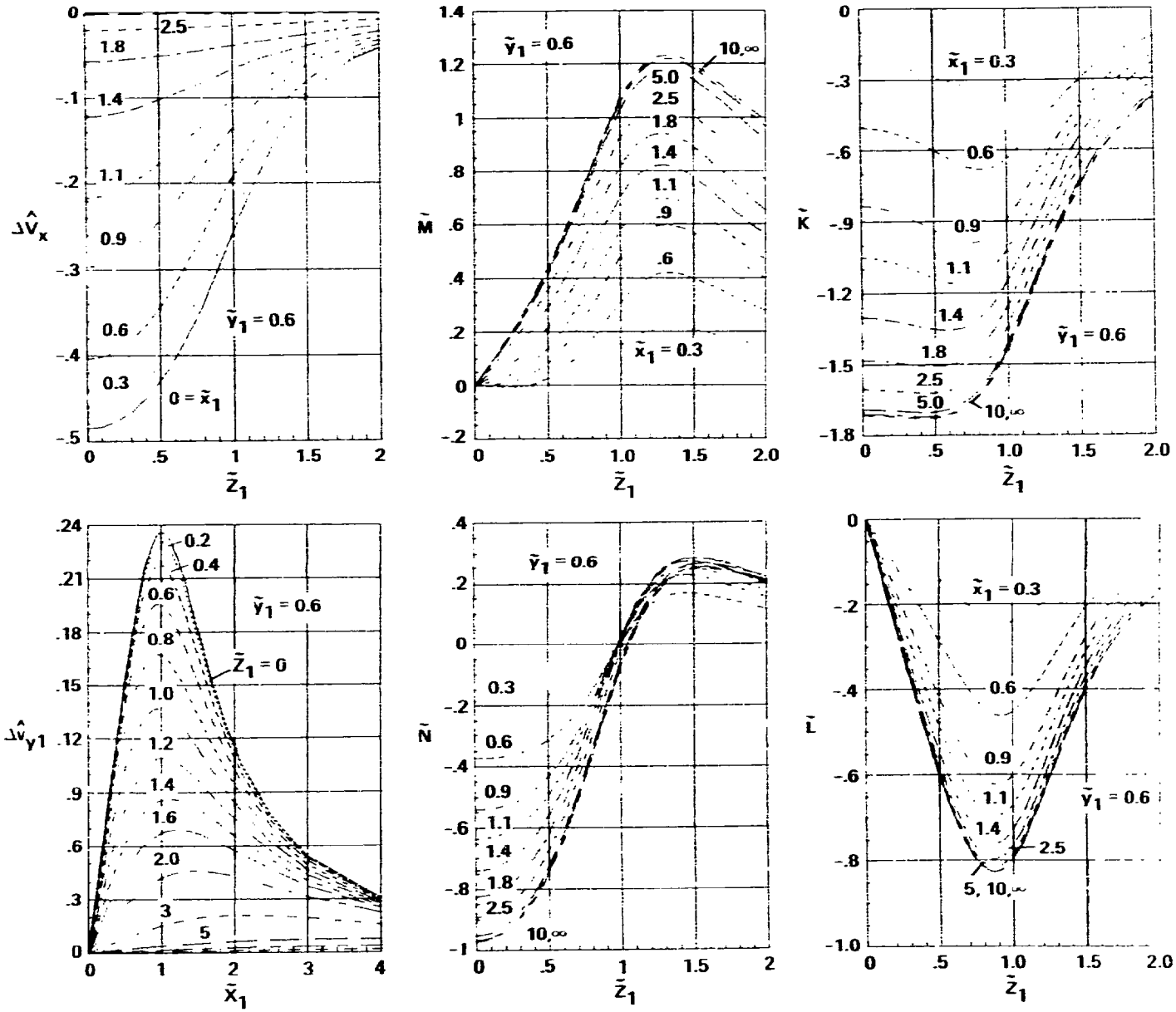

Figure 18. Examples of tabulated downwash functions.

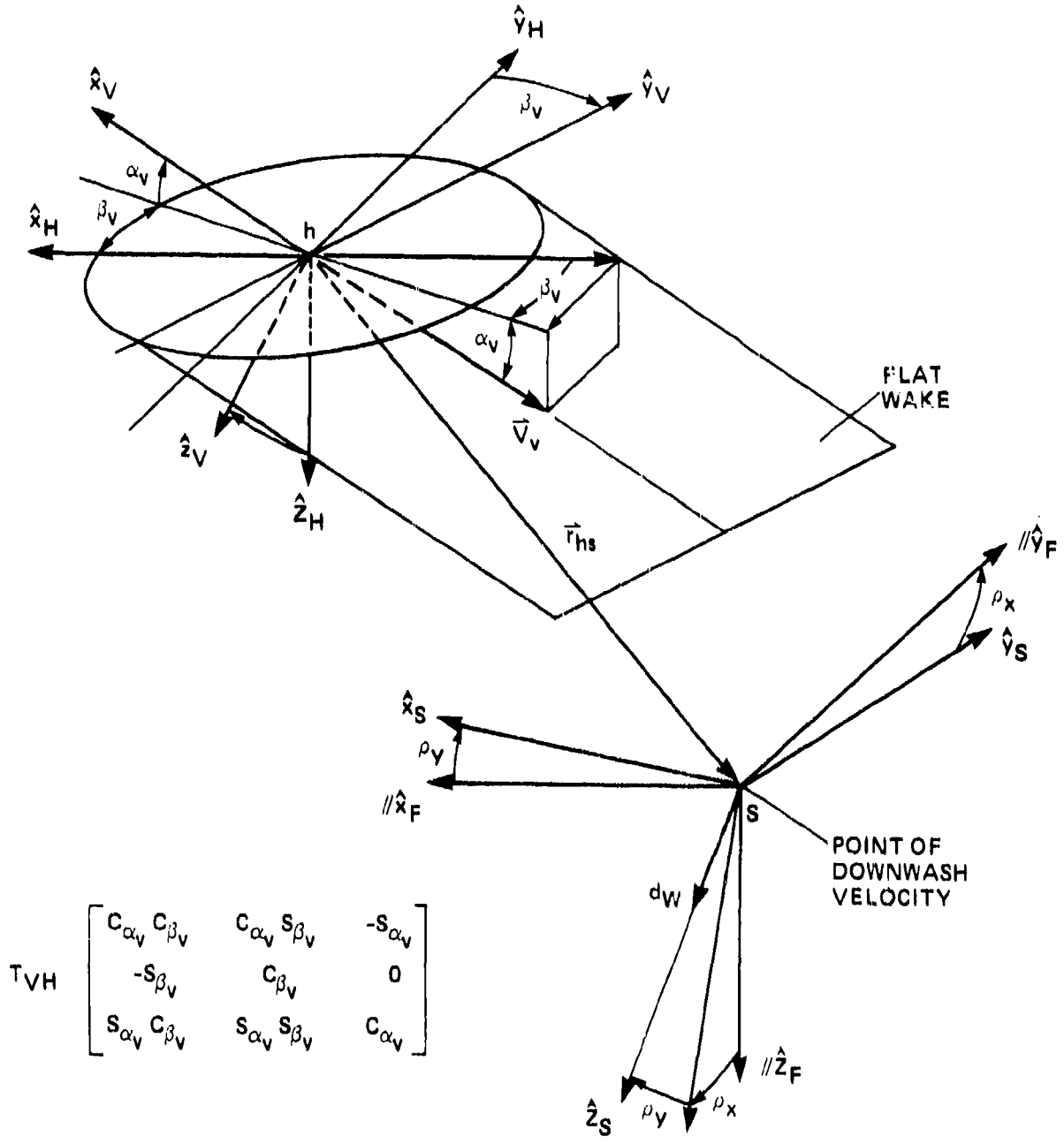

$$T_{VH} \begin{bmatrix} C_{\alpha_V} C_{\beta_V} & C_{\alpha_V} S_{\beta_V} & -S_{\alpha_V} \\ -S_{\beta_V} & C_{\beta_V} & 0 \\ S_{\alpha_V} C_{\beta_V} & S_{\alpha_V} S_{\beta_V} & C_{\alpha_V} \end{bmatrix}$$

Figure 19. Wake orientation for generating a surface downwash table.

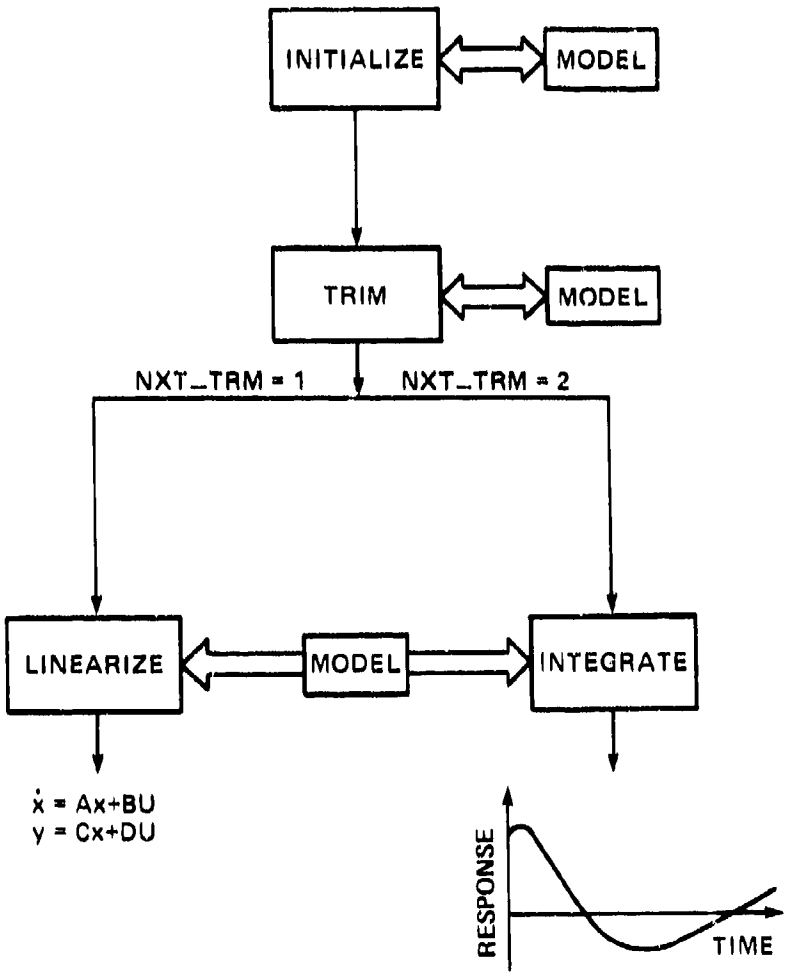

Figure 20. Overview of operations.

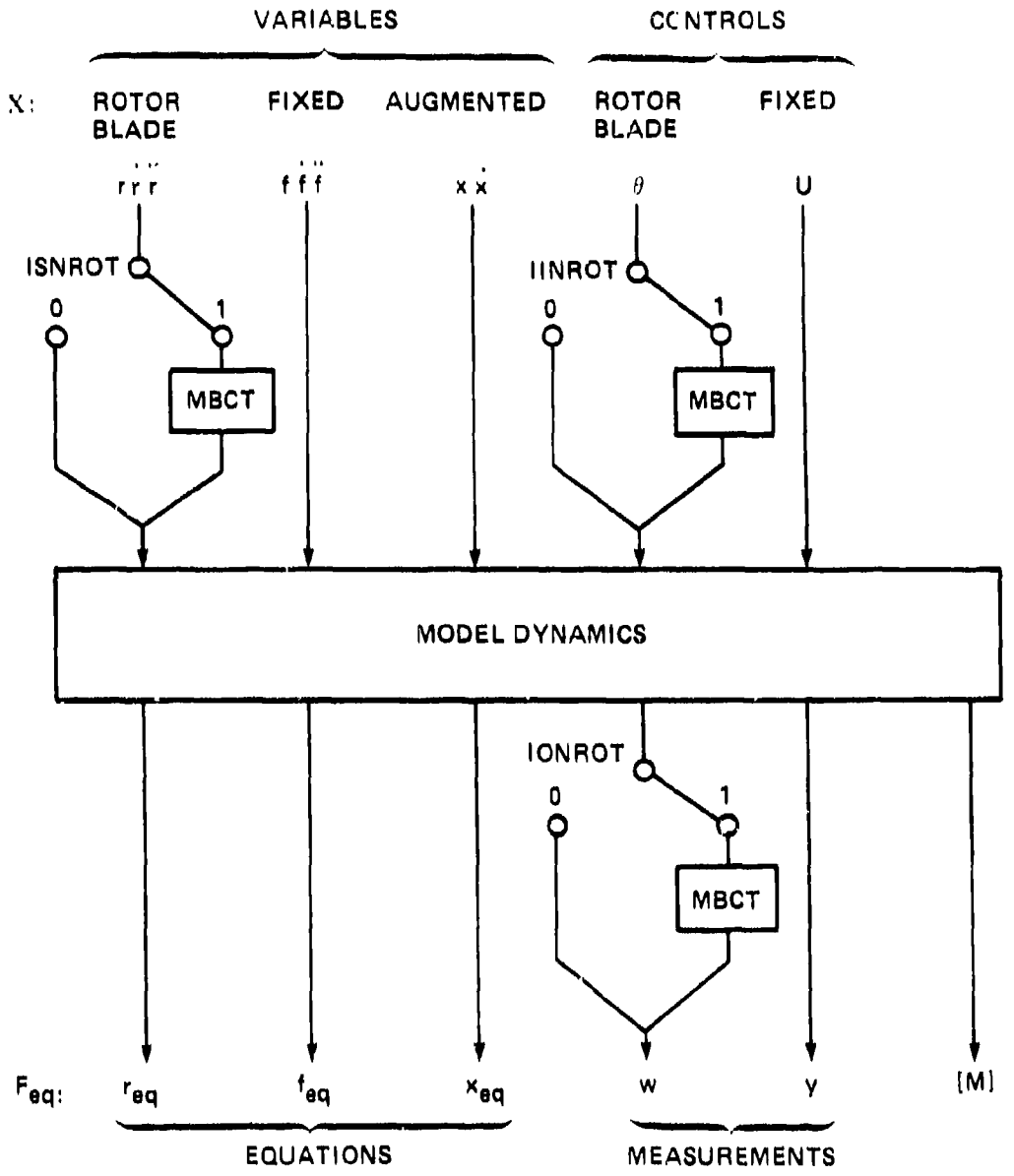

Figure 21. General input/output model structure used by trim,linearization, and integration operations.

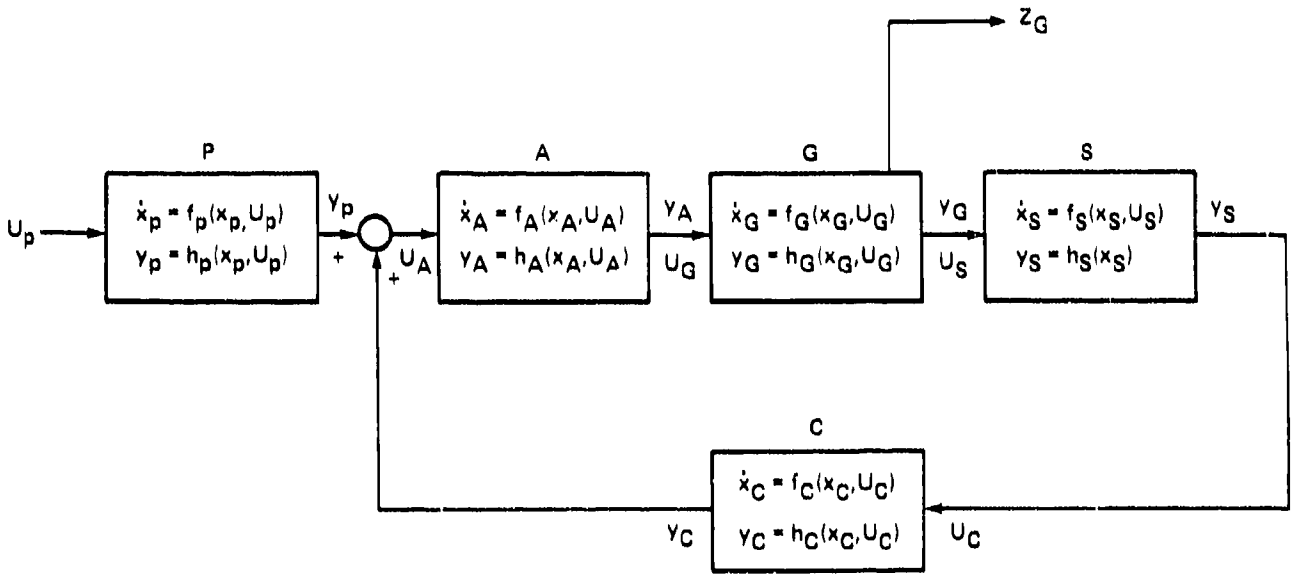

Figure 22. General system structure for integration.

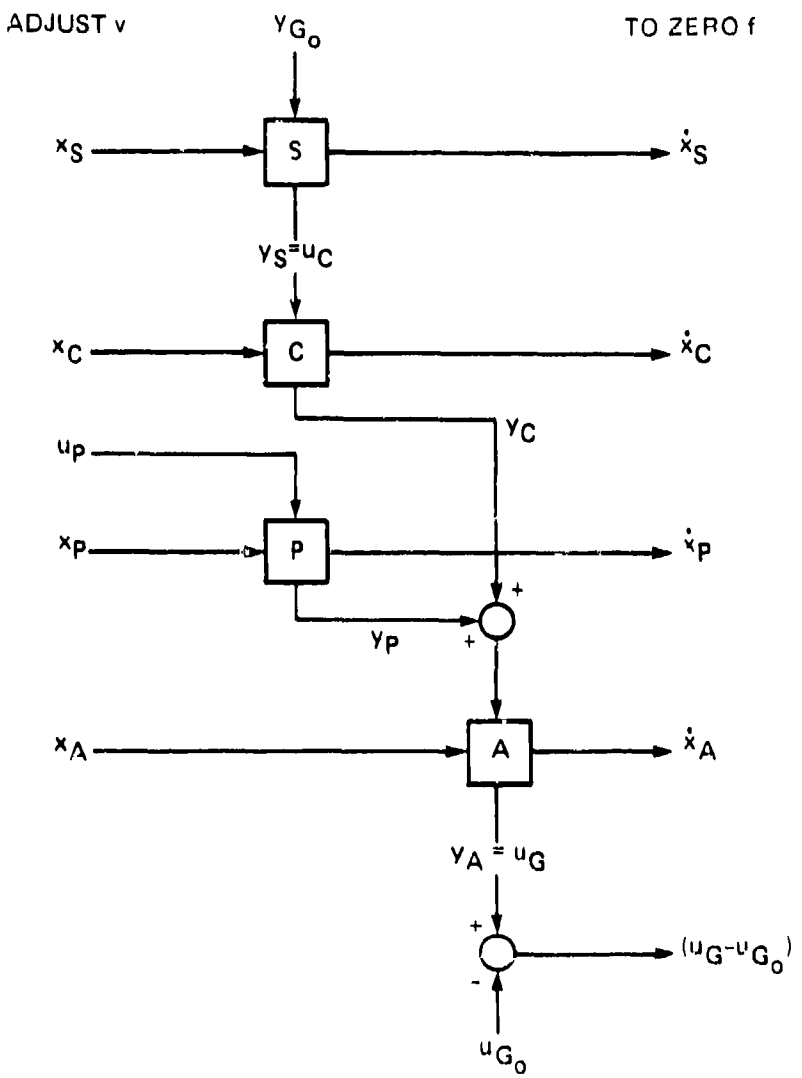

Figure 23. Flow of calculation to find the initial conditions of the system of figure 22.

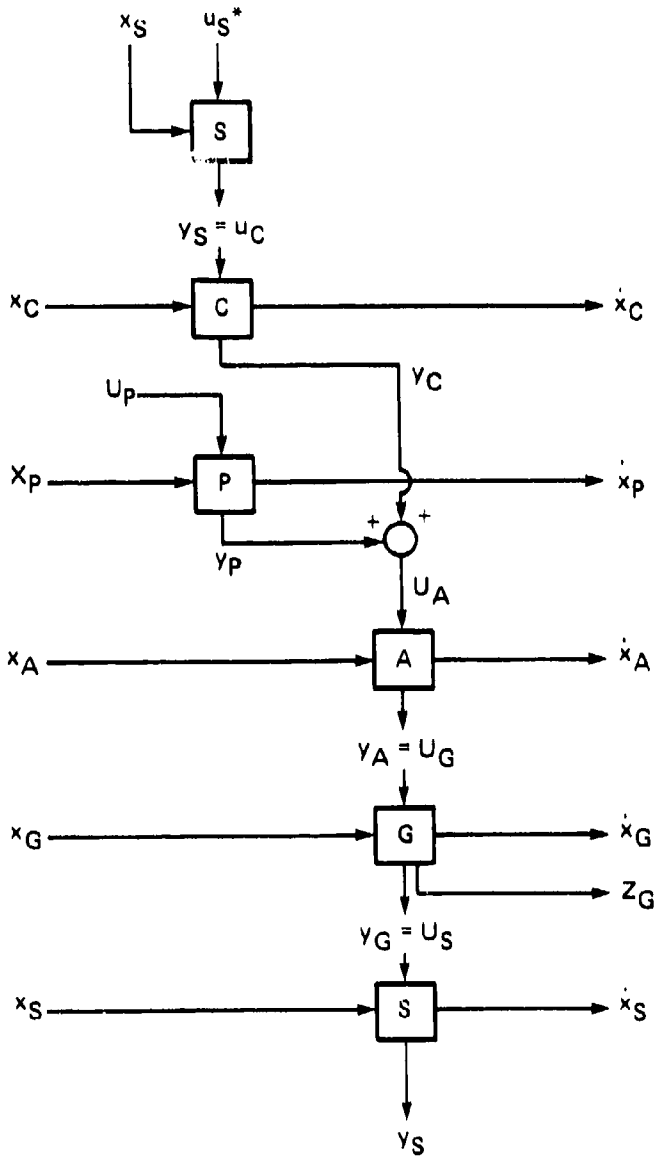

Figure 24. Flow of calculation to integrate the system of figure 22.

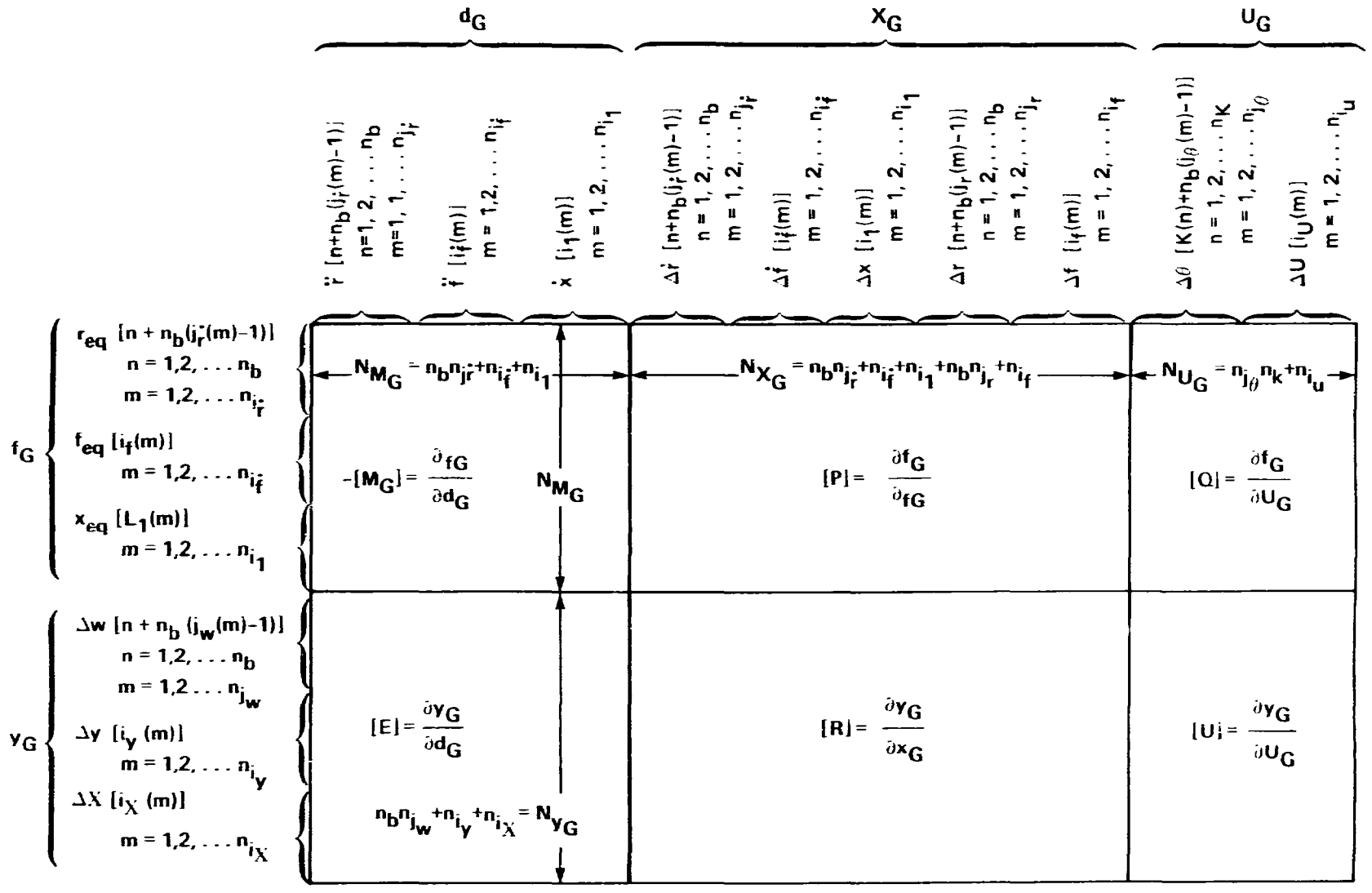

Figure 25. Partial-derivative matrix for model linearization.

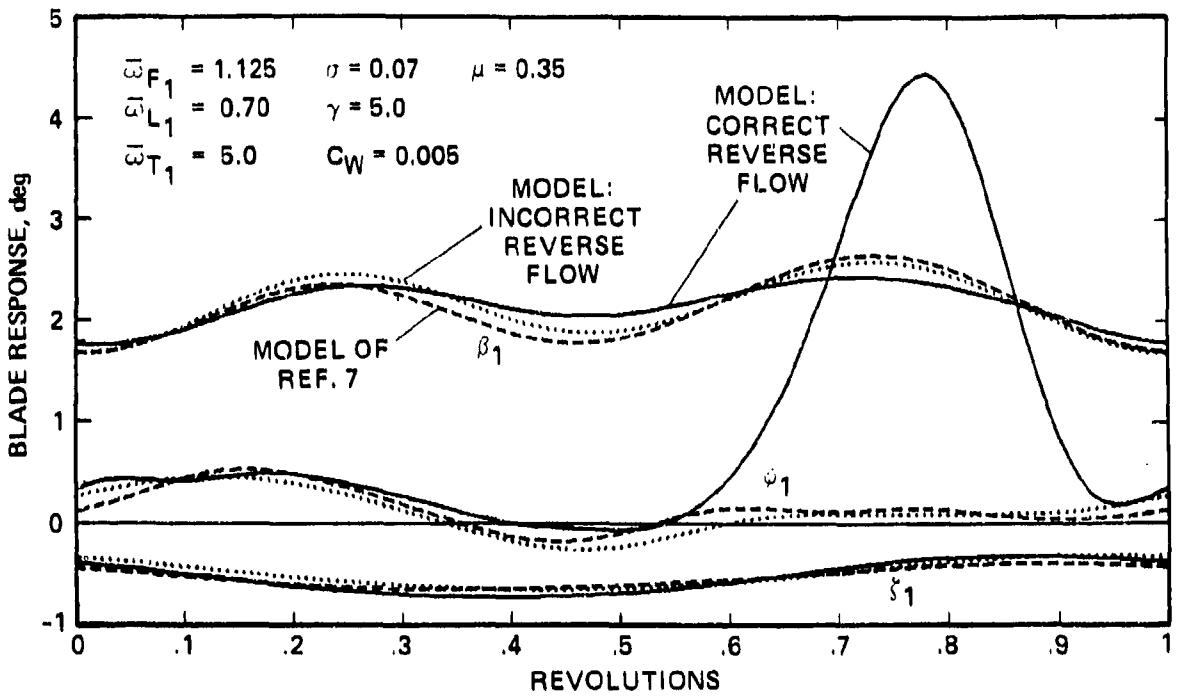

Figure 26. Blade responses from the present model compared with those from a flap-lag-torsion rotor in trim.

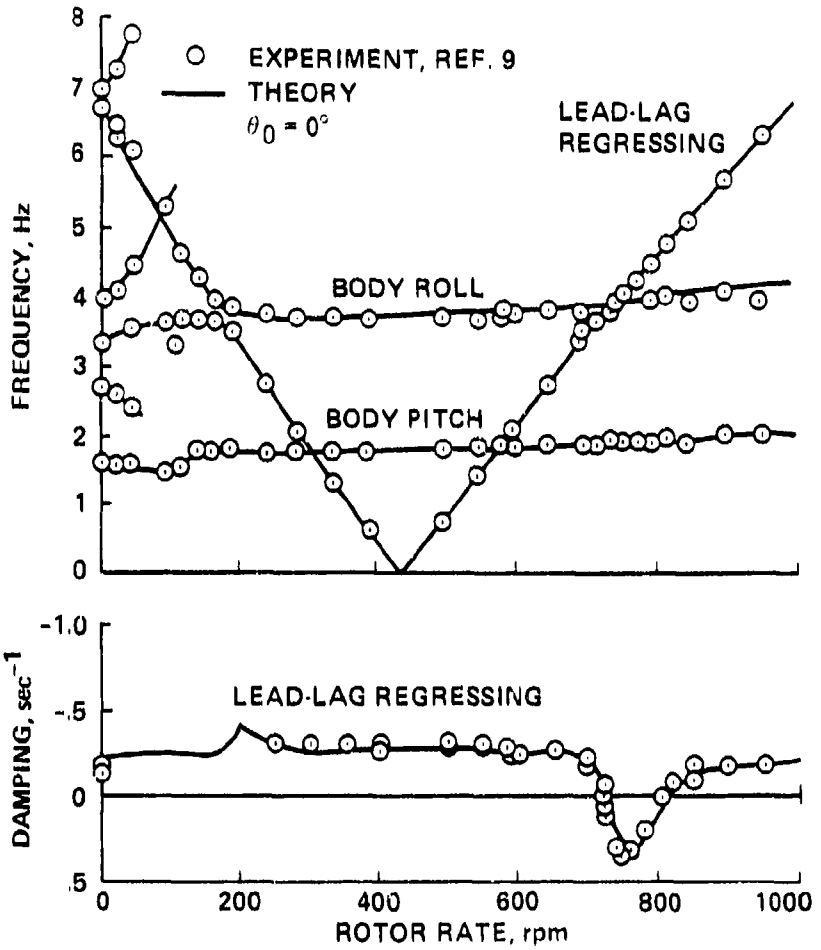

Figure 27. Modal frequencies and lead-lag regressing damping data from the present model compared with those from a flap-lag rotor/fuselage system at zero blade pitch.

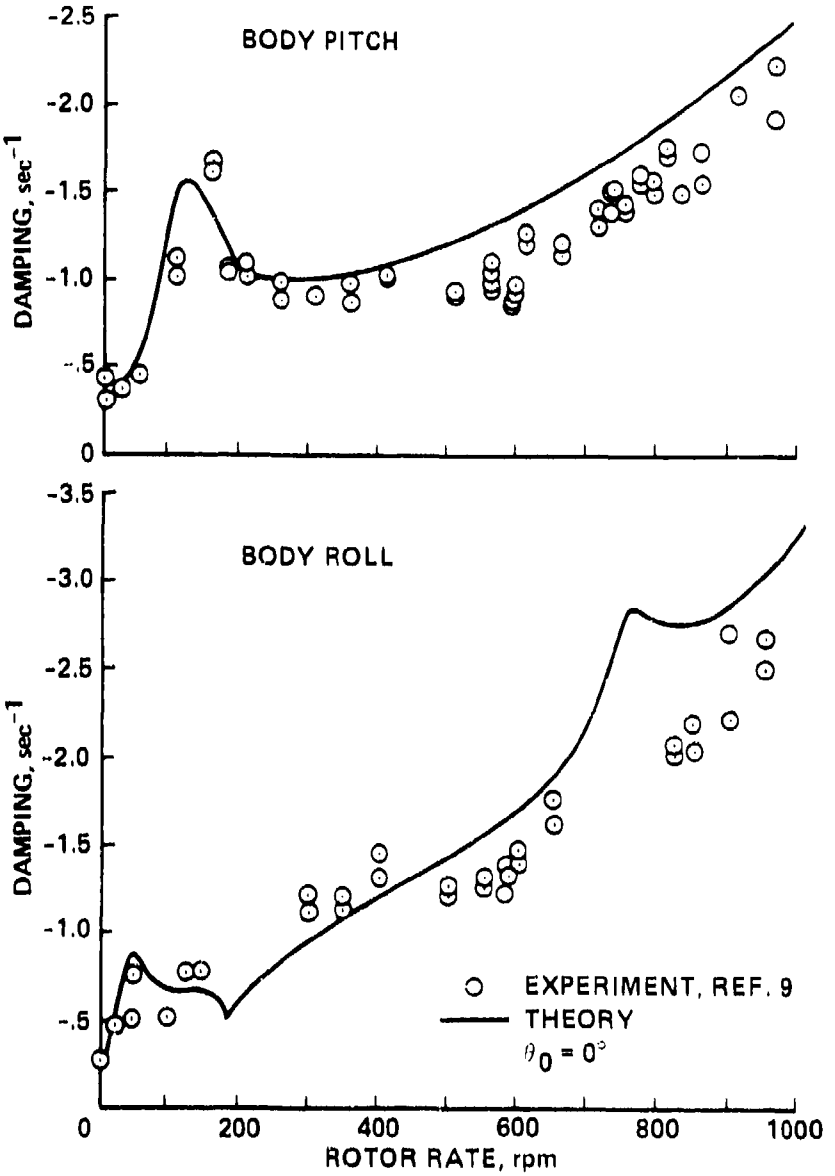

Figure 28. Body pitch and roll damping data from the present model compared with those from a flap-lag rotor/fuselage system at zero blade pitch.

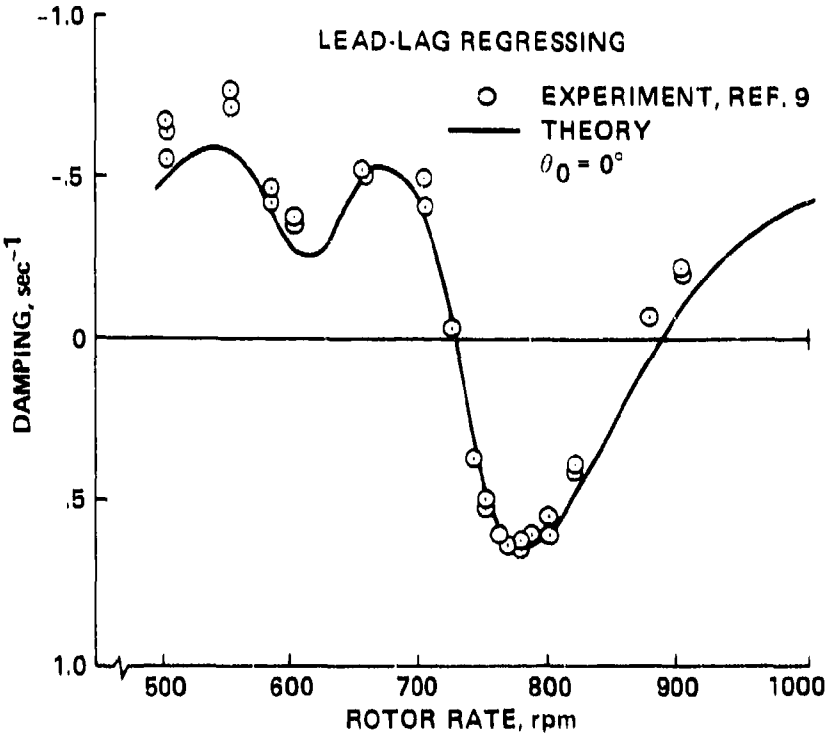

Figure 29. Lead-lag regressing damping data from the present model compared with those from a flap-lag rotor/fuselage system at 9° blade pitch.

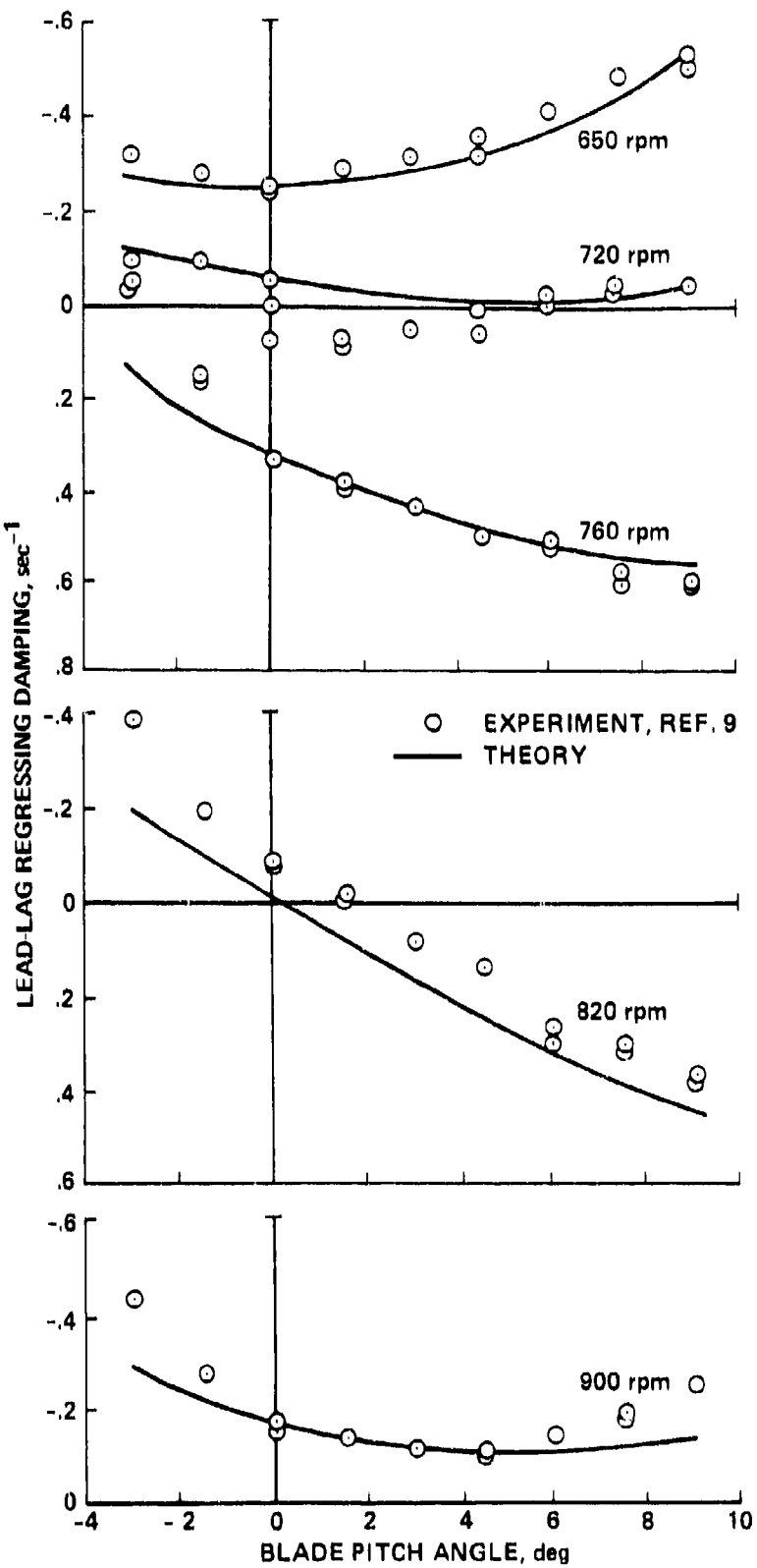

Figure 30. Lead-lag regressing damping data from the present model compared with those from a flap-lag rotor/fuselage system at various rotor speeds and blade pitches.

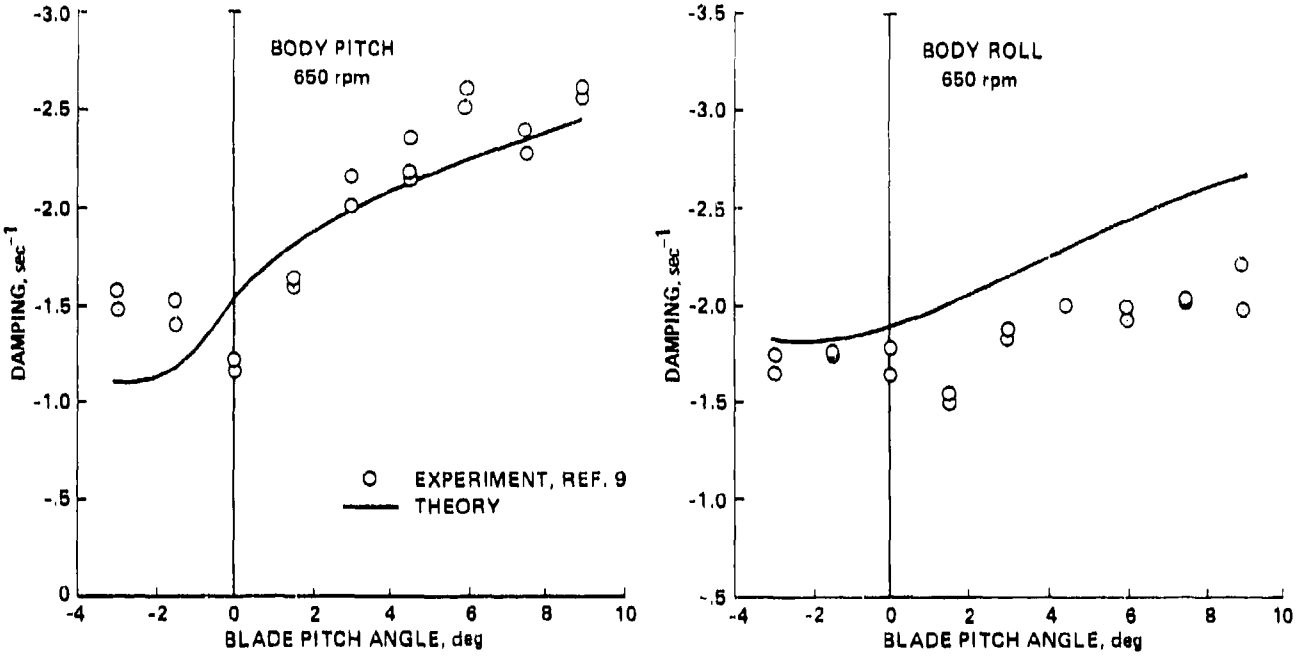

Figure 31. Body pitch and roll damping data from the present model compared with those from a flap-lag rotor/fuselage system at 650 rpm.

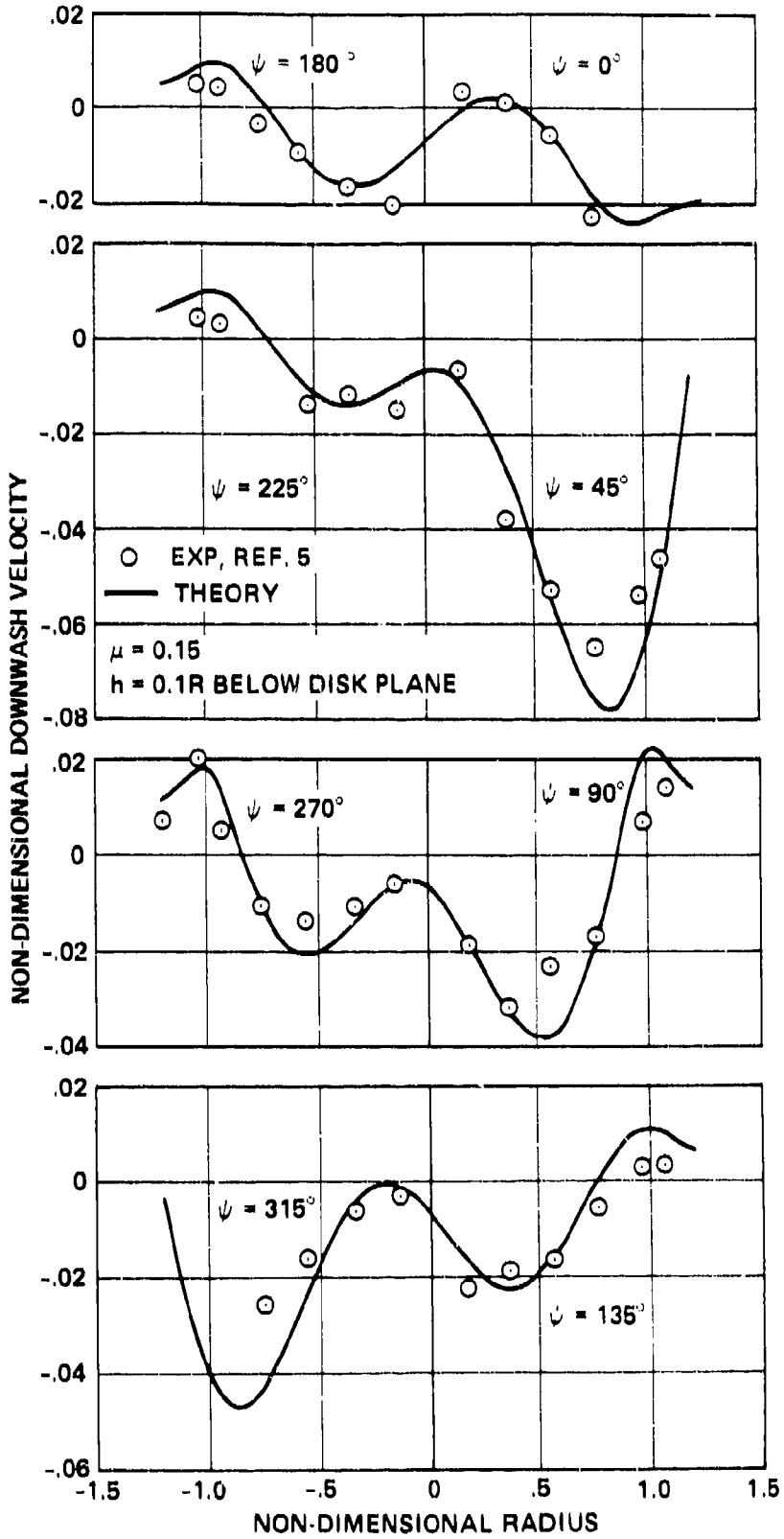

Figure 32. Downwash from the wake model compared with experimental results.

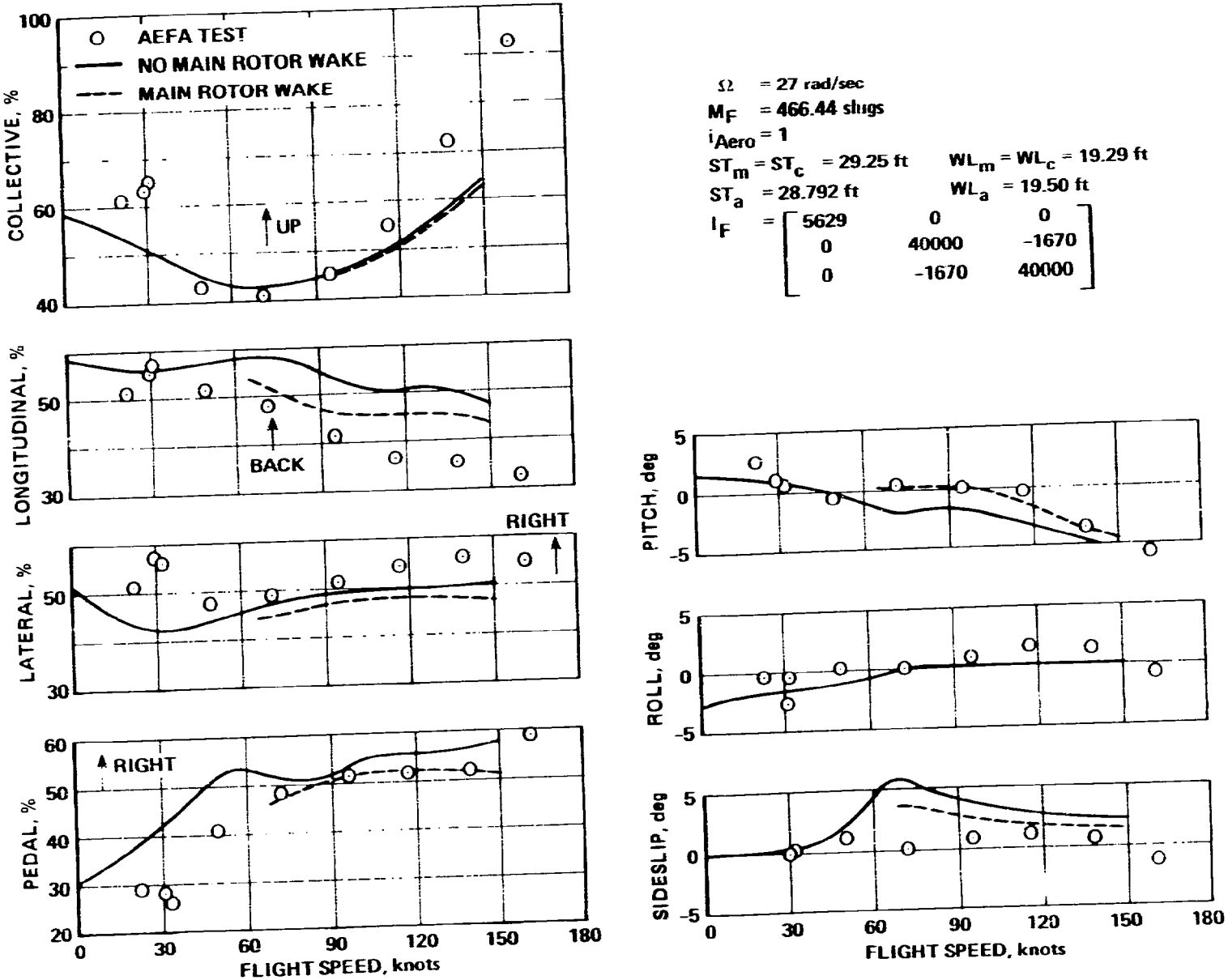

Ω = 27 rad/sec
M_F = 466.44 slugs
i_{Aero} = 1
$ST_m = ST_c$ = 29.25 ft $WL_m = WL_c$ = 19.29 ft
ST_a = 28.792 ft WL_a = 19.50 ft

$$I_F = \begin{bmatrix} 5629 & 0 & 0 \\ 0 & 40000 & -1670 \\ 0 & -1670 & 40000 \end{bmatrix}$$

Figure 33. Trim in straight and level flight of helicopter model compared with flight-test results.

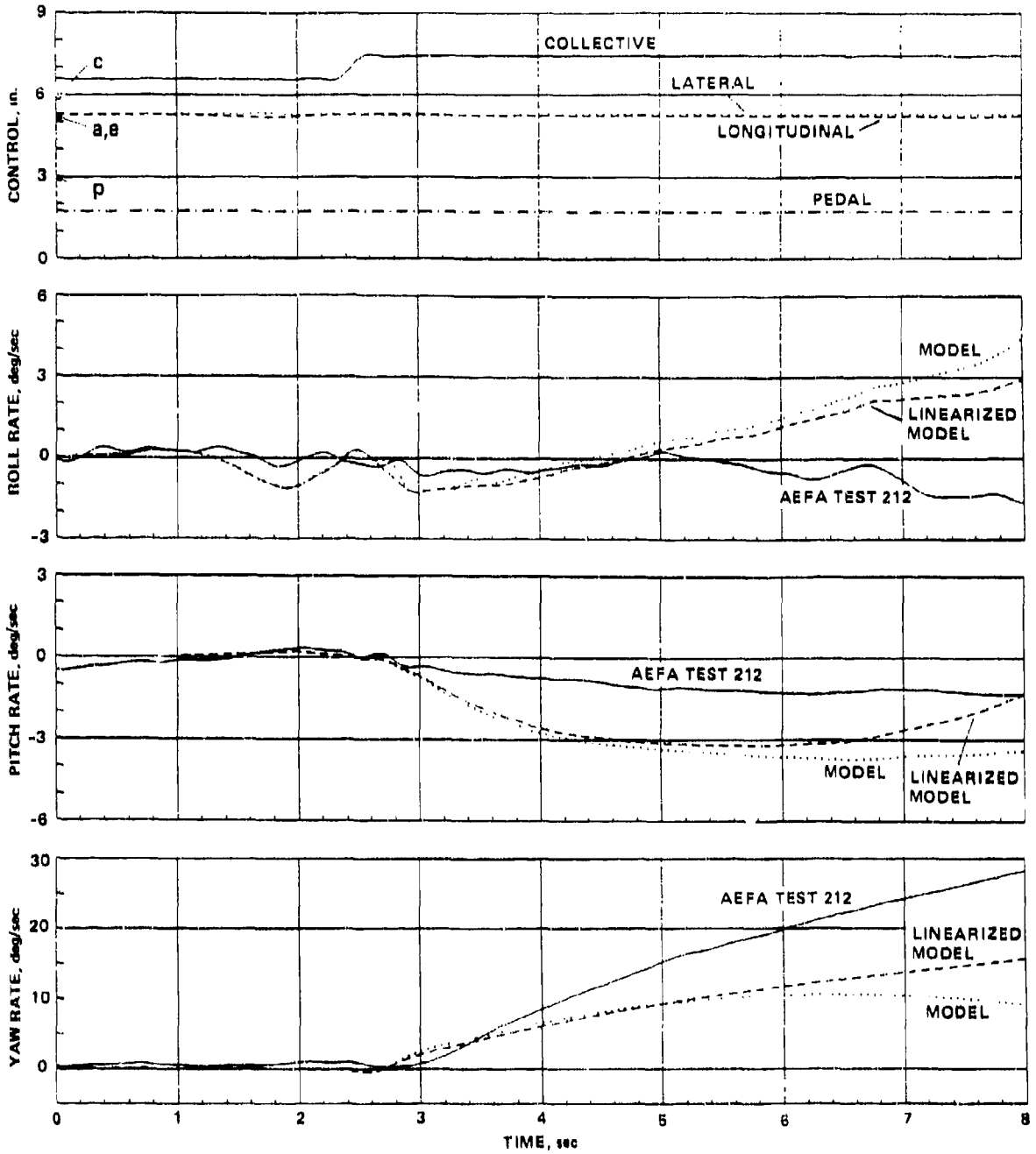

Figure 34. UH-60A model responses with 1-in.-up collective at 1 knot.

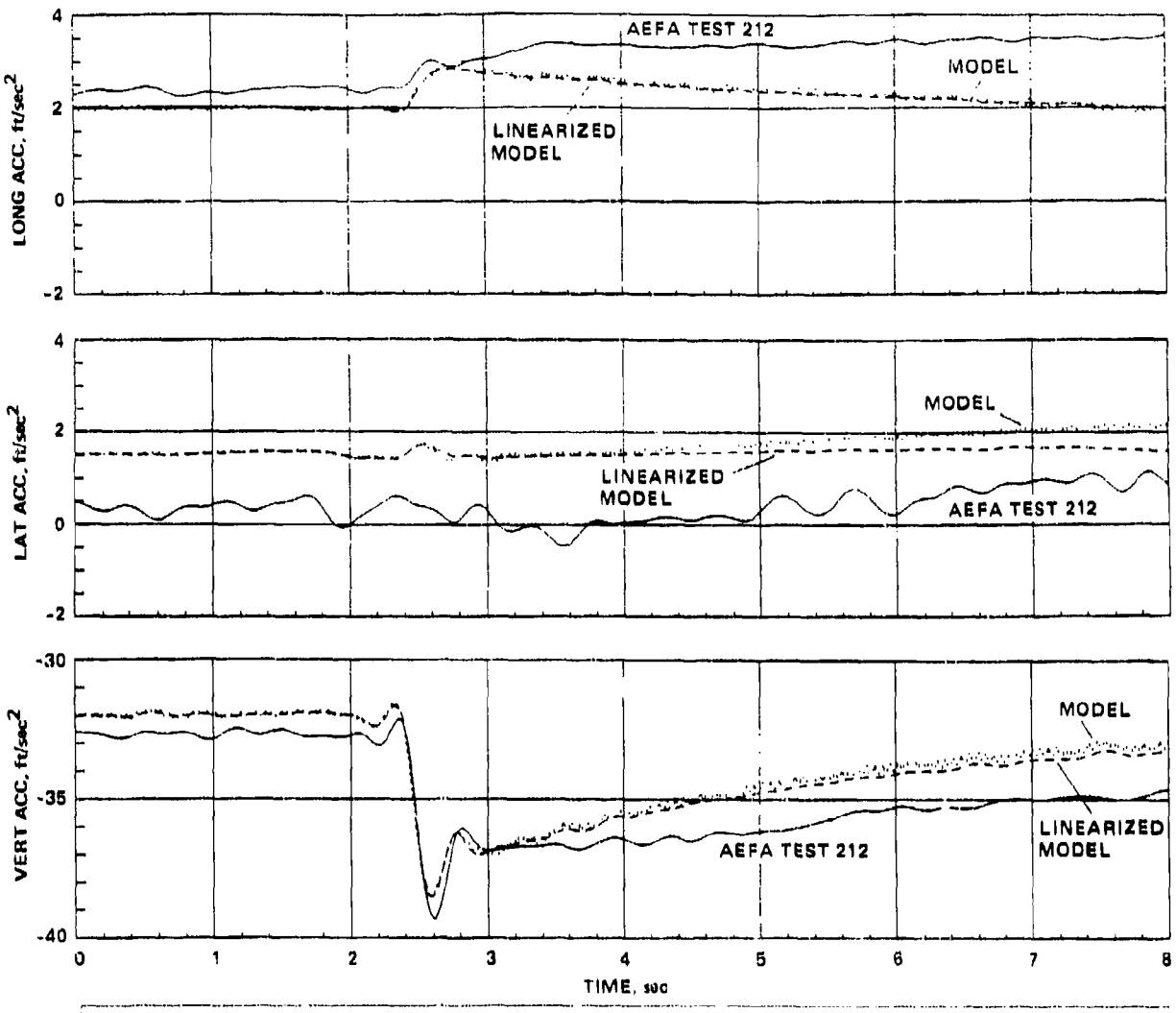

Ω = 26.882 rad/sec M_F = 467.36 slugs $ST_m = ST_c = ST_a$ = 29.95 ft f(4) = 1.68 ft/sec

$$I_F = \begin{bmatrix} 4659 & 0 & 0 \\ 0 & 38512 & -1882 \\ 0 & -1882 & 38512 \end{bmatrix}$$

$WL_m = WL_c = WL_a$ = 19.29 ft l_f = 1,2

σ_y = 0.0698, 0.0698, 0 rad

I_{Aero} = 0

IOPT5 = 1,1,1

Figure 34. Concluded.

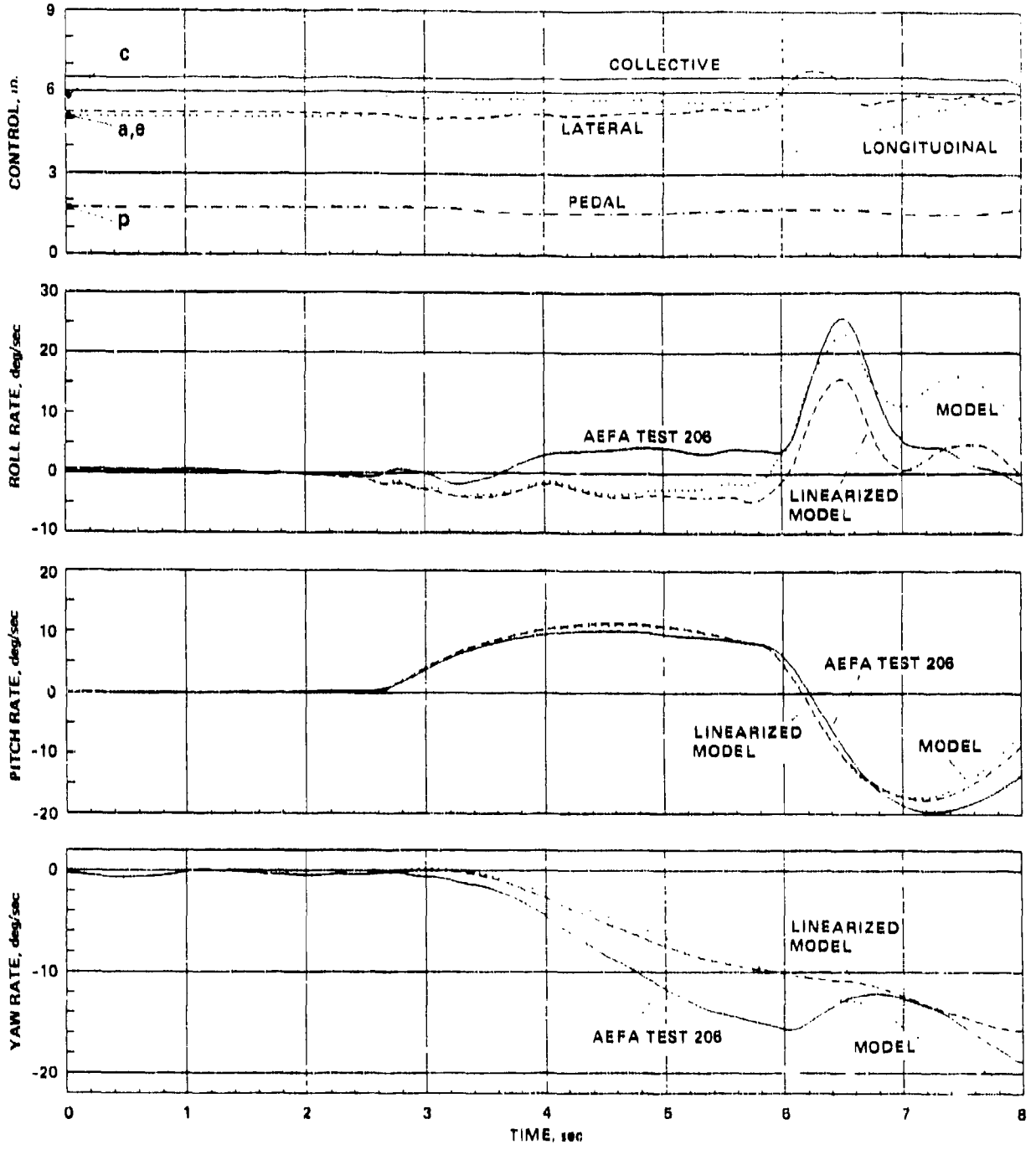

Figure 35. UH-60A model responses with 1-in.-aft stick at 1 knot.

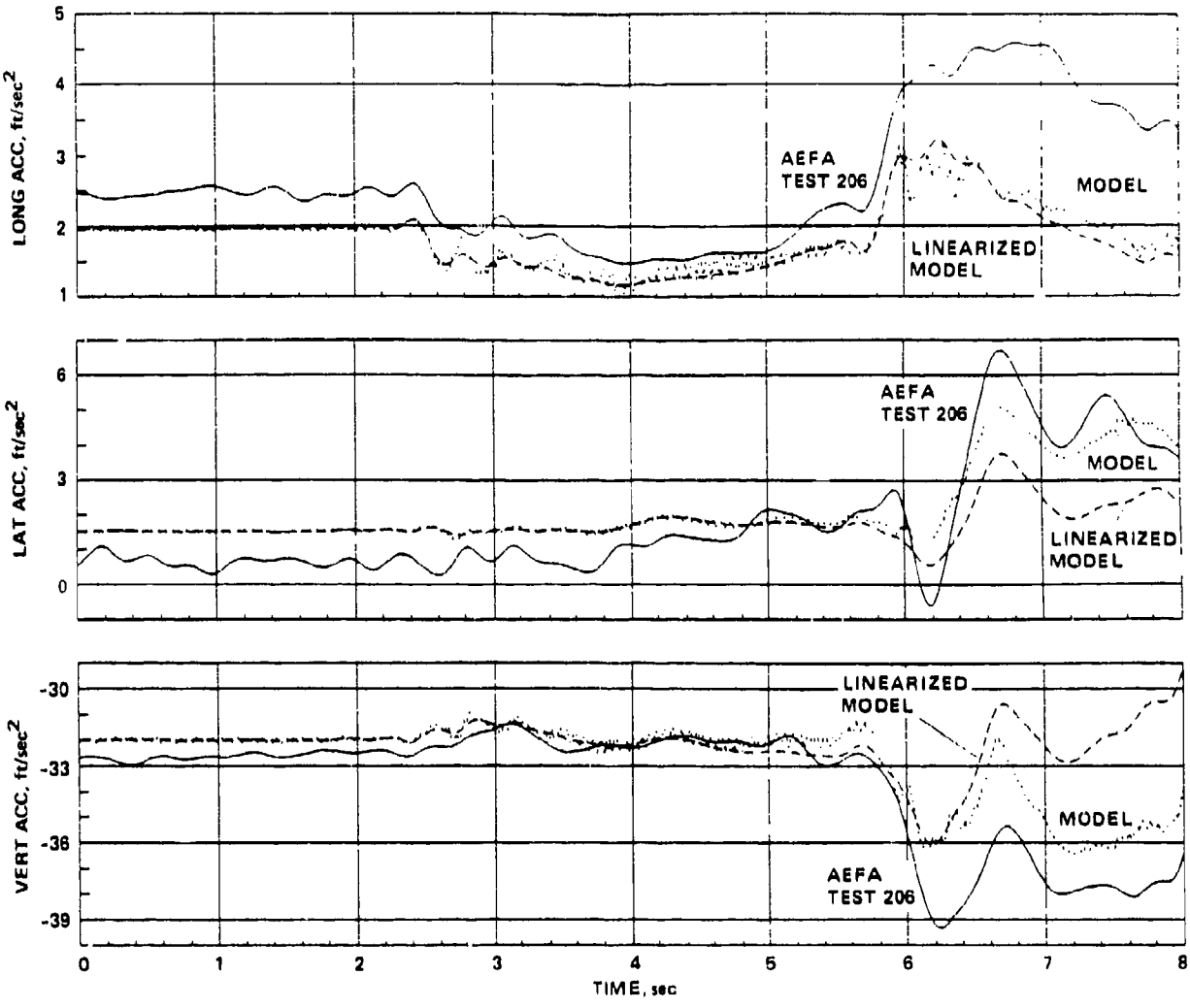

Ω = 26.987 rad/sec M_F = 457.71 slugs $ST_m = ST_c = ST_a$ = 29.93 ft f(4) = 1.68 ft/sec

$$I_F = \begin{bmatrix} 4659 & 0 & 0 \\ 0 & 38512 & -1882 \\ 0 & -1882 & 38512 \end{bmatrix}$$

$WL_m = WL_c = WL_a$ = 19.29 ft I_f = 1,2

σ_y = 0.0698, 0.0698, 0 rad

I_{Aero} = 0

IOPT5 = 1,1,1

Figure 35. Concluded.

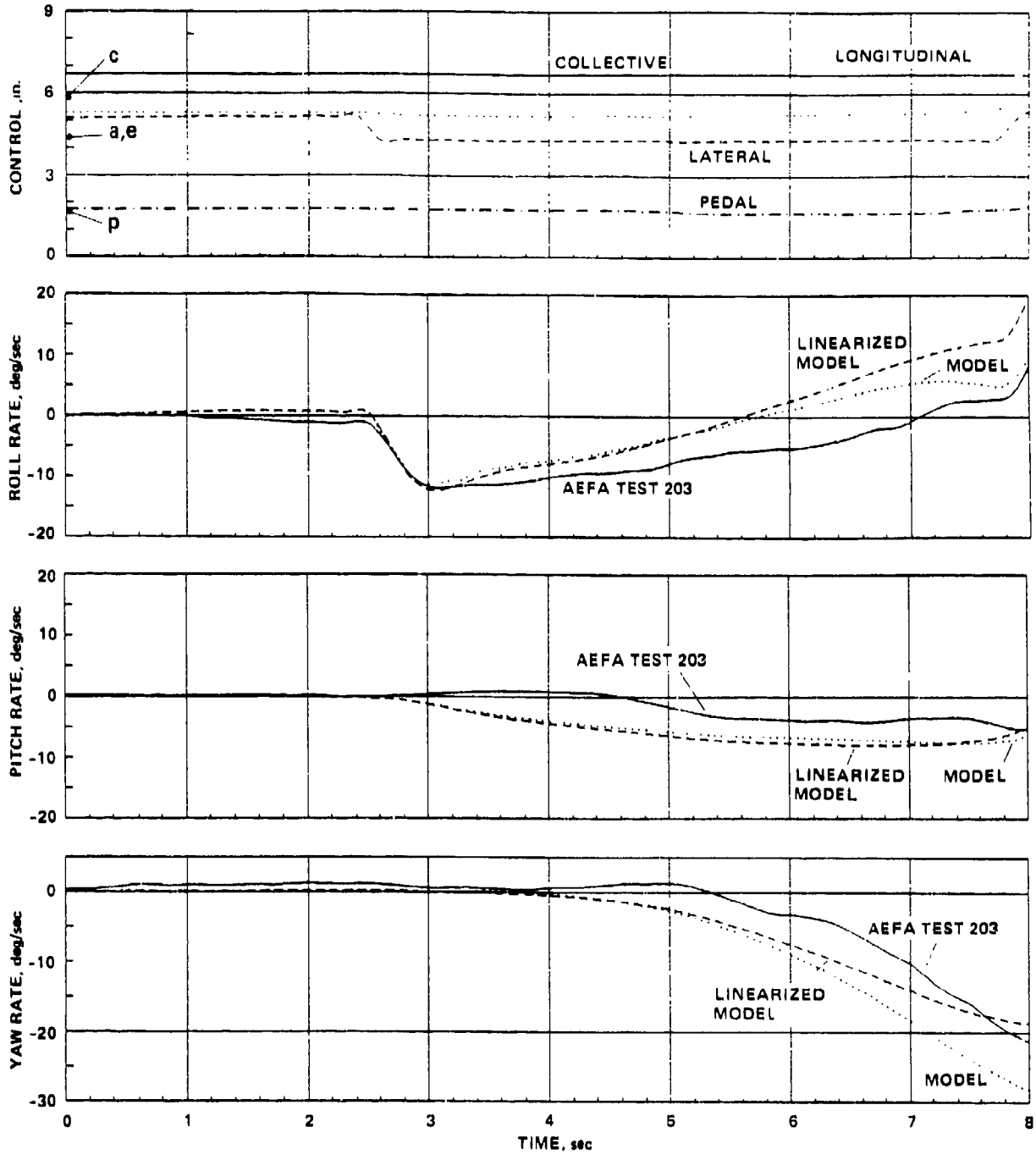

Figure 36. UH-60A model responses with 1-in.-left lateral stick at 1 knot.

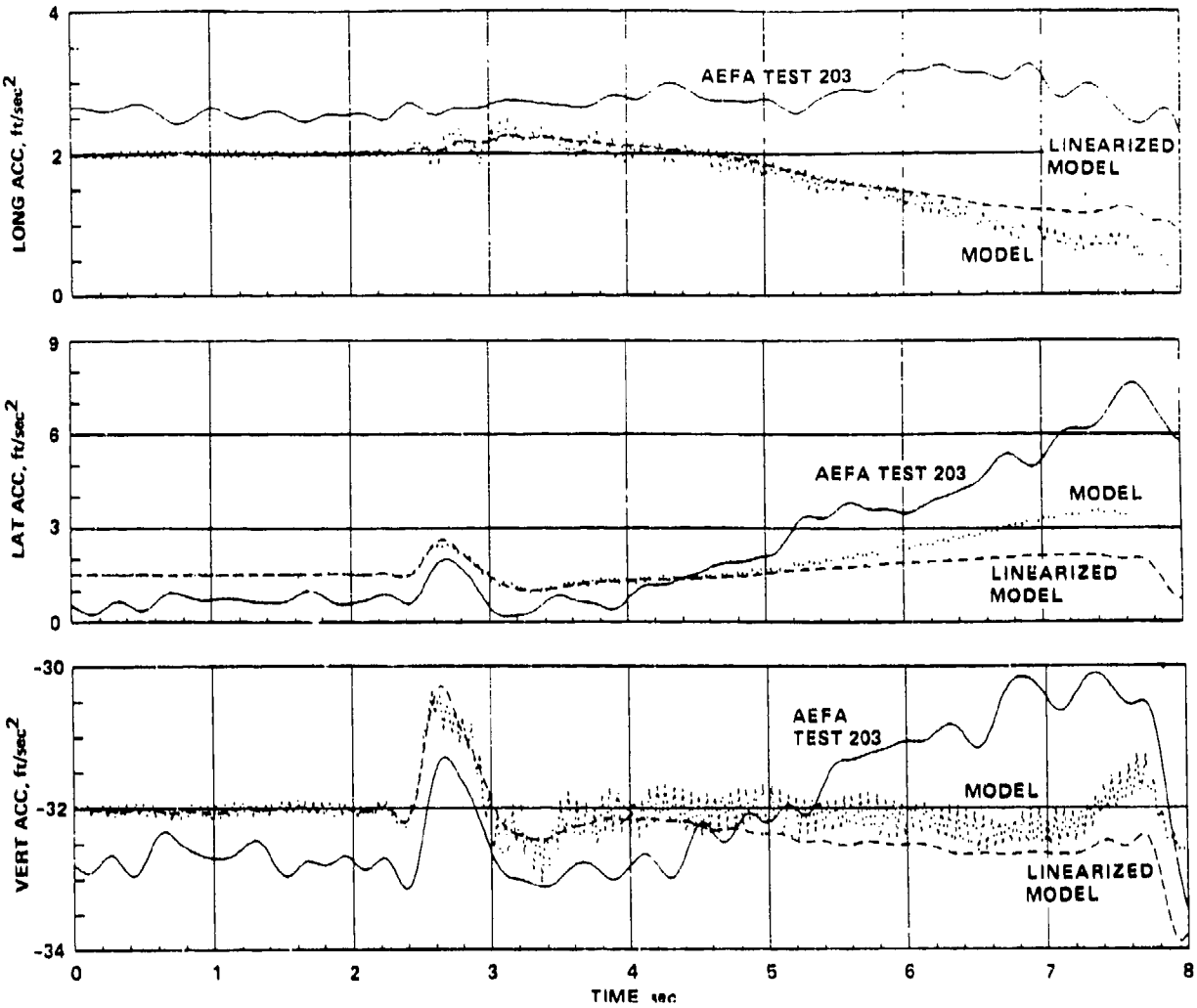

Ω = 26.996 rad/sec M_F = 458.64 slugs $ST_m = ST_c = ST_a$ = 29.94 ft f(4) = 1.68 ft/sec

$$I_F = \begin{bmatrix} 4659 & 0 & 0 \\ 0 & 38512 & -1882 \\ 0 & -1882 & 38512 \end{bmatrix}$$

$WL_m = WL_c = WL_a$ = 19.29 ft l_f = 1,2

σ_y = 0.0698, 0.0698, 0 rad

$I_{Aero} = 0$

IOPT5 = 1,1,1

Figure 36. Concluded.

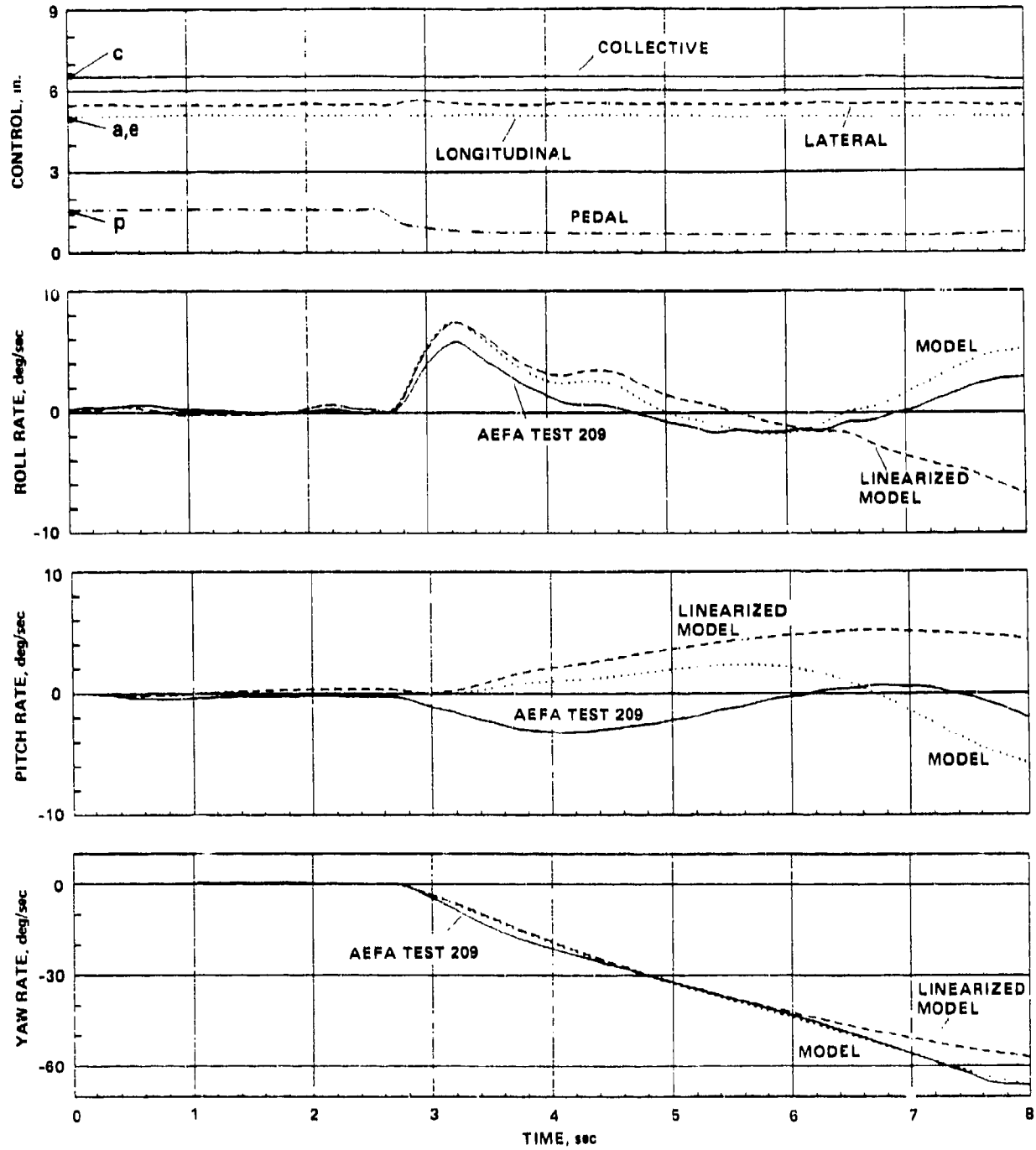

Figure 37. UH-60A model responses with 1-in.-left pedal at 1 knot.

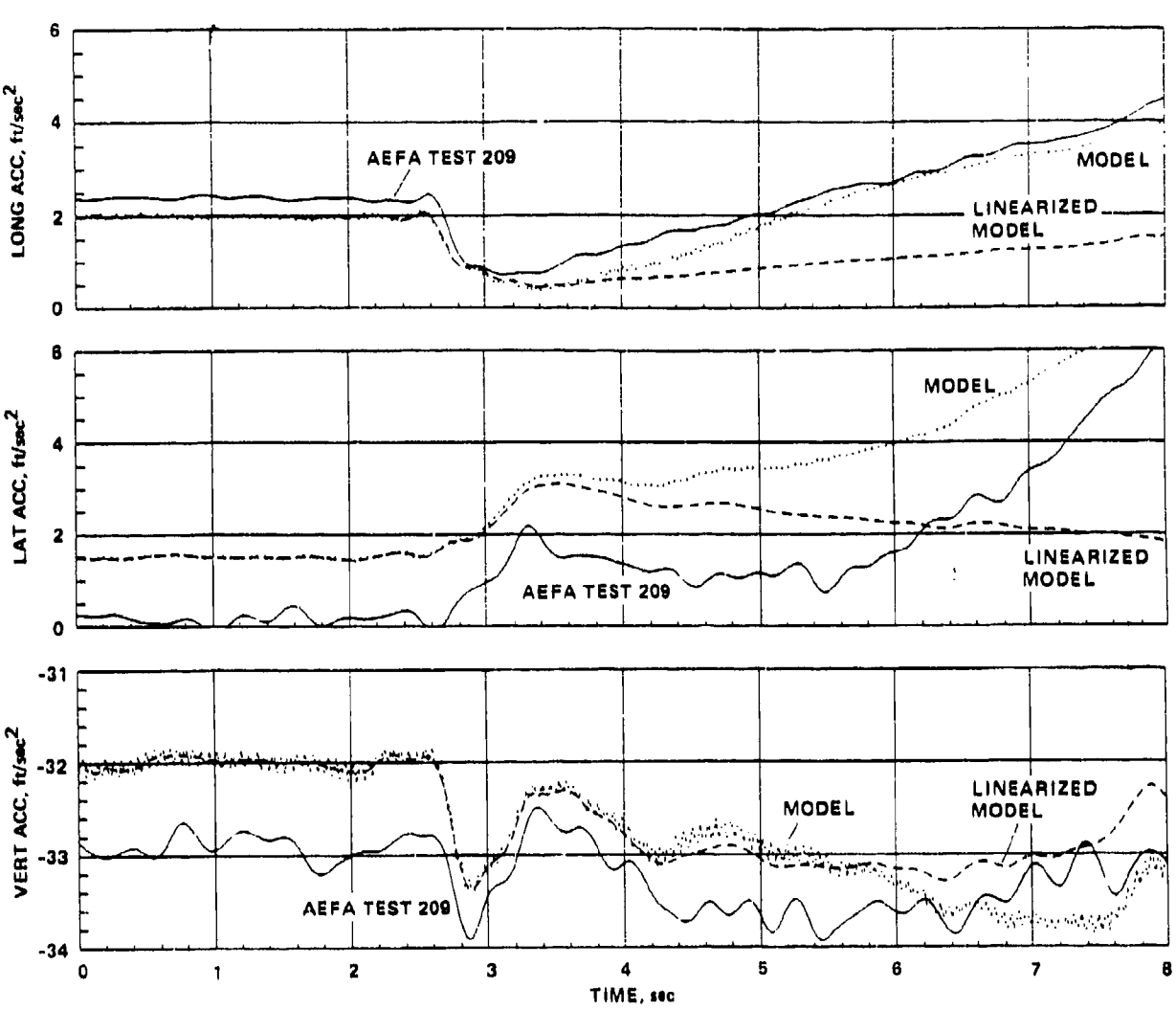

Ω = 26.925 rad/sec M_F = 458.64 slugs $ST_m = ST_c = ST_a$ = 29.942 ft f(4) = 1.68 ft/sec

$$I_F = \begin{bmatrix} 4659 & 0 & 0 \\ 0 & 38512 & -1882 \\ 0 & -1882 & 38512 \end{bmatrix}$$

$WL_m = WL_c = WL_a$ = 19.29 ft i_f = 1,2

σ_y = 0.0698, 0.0698, 0 rad

$I_{Aero} = 0$

IOPT5 = 1,1,1

Figure 37. Concluded.

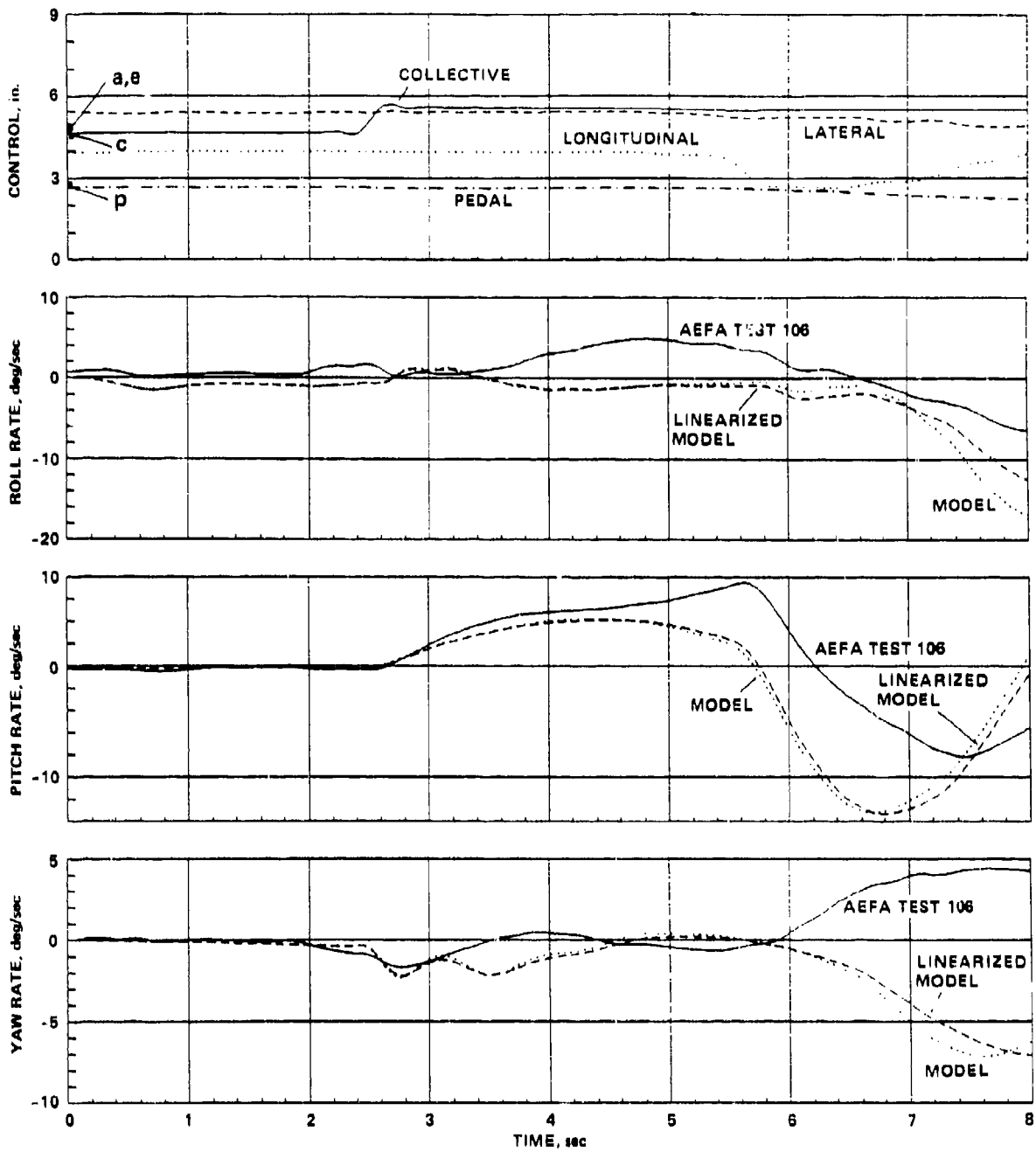

Figure 38. UH-60A model responses with 1-in.-up collective at 100 knots.

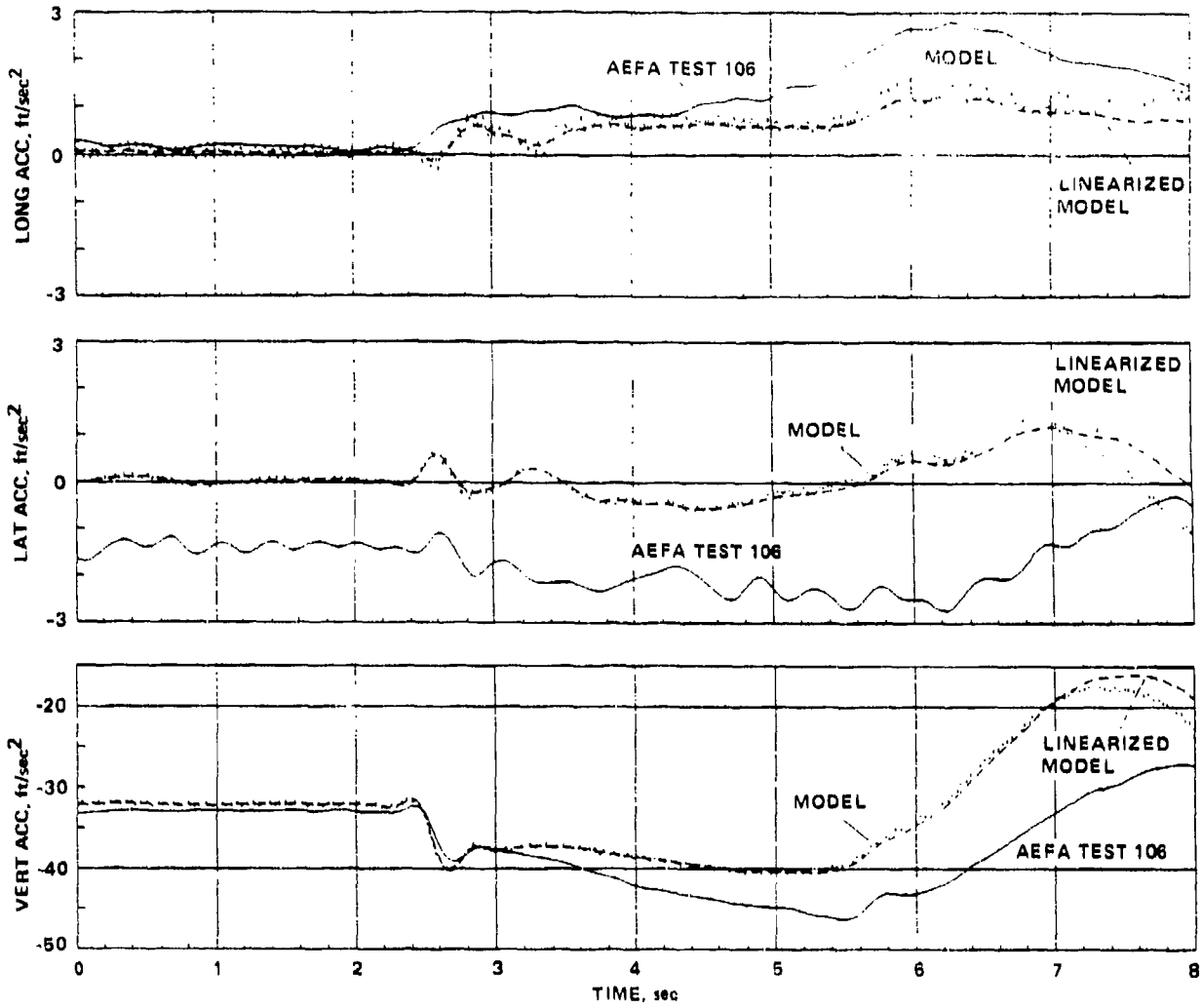

Ω = 27.018 rad/sec M_F = 456.15 slugs $ST_m = ST_c = ST_a$ 28.942 ft f(4) = 153.0 ft/sec

$$I_F = \begin{bmatrix} 4659 & 0 & 0 \\ 0 & 38512 & -1882 \\ 0 & -1882 & 38512 \end{bmatrix}$$

$WL_m = WL_c = WL_a$ = 19.29 ft I_f = 2,3

σ_y = 0.0698, 0.0698, 0 rad

$I_{Aero} = 0$

IOPT5 = 5,5,5

Figure 38. Concluded.

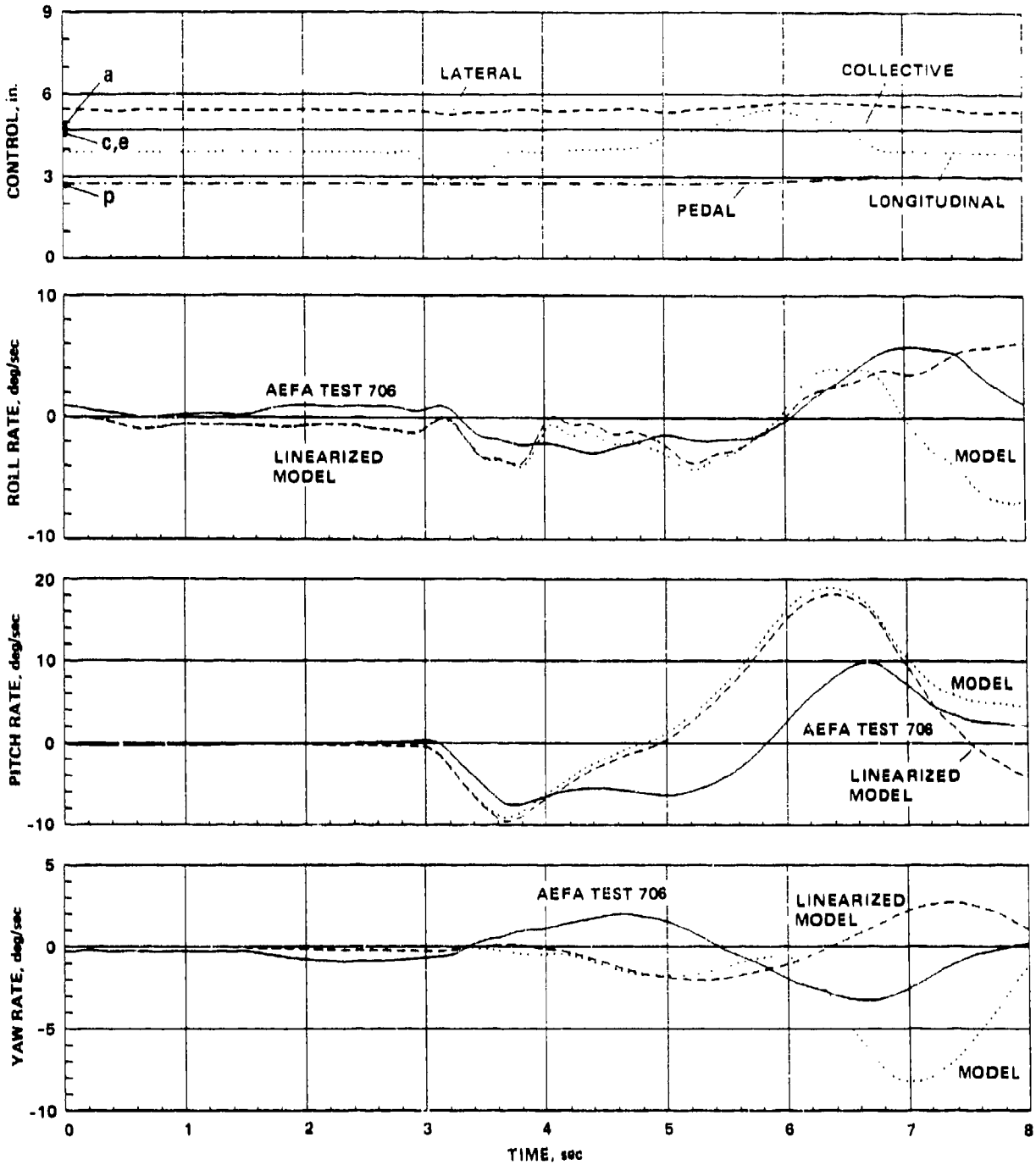

Figure 39. UH-60A model responses with 1-in.-forward longitudinal stick at 100 knots.

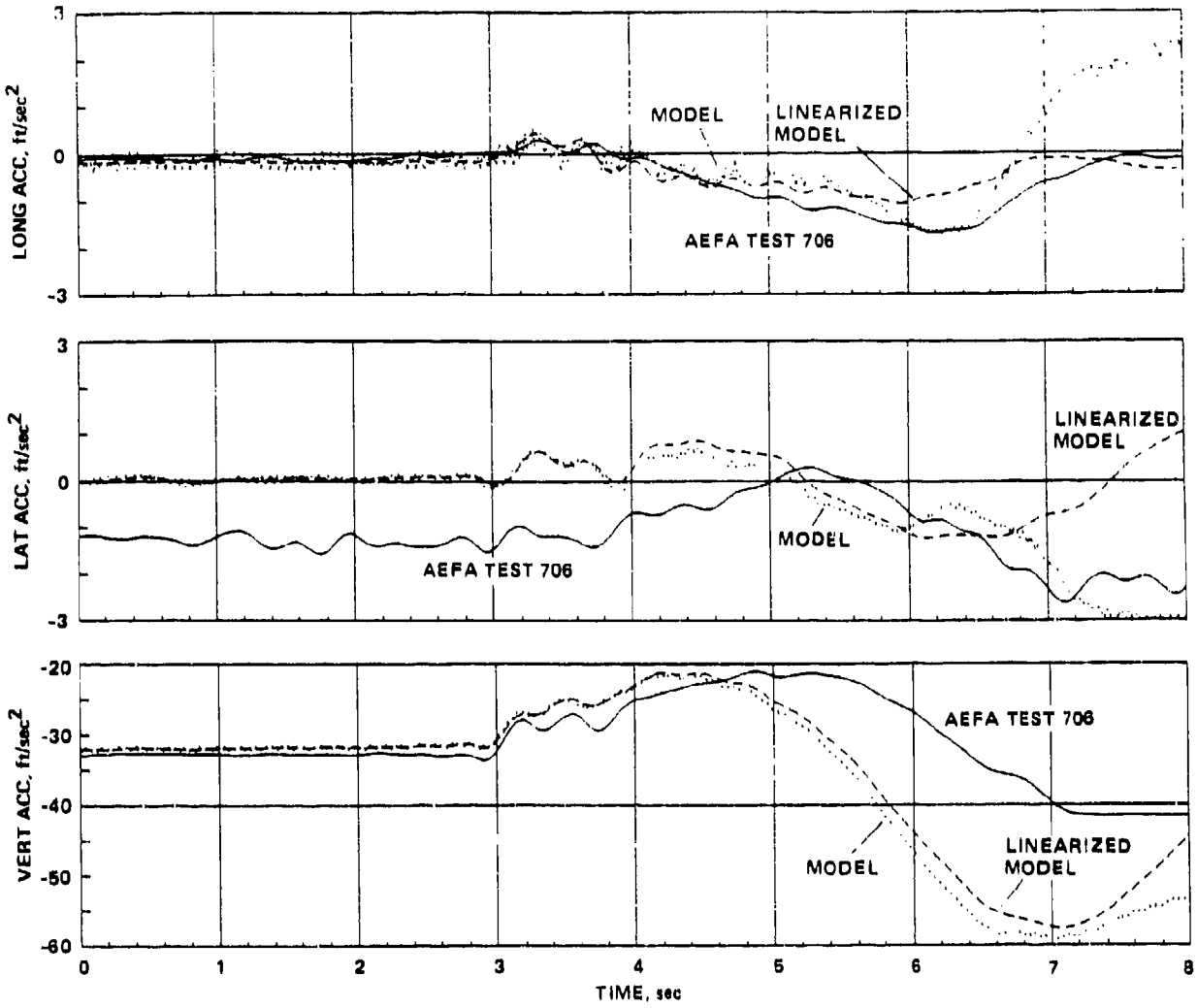

Ω = 26.887 rad/sec M_F = 448.05 slugs $ST_m = ST_c = ST_a$ = 29.325 ft f(4) = 175.6 ft/sec

$$I_F = \begin{bmatrix} 4659 & 0 & 0 \\ 0 & 38512 & -1882 \\ 0 & -1882 & 38512 \end{bmatrix}$$

$WL_m = WL_c = WL_a$ = 19.29 ft i_f = 2,3

σ_y = 0.0698, 0.0698, 0 rad

i_{Aero} = 0

IOPT5 = 5,5,5

Figure 39. Concluded.

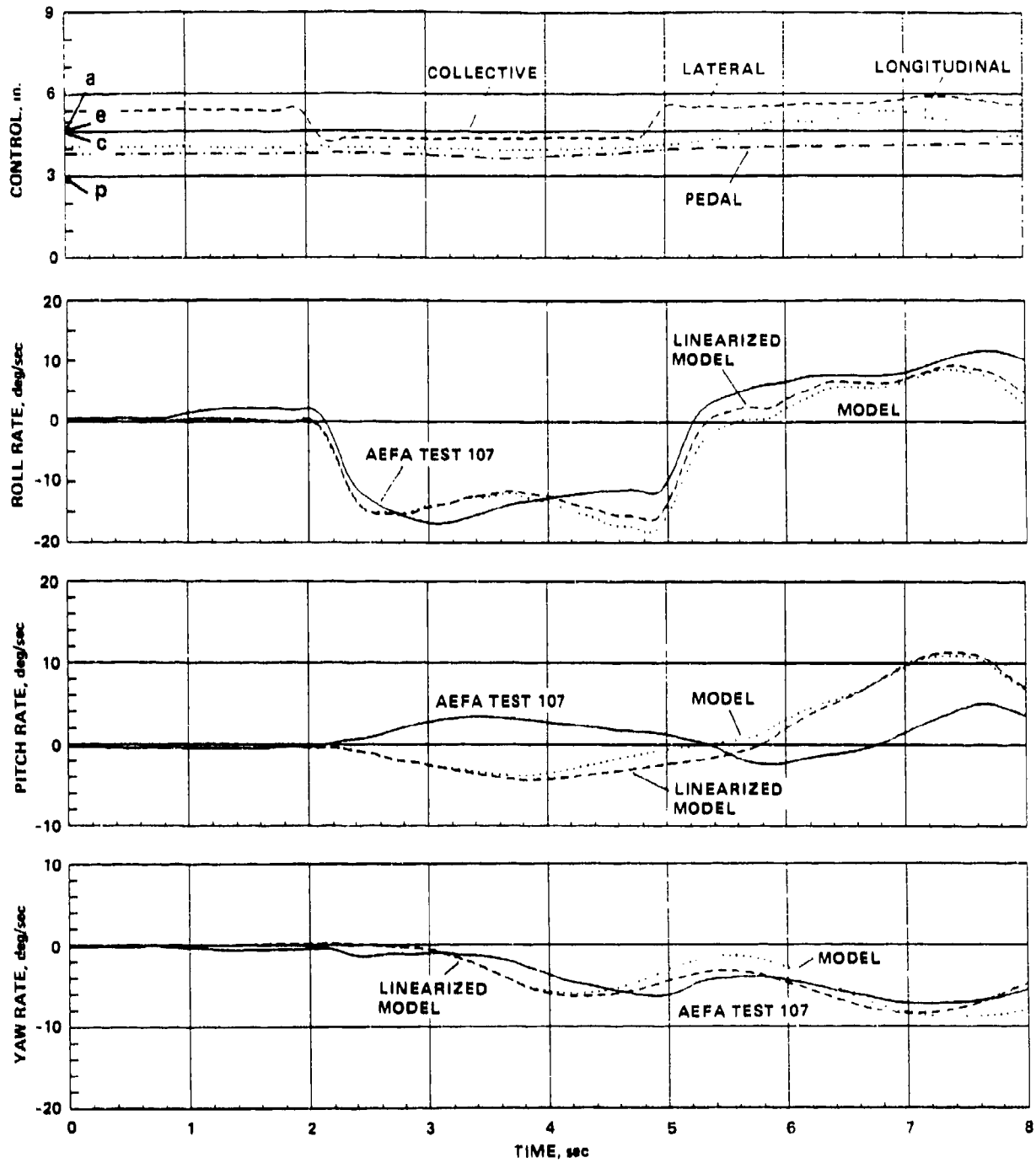

Figure 40. UH-60A model responses with 1-in.-left lateral stick at 100 knots.

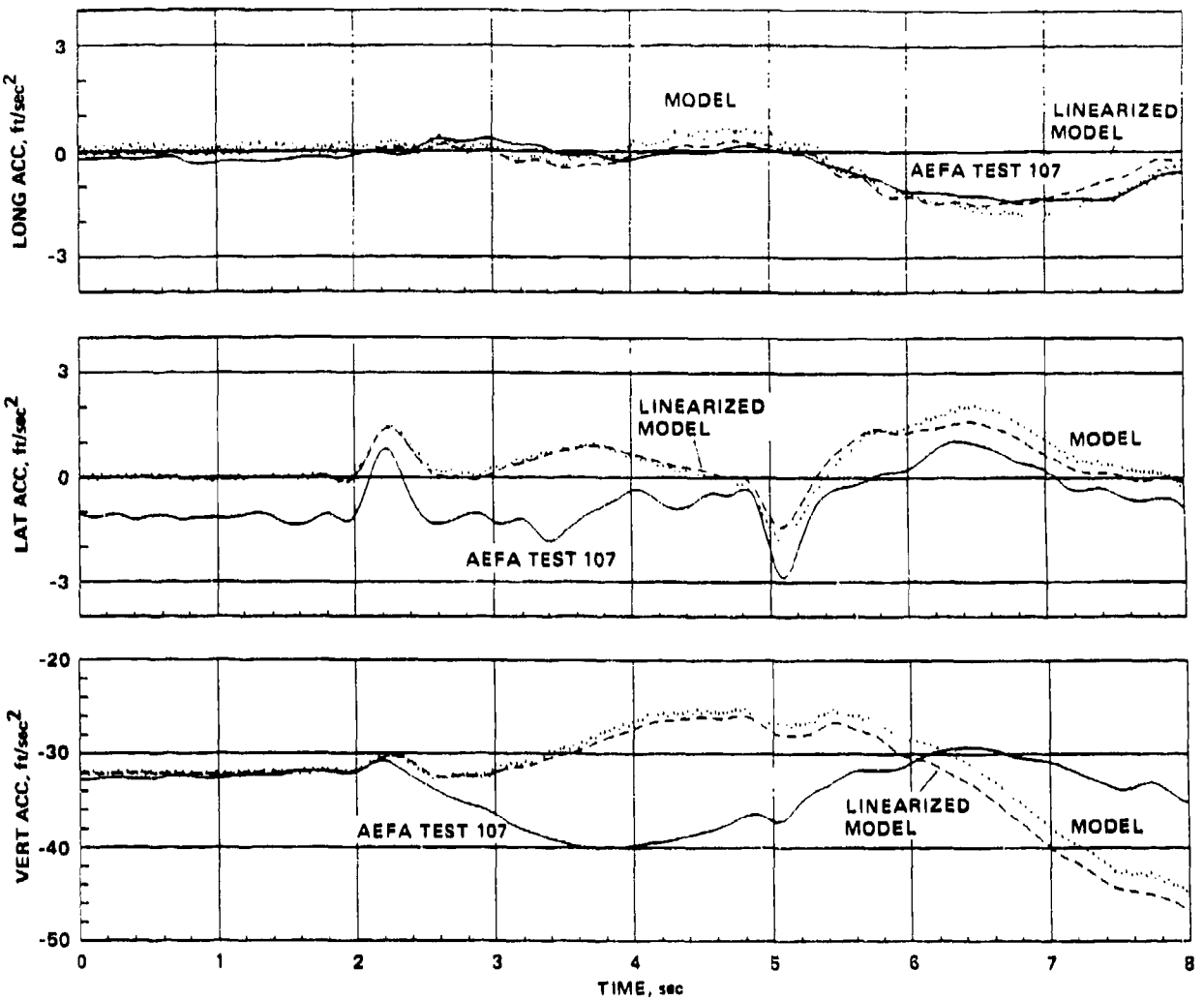

Ω = 26.798 rad/sec M_F = 465.50 slugs $ST_m = ST_c = ST_a$ = 29.058 ft f(4) = 159.8 ft/sec

$$I_F = \begin{bmatrix} 4659 & 0 & 0 \\ 0 & 38512 & -1882 \\ 0 & -1882 & 38512 \end{bmatrix}$$

$WL_m = WL_c = WL_a$ = 19.29 ft i_f = 2,3

σ_y = 0.0698, 0.0698, 0 rad

i_{Aero} = 0

IOPT5 = 5,5,5

Figure 40. Concluded.

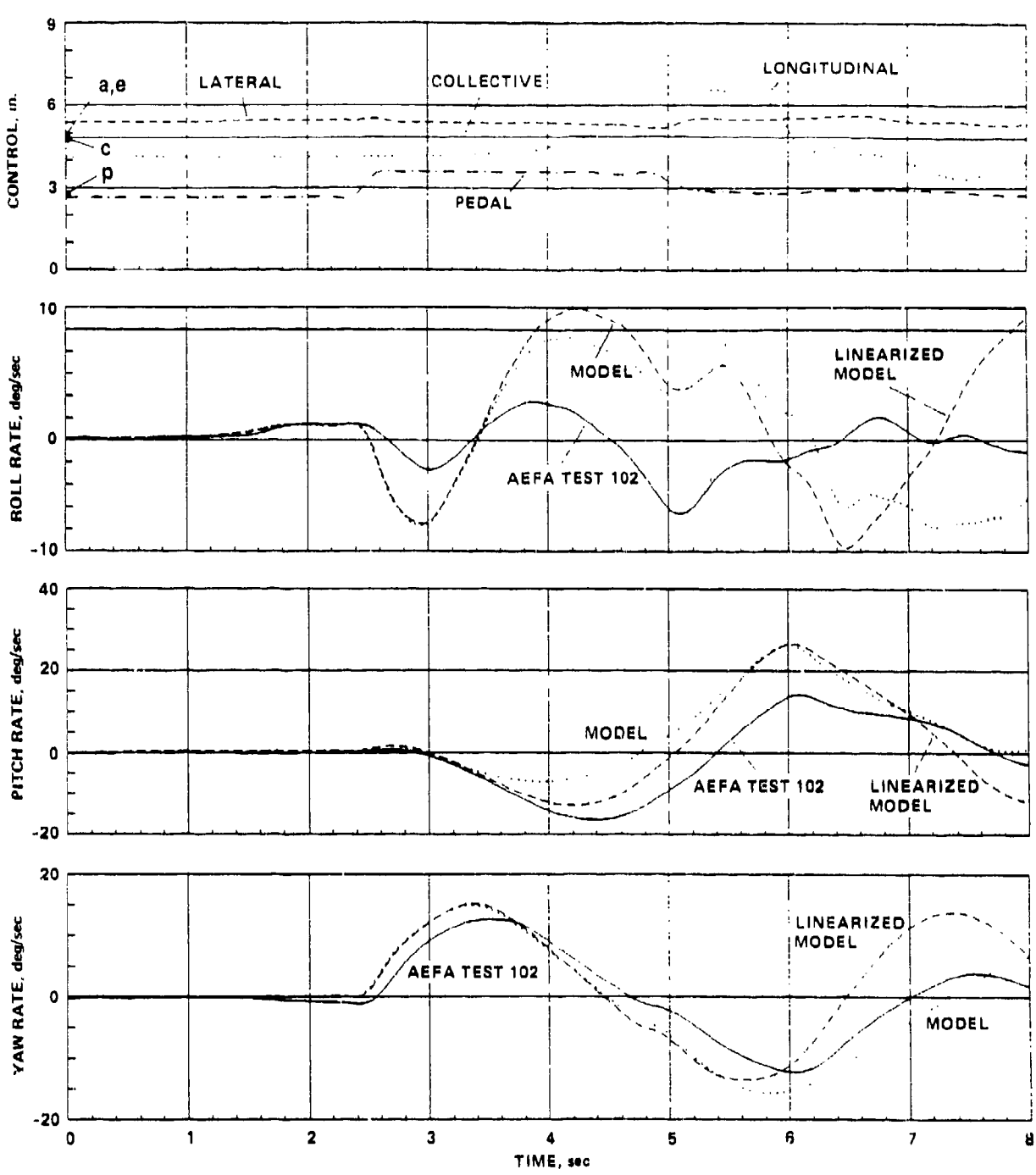

Figure 41. UH-60A model responses with 1-in.-right pedal at 100 knots.

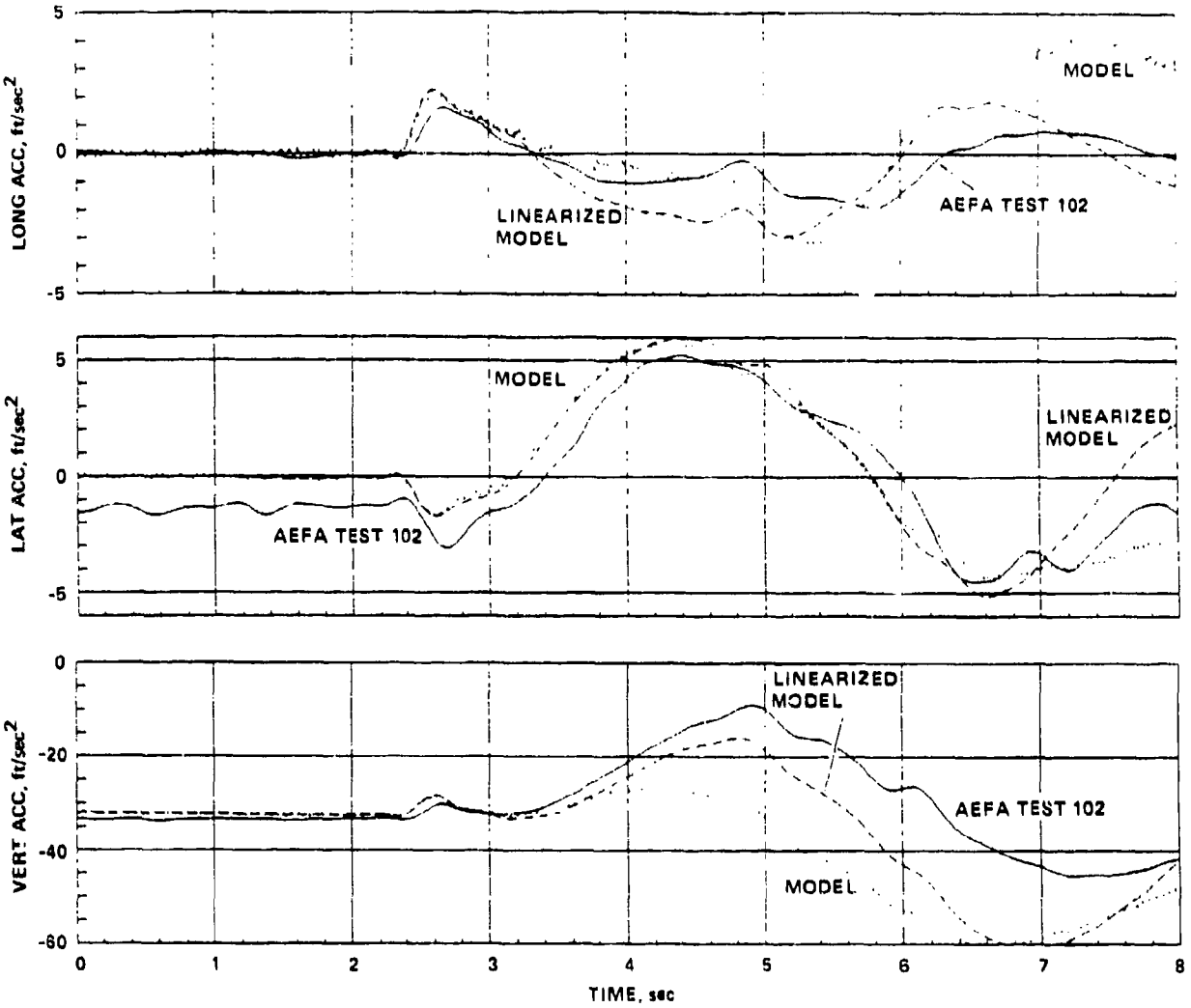

Ω = 27.023 rad/sec M_F = 465.81 slugs $ST_m = ST_c = ST_a$ = 29.058 ft f(4) = 161.6 ft/sec

$$I_F = \begin{bmatrix} 4659 & 0 & 0 \\ 0 & 38512 & -1882 \\ 0 & -1882 & 38512 \end{bmatrix}$$

$WL_m = WL_c = WL_a$ = 19.29 ft I_f = 2,3

σ_y = 0.0698, 0.0698, 0 rad

$I_{Aero} = 0$

IOPT5 = 5,5,5

Figure 41. Concluded.

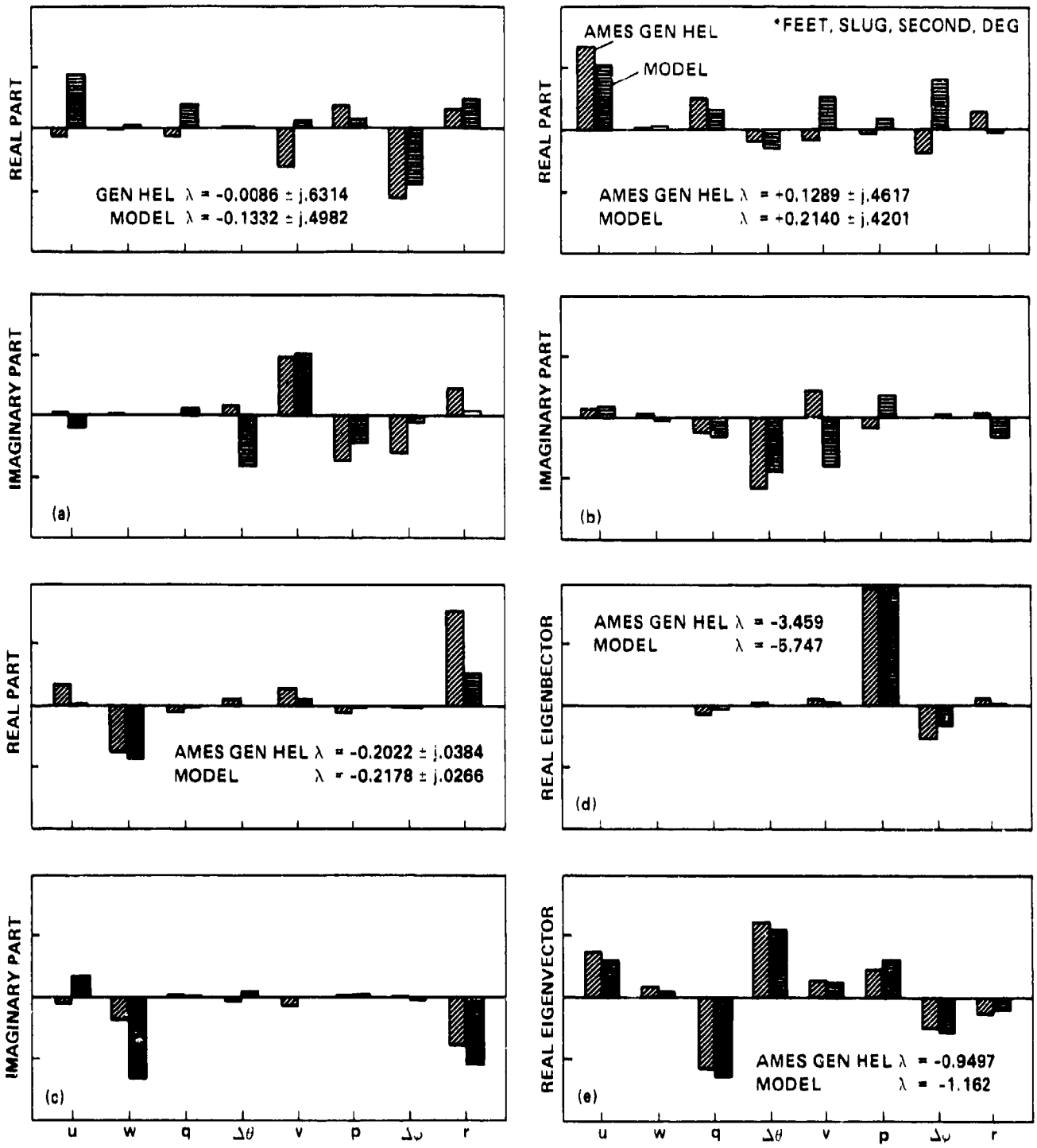

Figure 42. Eigenvalues and eigenvectors of this report's model and the Ames GEN HEL model at 1 knot.

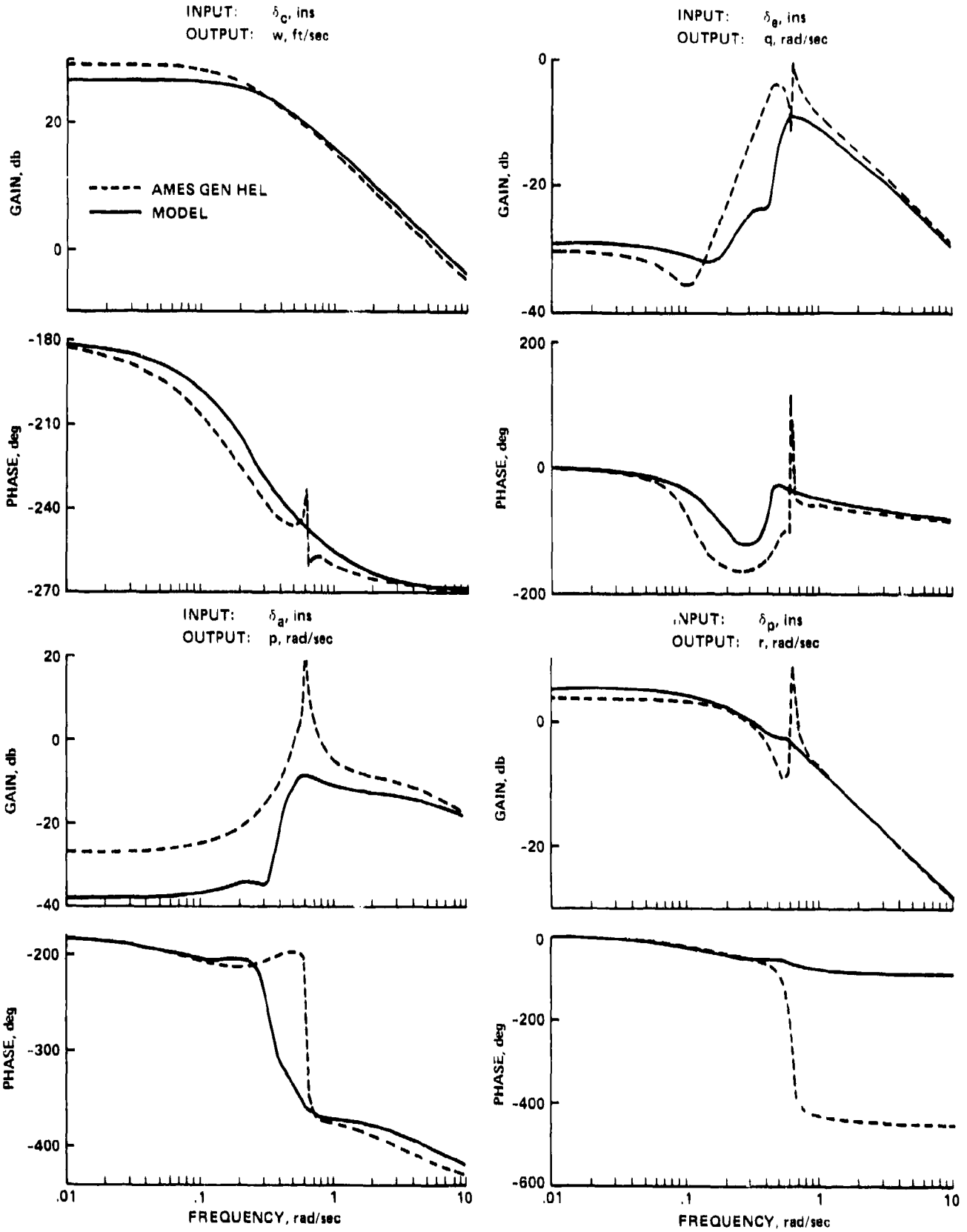

Figure 43. On-axis Bode plots of present model and Ames GEN HEL model at 1 knot.

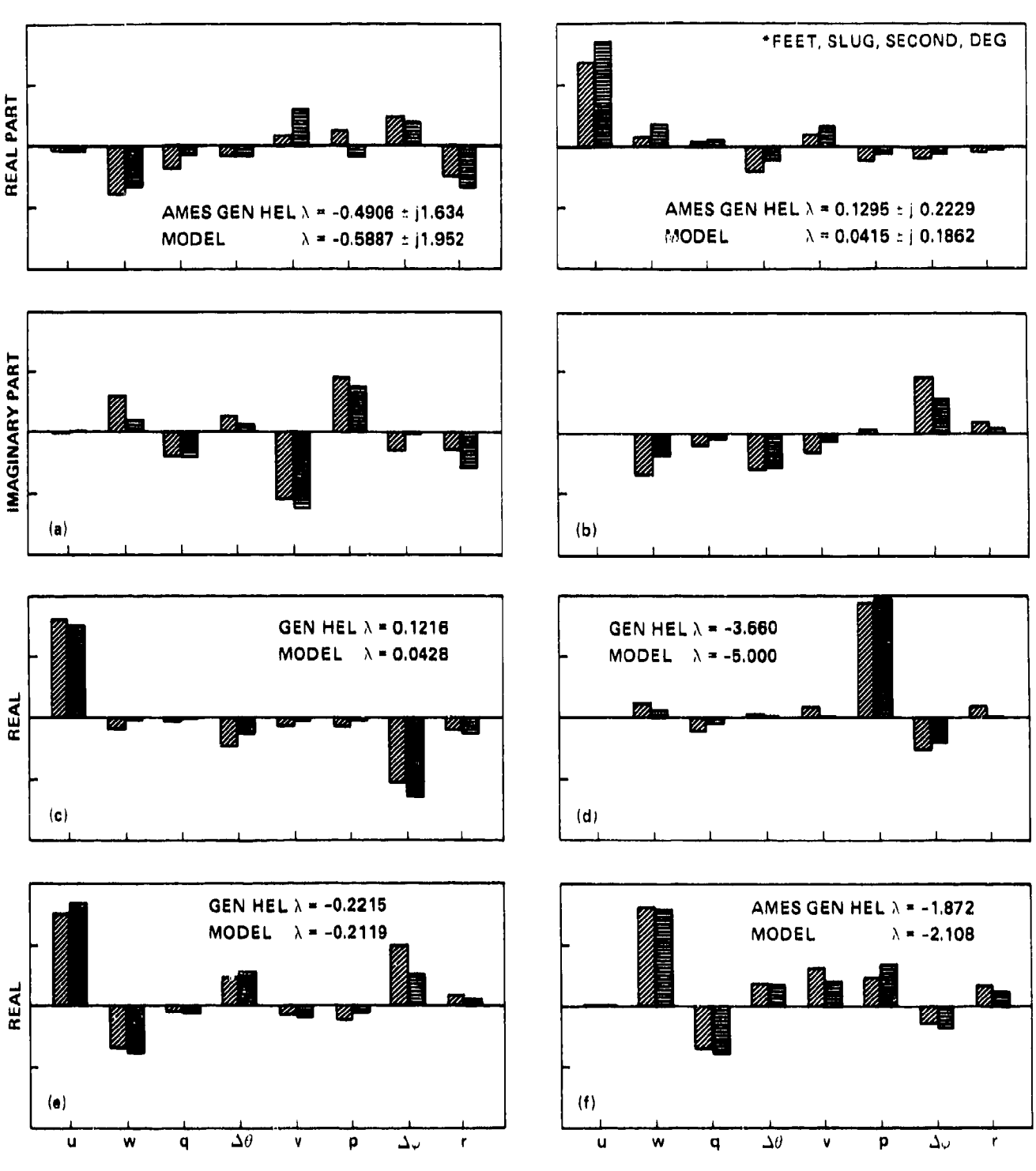

Figure 44. Eigenvalues and eigenvectors of present model and Ames GEN HEL model at 100 knots.

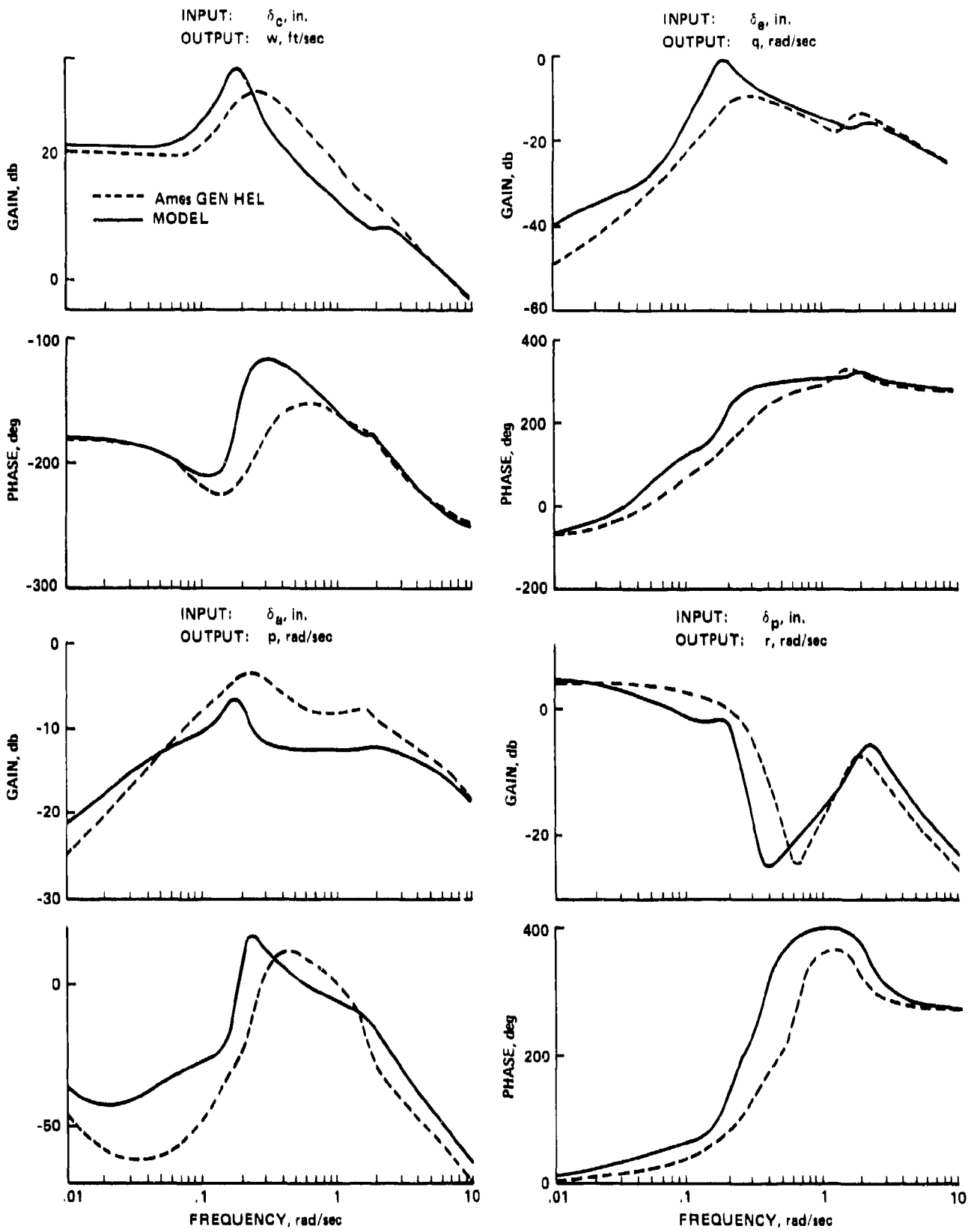

Figure 45. On-axis Bode plots of present model and Ames GEN HEL model at 100 knots.

NASA
National Aeronautics and Space Administration

Report Documentation Page

1. Report No.	2. Government Accession No.	3. Recipient's Catalog No.
NASA TM-102267 USAAVSCOM TM-90-A-004		

4. Title and Subtitle

A Flight-Dynamic Helicopter Mathematical Model with a Single Flap-Lag-Torsion Main Rotor

5. Report Date

February 1990

6. Performing Organization Code

7. Author(s)

Marc D. Takahashi

8. Performing Organization Report No.

A-90037

10. Work Unit No.

505-61-51

9. Performing Organization Name and Address

Ames Research Center, Moffett Field, CA 94035-1000 and Aeroflightdynamics Directorate, U.S. Army Aviation Research and Technology Activity Ames Research Center, Moffett Field, CA 94035-1099

11. Contract or Grant No.

13. Type of Report and Period Covered

Technical Memorandum

12. Sponsoring Agency Name and Address

National Aeronautics and Space Administration Washington, DC 20546-0001 and U.S. Army Aviation Systems Command, St. Louis, MO 63120-1798

14. Sponsoring Agency Code

15. Supplementary Notes

Point of Contact: Marc D. Takahashi, Aeroflightdynamics Directorate, USAAVSCOM Ames Research Center, MS 211-1, Moffett Field, CA 94035-1099 (415) 604-5271 or FTS 464-5271

16. Abstract

A mathematical model of a helicopter system with a single main rotor that includes rigid, hinge-restrained rotor blades with flap, lag, and torsion degrees of freedom is described. The model allows several hinge sequences and two offsets in the hinges. Quasi-steady Greenberg theory is used to calculate the blade-section aerodynamic forces, and inflow effects are accounted for by using a three-state nonlinear dynamic inflow model. The motion of the rigid fuselage is defined by six degrees of freedom, and an optional rotor rpm degree of freedom is available. Empennage surfaces and the tail rotor are modeled, and the effect of main-rotor downwash on these elements is included. Model trim, linearization, and time-integration operations are described and can be applied to a subset of the model in the rotating or nonrotating coordinate frame. A preliminary validation of the model is made by comparing its results with those of other analytical and experimental studies. This publication presents the results of research completed in November 1989.

17. Key Words (Suggested by Author(s))	18. Distribution Statement
Rotorcraft mathematical model Flap-lag-torsion rotor Helicopter	Unclassified-Unlimited Subject Category – 01

19. Security Classif. (of this report)	20. Security Classif. (of this page)	21. No. of Pages	22. Price
Unclassified	Unclassified	116	A06

NASA FORM 1626 OCT 86

For sale by the National Technical Information Service, Springfield, Virginia 22161